Experimental Study on Cyclic Behaviour of Riveted Stiffened Seat Angle Connections

by

Majid H.K.M. Sarraf

Thesis submitted to the School of Graduate Studies
in partial fulfilment of the requirements for the
Master of Applied Science Degree in Civil Engineering
under the auspices of the
Ottawa-Carleton Institute for Civil Engineering

September 1993

Department of Civil Engineering, University of Ottawa
Ottawa, Canada, 1993

ISBN 0-612-11601-8

UNIVERSITÉ D'OTTAWA
UNIVERSITY OF OTTAWA

Abstract

Riveted Stiffened Seat Angle Connections have been used as beam-to-column joints in many old steel buildings. These connections are generally categorized as flexible. A concern exists at to the lateral resistance of frames built with these connections, particularly under earthquake excitations which can cause these connections to undergo severe inelastic excursions. An experimental program was conducted to investigate the behaviour of two typical Riveted Stiffened Seat Angle Connections and the improvement in their behaviour when retrofitted using two suggested retrofitting techniques. Large inelastic cyclic tests were conducted on connections taken from an 83 years old building and their hysteretic moment-rotation curves were obtained. Preliminary models of their inelastic behaviour are developed. Practical recommendations for seismic rehabilitations are formulated.

To my wife, Samaneh

Acknowledgments

My great appreciations go to Dr. Michel Bruneau for his guidance, encouragement and support throughout this work. Dr. M. Saatcioglu and Dr. N.J. Gardner are greatly acknowledged for their additional assistance. I would like to thank Mr. Peter McCourt, Chief, Private Sector - Joint Projects Real Estate Development, National Capital Commission, Mr. John G. Cooke, P.Eng., President, Cooke & Associates Ltd., Consulting Engineers, and Mr. Paul Greenspoon, Vice President, Operations, Bros. Ltd., Demolition Experts, for their cooperation in obtaining the tests' specimens and also the University of Ottawa, Dept. of Civil Engineering machine shop technicians and Structures laboratory technicians for their efforts in building the set-up.

My deepest thanks also go to my parents for their encouragement and moral support throughout my life.

Table of contents

CHAPTER 4

CHAPTER 5

CHAPTER 6

List of Tables

List of Figures

Notations

C_r	factored compressive resistance of a member, kN
d_1,.d_4	displacement measured by LVDTS at the location shown in Fig. 3.9, mm
F_u	tensile strength of steel, MPa
F_v	shear strength of steel, MPa
F_y	yield strength of steel,
h	hight of beam, mm
h_1,.h_4	distance between the LVDTS and beam as shown in Fig. 3.9, mm
M	moment applied to connection, kN.m
T_r	factored tensile resistance of a member, kN
θ	average rotation developed in connection, radians
θ_R	angle of rotation in the right side of joint, radians
θ_L	angle of rotation in the left side of joint, radians
ε	strain, mm/mm

CHAPTER 1

Introduction

1.1 General

Beam-to-column connections commonly used in steel frames are generally categorized in three groups; flexible, rigid and semi-rigid. In theory, a perfectly flexible connection in a typical beam-column joint allow free rotation of the beam without any moment resistance. By contrast, a perfectly rigid connection resist moments without developing any rotation. Semi-rigid connections, therefore, are those which can resist moment while allowing some rotation to occur. Rigid and flexible types of connections have been used extensively in steel structures in a large part because the structural analysis of frames is greatly simplified when only these two types of connections are present, as opposed to when semi-rigid type of connections are used. In the past, to achieve maximum agreement between the theoretical and true behaviours, these two types of connections were designed such that they performed as closely as possible as purely rigid or flexible connections. However, experimental and analytical studies on the various types of connections traditionally used in structural steel frames have proved that most connections, to some extent, can be considered as semi-rigids to various degrees.

Numerous investigations have already been conducted to understand the differences between true and assumed connections behaviour when analyzing frames. Experimental and analytical approaches have been used in the past to obtain the monotonic moment-rotation relationship of various types of connections. Semi-rigid types of connections have received special attention in this regard, since this group includes a variety of different connections.

Over the years, many buildings have suffered damage during severe earthquakes. In structural

steel frames subjected to such severe earthquakes, connections normally undergo large and numerous cyclic inelastic excursions. The seismic-survival of steel buildings is obviously closely tied to the vulnerability of the beam-to-column connections. Therefore, knowledge on the ultimate inelastic cyclic behaviour of connections, particularly semi-rigid ones, is very important.

1.2 Knowledge on Cyclic Behaviour of Existing Semi-rigid Connections

In absence of earthquake design requirements in the past, very little constraints existed against the common use of semi-rigid and flexible connections in designing the beam-to-column joints of steel frames. Ensuing from a better understanding of the damaging effect of earthquakes, building codes requiring that frames be designed to resist earthquakes have been progressively established, and have become more stringent with time. Engineers realized that buildings with flexible connections could difficultly meet these requirements and these connections fell out of favour. Still, as these developments are relatively recent, there remains in existence many old building frames with semi-rigid and flexible connections which were not designed to resist moments. At first glance, these frames seem to lack the needed lateral resistance to survive earthquakes. Absence of better knowledge on the lateral resistance of these frames would eventually translate into the demolition or the need to perform major retrofit of many steel buildings when investigated by practising engineers, unless it can be demonstrated that these connections, and consequently their frames, have some inherent resistance.

Studies on flexible connections have shown that some type of flexible connections are capable of resisting moments. Therefore, these could be treated as semi-rigid connections and the frames built with such connections would even have some capacity to resist lateral loads. Such previously overlooked potential resistance need not be neglected. In fact, in some cases, this resistance may be found to be sufficiently large to demonstrate that only minor, or even no, retrofit of these frames is required in zones of minor or moderate seismicity. The challenge lies in establishing the magnitude, nature, and reliability of this potential resistance.

Riveted stiffened seat angle connections are normally considered as flexible types of connections. They have been commonly used in the beam-to-column joints of many steel frames in the past. However, ability of riveted stiffened seat angle connections to behave as semi-rigid types of connections remains unquantified. Analytical studies on the performance of steel frames having such connections and subjected to earthquakes or other cyclic lateral loads, can only be made if the cyclic non-linear inelastic moment-rotation relationship of such connections is known. However, to date very little of this knowledge is available.

1.3 Objectives of This Research

The objective of this thesis is: (i) to obtain experimental results on the behaviour of typical riveted stiffened seat angle connections subjected to cyclic loads, with a particular emphasis on establishing their non-linear inelastic moment-rotation relationships and; (ii) to investigate the improvement in cyclic behaviour of these connections provided by the two proposed retrofitting techniques.

1.4 Scope of Work

An experimental study has been accomplished by conducting 4 tests, including two retrofit strategies, on two different existing joint configurations. Each of the two specimens includes two identical connections generating two sets of data for each test. The two specimens were obtained from an 83 years old building.

The obtained experimental results are applicable to similar connections of different size, with minor adjustments, as demonstrated by analyses and comparison of the results with those obtained using suggested physical models. Moreover, since the experimental approach used in this study was intended to produce more broadly applicable results, the specimens were set-up to eliminate the effect of panel zone deformations in the columns.

1.5 Outline of the Thesis

Existing literature on the behaviour of semi-rigid connections is reviewed in Chapter 2. Description of the test specimens, prediction of capacity of the connections and the experimental procedure are explained in Chapter 3.

The test observations and experimental results are provided in detail in Chapter 4 and the test results are interpreted and compared with their predicted values in Chapter 5. Finally, in Chapter 6, conclusions and practical recommendations are made based on the test results.

CHAPTER 2

Literature Review

2.1 General

Semi-rigid types of connections, as stated earlier, do not fall in the categories of either rigid or flexible type of connections, since theoretically, in the former no connection rotation can develop, and in the latter no moment can be resisted by the connection, two constraints violated by semi-rigid connections.

Practically, there is no such thing as perfectly rigid or flexible connections. In fact all connections, even those classified as flexible, are capable of resisting some moment, and those categorized as rigid allow some degree of rotation when subjected to moments. Therefore, all connections can be thought of as semi-rigid with different moment-rotation (M-θ) characteristics. However, for simplicity in structural analysis, practising engineers commonly model connections as perfectly rigid or flexible whenever their behaviour is sufficiently close to one of these two types.

To quantify relative fixity of connections, the term "degree of restraint" is often used, in existing literature (Salmon and Johnson 1980). It is defined as the ratio of the end moment of a beam developed in its connection to that of a beam with fully fixed support conditions. In steel frames, connections are typically referred to as rigid if they can develop an end restraint greater than 90% of the end restraint produced in the fully fixed beam. In other words, connections with a degree of restraint of 90% or more are classified as rigid. If a connection's degree of restraint is less

than 20%, it is considered as flexible. For all other cases, connections are categorized as semi-rigid.

For example, T-Stub, End-Plate and fully welded connections are treated as rigid. Seat-angle connections with or without stiffener, and simple web-angle connections are generally considered as flexible, but test results show that even these connections, particularly stiffened seat angles, can be considered as semi-rigids. Fig. 2.1 illustrates some typical connections.

As found in old steel design handbooks (e.g. Scott 1904, Ketchum 1924), at the turn of the century, most connections were also designed to perform as either rigid or flexible. For many years, engineers have known that connection rigidity can have a major impact on behaviour of a steel frame and that taking advantage of end restraints could translate into the use of lighter beams. Unfortunately, during the first half of this century, knowledge on behaviour of semi-rigid connections was primitive and engineers lacked the analytical tools which would have been necessary anyhow to consider true semi-rigid properties of connections in their analyses.

Since most engineers believed that gravity loads governed the design of steel frames, and since only buildings were specifically designed to resist wind loads (many engineers indirectly relied on the heavy cladding typically found in older buildings for that purpose), early investigations on the behaviour of semi-rigid connections were solely focused on determining their degree of restraint under monotonic loading caused by gravity loads. Eventually, some cyclic loading tests were conducted mainly to investigate steel frame drift due to wind loads.

When earthquake-resistance became a design concern, major changes occurred in the understanding on the general behaviour of structural frames subjected to lateral forces. Rare and intense earthquakes, by their nature, cause structural frame connections to undergo high cyclic deformations far beyond the elastic range. Therefore, researchers started to investigate the performance of connections with more emphasis on developing experimental or analytical models which can predict M-θ relationship of connections under cyclic loading, well into their non-linear inelastic range.

Therefore, early investigations on semi-rigid steel connections are different in emphasis from the more recent ones. In the former, the objective was mostly to find the rigidity of connections under monotonically increasing loads within the elastic range, whereas in the latter the goal was tc finding models which can represent the inelastic cyclic behaviour of connections and be used in more accurate seismic analysis of frames. As this later concern is relatively recent, this is reflected by the scarce coverage it has received in the literature on this topic

2.2 Experimental Investigations

The exact behaviour of any given connection can only be determined experimentally (although some complex modelling strategies can very accurately replicate this behaviour). However, conducting experiments for every connection type to be used in a frame is neither practical nor economical. Thus, simple analytical models which can closely predict the real behaviour of connections are needed. On the other hand, because of the broad variety of possible connections, and owing to differences in size and arrangement of parts of these connections, it is impractical to develop a single model which can give M-θ characteristics for all types of connections. Therefore, models have often been developed to fit specific type of connections, based on experimental data.

2.2.1 Monotonic Tests

Riveted types of connections were commonly used in steel frames from the beginning of steel construction until the mid 1900's. In those days, researchers paid a special attention toward experimentally determining the rigidity of riveted connections. Early investigations of riveted connections started when a series of tests were conducted by Moore and Wilson (1917). Later, Young and Jackson (1934) studied different types of riveted connections to compare their rigidity against welded ones. In their study, they also applied reversed loading on typical wind resisting connections to inspect connections rigidity subjected to wind loads. However, the level of load applied in their tests was limited, due to the fact that working stress design method was

commonly used at that time, and tests were not conducted to either fail or cause large inelastic deformation of connections. Rathbun (1935) conducted experiments on typical riveted connections such as seat angles, seat and web angles, and T-Stub types, which were known as "shallow wind bracing". Specimens used were standard connections from handbooks published by steel mills and were subjected to monotonic loading. From that experimental investigation, it was concluded that for seat angle connection, large deformations of angles occurred without major change in connection shear capacity. It was also inferred that thickness of the angles was a major factor affecting these deformations, and that replacing angles by thicker ones would improve connection rigidity.

To investigate further the role of angle deformations on the behaviour of semi-rigid connections, Lewitt et al. (1966) conducted experiments by subjecting angles to both tension and compression in a monotonic manner, and used the results to formulate an analytical model. The results showed that angles in tension develop three yield lines (Fig. 2.2), and that load deformation relationship of angles could be expressed by an exponential function.

A number of other tests were conducted by other researchers (e.g. Marley 1982; Hetcman et al. 1947; Maxwell et al. 1981) to enhance the understanding of the behaviour of connections under monotonic loadings. The results of these tests were used by others to develop experimental models. Although behaviour of semi-rigid connection under monotonic loading is not within the scope of this study, some ideas which resulted from these investigations can be applicable. Therefore, some of the models developed by others are reviewed in section 2.3.

2.2.2 Cyclic Tests

In recent years, attempts have been made to obtain the M-θ relationship of semi-rigid connections under cyclic loading, and understand the performance of such connections in steel frames subjected to severe lateral loads. Radziminsky et al. (1986) conducted experiments on a type of semi-rigid connection consisting of double angles with top and seat angles, and subjected this

type of connection to low-amplitude cyclic rotations. Astaneh et al. (1989a) later performed experiments on double web angles under large cyclic rotations until failure of the connections. Astaneh et al. (1989b) also conducted shake-table experiments with both the type of double web angles they previously tested, and the same type of semi-rigid connections used by Radziminsky et al., by employing them in frames subjected to simulated earthquake loads. Another study (Charles et al. 1993), still in progress at the time of this writing, investigates the cyclic behaviour of some selected types of bolted and riveted semi-rigid connections. Progress reports have reported that moment-rotation curves obtained are pinched and that riveted connections show slips when unloading. This last experimental study is noteworthy since it is, with the work related to this thesis, the only reported cyclic test program of riveted connections. However, Charles et al. have simulated old connection by developing in-laboratory capability for riveting new steel sections, regardless of aging of riveted steel.

2.3. Experimentally Based Models

Using experimental test data and different curve fitting techniques, many researchers have attempted to develop M-θ relationships which could describe the monotonic behaviour of semi-rigid connections.

2.3.1 Linear Models

The simplest developed model is the single stiffness linear model by Rathbun (1936). It was improved by Monforton et al. (1963), and later Lightfoot et al. (1974) who developed single stiffness model for different types of connections. After that Trapy et al. (1981), and then Lui and Chen (1983) developed bi-linear piecewise linear models (Fig. 2.3) Although these models can be used easily to represent M-θ relationships, their sudden change in slope creates difficulties for practical applications.

2.3.2 Polynomial Model

Fry and Morris (1976) utilized polynomial functions to express θ as a function of moment. The parameters used in their model were curve fitting constants and a factor related to the type of connection. The model is more accurate than other simple models, but it can produce negative stiffness if used at very large deformations.

2.3.3 B-Spline Model

Using B-Spline method of curve fitting, Jones et al. (1982) proposed another M-θ relationship. Their model, while improving accuracy, needs a considerable number of data points for calibration.

2.3.4 Exponential and Power Models

Power models were independently introduced by Richard et al. (1980) and Colson et al.(1983). They proposed a three-parameter power model in which moment and stiffness of connection are taken into consideration. Later, Ang et al. (1984) introduced a power model with four parameters. Chen and Lui (1985) and Lui et al. (1986) also used an exponential function in which, besides curve fitting constants and other parameters, a connection strain-hardening parameter was introduced. This model was adjusted by Kishi and Chen (1986) using Heaviside's step function, for better representation of abrupt changes in slope of M-θ. Kishi and Chen (1990), also proposed a three parameter power model similar to Colson's et al. (1983).

It is noteworthy that in spite of these various refinements, all these above models are valid only for monotonic behaviour of connections and their applicability to cyclic loads is not established. Moreover these experimental models are based on curve fitting techniques to experimental results and in some cases require a considerable number of data points. Also, the applicability of an experimental model to other connections of the same type but with different size must be

demonstrated rationally, otherwise the model is only valid for the tested connections. For the above and other reasons, the use of analytical models, which attempt to physically and more generally explain the behaviour of a given type of connection, is preferred. Again, the existing analytical models which have been proposed by researchers cannot be directly used for the case at hand, but the physical descriptions of behaviour for the connection parts in those models is instructive. A few relevant studies are reviewed in the following section.

2.4 Analytical Approaches

Due to complexity of analytical approaches for most cases, limited studies have been made to model the behaviour of semi-rigid connections subjected to cyclic loadings. However, a number of analytical models have been proposed to predict the M-θ relationship of these connections under monotonic loadings.

The first analytical study on the behaviour of semi-rigid connections was undertaken by Lewitt et al. (1966). He developed a physical model for double angles subjected to axial forces, and enhanced it to predict the behaviour of web-angle connections under monotonic loading. In Lewitt's model of the connection, the important parameters are centre of rotation, which varies as a function of angles stiffness and geometry, and load deformation characteristics of the angles in tension.

More recently, Kishi and Chen (1990) studied semi-rigid bolted connections consisting of top and bottom seat angles. Their analytical model was developed to predict the moment rotation characteristics of connections under monotonic loadings. In this model, initial stiffness and ultimate moment capacity of the connection are the key parameters, and a shape parameter from curve fitting of experimental data is applied to establish a three-parameter power model. In determining initial stiffness it is assumed that: a) centre of rotation is located at the fillet of bottom seat angle leg; b) top angle leg is modeled as a cantilever; c) resisting moment of seat angle is ignored. However, for the calculation of ultimate moment capacity, it is also assumed

that: a) top angle develops two plastic hinges; b) Bottom angle hinging moment is taken into account. These assumptions for initial and ultimate condition of the connection are illustrated in Fig. 2.4.

Among semi-rigid types of bolted connections, the top and bottom angle one was also studied by Youssef-Agha et al. (1989). The main characteristics of the model are initial stiffness and strain hardening behaviour of the connection. Having established a monotonic load deformation relationship for the top and bottom angles in elastic range and calculating the yielding moment as a transition point for changes in behaviour of the connection, they developed an analytical bi-linear model to predict the M-θ relationship (Fig. 2.5). In this model, the effect of column flange deformations was also taken into account. However, deformations due to slippage of bolts were ignored and elongation of bolts under tensile load was assumed to be linear. The significance of this bi-linear model of the M-θ relationship is that all its parameters can be established from the geometry of the connection, and thickness of the parts. Only a constant to account for strain hardening, tentatively taken as 0.15 based on test results by Marly et al. (1982) and Stelmack et al. (1986, 1983), is empirical. Although they developed this model based on assumptions regarding the monotonic behaviour of this type of connection, they also attempted to extend its applicability to the case of cyclic loading. Therefore, Youssef-Agha et al. compared the results from their model integrated into a computer program to perform cyclic non-linear inelastic earthquake response analysis, with experimental results by Stelmack (1983) and Marly et al. (1982) for one-story and two-story frames having this type of connection and subjected to low intensity seismic loads. As shown in Fig. 2.6, the analytical model produce results in good agreement with the experimental ones. However, adequacy of application of this model for the connections in the frames subjected to more severe earthquake levels (which would cause larger inelastic deformations) remains unknown.

CHAPTER 3

Experimental Approach

3.1 General Description of Specimens

Contrary to most experimental studies where the specimens are first designed and built to fulfil the purpose of a specific investigation, in this study the specimens were primarily parts of steel frame of Daly Building, located at Rideau and Sussex street in downtown Ottawa, which was constructed in 1910 and demolished in 1992. Therefore, in this investigation, it is the actual beam-to-column connections of the building and the physical property of old steel which are tested.

The building can be described as a seven story office building 155 ft x 189 ft in plan, 5 bays and 8 bays of approximately 20 ft in the East-West and North-South directions respectively. The structural system for the southern half of the building consisted of steel frames spaning in the East-West direction. The northern half of the building was made of concrete space-frames with very thick slab and small walls around a staircase. The building envelope consisted of stone masonry with large window openings. Based on a survey of past seismicity, the most noticeable earthquake excitation felt at the site of this building over its life is estimated to have produced a peak ground acceleration of 3.2% g (Robert Wetmiller, Seismologist, Geological Survey of Canada, personal communication). It was produced by the 1944 Cornwall-Messina earthquake of Richter Magnitude 5.6.

The specimens, consisting of beams, columns and their connections, were first flame-cut from the building frame on site, with cuts made as far as practically possible from the joints, contrary to normal demolishing procedure, so that the connections with part of members could be carried whole to the laboratory. Since the specimens did not appear to be vulnerable to loads due to

handling, they were given an ordinary care and, laid on a deck of a flat truck, they were shipped to the laboratory. The specimens had no significant rust and they were stored in a dry-space for a few months before being tested.

All the specimens, connections were of the top and stiffened seat angles type, and entirely riveted. However, due to differences in size and arrangement of fasteners the specimens are divided into two groups, for the purpose of this study. In the first group, the column consists of only a single I-shape steel section. In the second group, the column is a built-up section encased in a weak concrete used for fire proofing of the steel frame not for structural purposes. Details of the beam-to-column connections corresponding to each group, referred to herein as connection detail 1 and 2, are shown in Figs.3.1(a) and 3.1(b). Four specimens were tested in this study. The first three (specimens 1,2 and 3) were built of the connection detail 1, and the last one (specimen 4) of the connection detail 2.

3.2 Preliminary Tests

In order to determine physical properties of the old steel members and to find the material characteristics of the rivets, a series of preliminary tests were conducted. Description of these tests follows.

3.2.1 Tensile and Weldability Tests of the Steel

A series of tests were conducted. In the first two tests, the objective was to determine the stress-strain relationship of the existing steel, while in the third test, weldability of that steel was to be established. Therefore, three coupons of steel were prepared; Two were taken from the flange (at its quarter width) and one from the web (at its quarter height) of a typical beam. All of the coupons were machined to a standard size in accordance with ASTM E8. The specimen used for weldability test was also cut at the middle, machined, and re-joined by welding (Fig. 3.2). For the simple tensile tests, each specimen was put in the testing machine and loaded until it failed.

For the weldability test the coupon was groove welded with E70 electrodes at its middle using a double bevel welded joint configuration. However, when tested, this specimen failed through the weld because of poor weld quality and incomplete penetration. Therefore, the same specimen was welded again, this time using a full penetration grove weld of double v joint configuration, and better quality control. Then, this specimen was tested assuming it to be the continuation of the prior test. It failed in a ductile manner at a distance away from the welding zone, confirming the weldability of the base material.

The result of the two tensile tests indicated that the specimens are of a mild steel with average yield point of F_y=225 MPa, and average tensile strength of F_u=400 MPa. Stress-strain relationship for the three tests are shown in Fig. 3.3.

3.2.2 Rivet Tensile Test

In determining the tensile strength and stress of the rivet any test procedure which causes changes in property of the rivets must be avoided. Therefore, it was elected not to remove rivets from the connections and to conduct a test on a selected rivet in an existing connection. Therefore, another connection, similar to those used for the specimens, was taken from the same steel frame and one rivet with its connected plates was isolated and cut out. Then two large solid steel bars, machined to have half-spherical voids at their end, were placed on each side of the specimen, covering but having no contact with the rivet heads. The bars were then welded to the plates. In this manner, the tensile load is transferred through the surrounding plates to the head of the rivets, with the plates pulling away the heads of the rivet. Drawing of this specimen is shown in Fig.3.4.

A tensile strength of 162 KN was obtained. At first, this tensile capacity of the rivet appeared to be higher than expected when compared to the values reported in the existing literature (Ketchum 1932). However, in the initial calculation of the expected rivet tensile capacity, the nominal diameter (3/4 inch) of the rivet was used, as deducted from rivet head diameters (Kulak

et al. 1987), instead of the hole diameter (13/16 inch). Indeed, when driving a hot rivet, the rivet steel is sufficiently soft and malleable to deform and fill its hole; consequently the diameter of the rivet changes to that of the hole. Taking this correction into account, yield and tensile stresses of the rivet of F_y=258 MPa and F_u=483 MPa were obtained respectively, and the rivet failed in a very ductile manner. The resulting stress-strain diagram is shown in Fig.3.5, and is comparable to that typically obtained for ASTM A502 grade 1 rivets (Kulak et al. 1987).

3.2.3 Rivet Shear Tests

Again, to avoid testing procedures which would change the property of the rivet, another part of connection having four plates connected by rivets was deemed adequate for a double-shear test on a single isolated rivet and plates cut-out sub-assembly. To allow insertion into an uniaxial testing machine, other pieces of steel plates had to be welded (as shown in Fig.3.6) on each side of the specimen. The specimen was then loaded until failure occurred. Test results showed a rivet ultimate shear capacity of 96 KN, and corresponding stress of F_v=288 MPa (based on the rivet hole diameter). This reflects a shear to tensile capacity ratio of 0.6 which is less than the average value of 0.75 reported in the existing literature (Kulak et al. 1987). Distortion of the specimen after failure indicated that the measured shear capacity could have been affected by combined state of shear and tension. Stress-strain relationship for this test is shown in Fig.3.7.

3.3 Preparation of the Specimens

3.3.1 General

Experimental set-ups used to investigate the cyclic behaviour of beam-to-column joints vary in configuration between two philosophies. At one end of the spectrum, a connection is isolated, for example by connecting a member to a very rigid and strong supporting structure, and behaviour of this connection is treated individually. At the other extreme, joint behaviour is regarded as the combined behaviour of a connection as a whole, including all contributions to

performance, such as deformations in panel zone of the column and of the column flanges. Since in a building subjected to lateral loads, connections, beams and columns of the structural frame simultaneously undergo cyclic loads, it seems that the second method is more rational. However, the problem with the second method is that a very large number of tests would be needed to obtain results directly applicable to other joints having the same type of connection but different interaction of elements, such as panel zone. Thus here too, the first method appears to be more efficient and became the adopted approach as much as possible for all the experiments of this study. Thus, the test results are not intended to include effect of the panel zone in the columns, or other case-specific failure modes of columns and beams which could detract from the main scope of work.

Although in this study the connections were tested with their actual beams and columns, the effect of column behaviour on the results was minimized by applying moment to the connection on both sides of the columns, in a symmetric manner, using the beams as a double cantilever for this purpose. For the specimen configurations selected, the beams themselves were not susceptible to any undesirable failure modes in their as-is condition.

Moments at the connections can be created by applying a point load on the beams at a distance from the column face. Estimate of the moment capacity of all connections to be investigated revealed that the needed length of the cantilever beam exceeded that on the existing beam-to-column connections in their "as-received" condition. Therefore, an extension arm was connected to each beam. In order to save time and efforts, the two extension arms and the beams of the connections were cut to a pre-determined length and bolt holes were drilled at a pre-set configuration so that the extension arms could be easily removed and reused for testing other specimens. The extension arms were structural shapes identical to the beams present in the connections to be tested as they were taken from an identical frame in the same building. They were connected to the beams by using web and flange splices and high strength bolts. The fasteners and splice plates were designed to resist the maximum expected shear and moment that would be developed at that section during the experiments. To minimize slippage of the bolts inside the holes of the splice, clearance between the holes and high strength bolts was as low as

0.79 mm (1/32 inch).

In the test set-up, the point loads applied to the beams are in fact reaction forces resulting from large size bolts anchored to the floor, as will be shown later. Other than the point loads, acting perpendicularly to the longitudinal axes of the beams, the presence of any other forces, such as friction at the supports, is not desirable. Therefore, a hole was flame-cut in the web of each extension beam and a machined piece of cold rolled steel with a slotted hole was welded onto these webs to provide a fully hinged condition at the reaction points. The hole was purposely made slotted, in order to avoid developing axial forces in the beam when the distance between the specimen and the hinge supports slightly changes due to rigid-body rotation of the beams about an eccentric connection contact point during the tests.

The role of the columns in all the specimens, as described later in Sec.3.4, was mainly to transfer load from the hydraulic jacks to the specimens; therefore, they are working in compression. Thus, to avoid buckling, the columns were cut to a short length. Also, to prevent specimens from lifting in the direction perpendicular to the floor, under a possible shear component of the axial force from the hydraulic jacks, a pair of slotted holes were provided at the column web; a threaded rod was passed through each hole and anchored to the floor to provide a lateral bracing system. The detail of this can be found in Fig.3.8 of the set-up.

As mentioned in Section 3.1, two different connections details were encountered in the specimens. The summarized description of the specimens for each each experiment is given in Table 3.1. The connection detail 1 exist in specimen 1, 2, 3 and the connection detail 2 is only in specimen 4. For each specimen, based on knowledge of the steel and rivet properties as obtained from the preliminary tests reported earlier, and using ultimate resistance models and/or simple Limit States Design concepts for structural steel (Canadian Institute of Steel Construction, 1991) but omitting the performance factor ϕ, the moment capacity of the connections was calculated for a number of possible failure modes to provide an assessment of the adequacy of existing engineering procedures in predicting the ultimate strength of these connections, while providing useful information for design of the set-up (details are given in Appendix A). These

results are summarized in Tables 3.2 to 3.5 for specimen 1 and 4. These are best understood by referring to Fig 3.1 showing the connection details 1 and 2. These specimens are reviewed in details in the following sections.

3.3.2 Specimen 1

Specimen 1, made of connection detail 1, was used to investigate the cyclic behaviour of the connection in a condition identical to that found in the actual building. However, calculations showed that, considering the inherent uncertainty of experimental work, the column's flanges and web could fail or undergo plastic deformations prior to connection failure. Therefore, to conduct the experiment without risking failure in the column, web stiffeners were designed, built and welded to the flange and the web of the column. Besides this, the connection itself was not altered in any way.

The specimen's connection and instrumentation is illustrated in Fig.3.9. Detail of this instrumentations are presented in Sec.3.5.

3.3.3 Specimen 2

As will be further explained in the chapter on test results, specimen 1 failed due to shear failure of the one of the rivets which connect the beam bottom flange to its associated seat angles. Since the replacement of a few judiciously selected rivets is a very simple retrofit procedure, another test was conducted to investigate the changes in behaviour and failure mode which would occur in connection detail 1 when retrofitted by simply replacing the few rivets that were expected to fail in shear with high strength bolts. Therefore, specimen 2 is simply identical to specimen 1 with the difference that four rivets have been replaced with high strength bolts. The connection with the replaced fasteners is shown in Fig. 3.10. No other changes were made in this connection and the same instruments, checked to be still operational and reliable, were re-usable.

3.3.4 Specimen 3

Retrofitting of the existing structures remains, to this day, more an art than science. Many retrofit strategies are proposed in the existing literature (FEMA, 1992), but these are mostly provided for guidance. The best strategies will vary depending on the circumstances and conditions pertaining to each particular project. A commonly recommended procedure is the addition of new structural braced or rigid steel frames in a existing building. This approach is well established, effective, and conventional, but could be very costly, since in most cases new foundations and floor diaphragm reinforcements may be needed to accommodate the new load-paths not compatible with the original one. Moreover, this approach entirely neglects the potential contribution to lateral load resistance of the existing structure, and in some cases where very rigid new structural elements are introduced in the structure, overwhelms it. This may be unavoidable when the existing structure is of a brittle constitution (e.g. unreinforced masonry or non-ductile concrete), but it could be very conservative when a steel structure is already present. Moreover, current intentionally accepted preservation goals for buildings of heritage value also require that a retrofitting techniques be as little intrusive as possible, and even fully reversible to allow the future integration of new and disruptive retrofitting techniques if ever developed in the future. A solution which can more harmoniously be integrated into the existing fabric of a building would help achieving these goals.

In answer to such concerns, particularly that of making efficient use of the already existing steel structure, braced frames are not necessarily an ideal solution, particularly in regions exposed to medium and small seismic risk. Bracing a few selected existing bays may require considerable reinforcement of the beams and columns of the frames never intended to carry large axial forces and again new foundations and diaphragm strengthening, at great disturbance to the occupants if the retrofits are to accomplished while the building remains in service. Even more difficulties may be arise in strengthening, of these members if they are not of weldable steel.

Thus, alternative retrofitting methods are welcome and specimen 3 is used to investigate the effectiveness of one such concepts: the local reinforcing of individual beam-to-column by adding knee-braces. In this method, retrofitting activities would be localized and performed sequentially throughout the building, causing minimum disturbance to occupants. Knee-braces could also be easily detailed for the case of non-weldable steel structures. It would also allow seismically-induced hysteretic energy dissipation to be uniformly distributed throughout all the frame joints. Another advantage of this method is that knee braces are inexpensive structural element and easily replaceable if inelastically deformed, although even this could be avoided if used with frictional type of fasteners (Tremblay and Stiemer 1993, Grigorian et al. 1992). The drawback of such a system is its potential intrusiveness at floor levels. However, as heavy non-structural partition walls in old buildings are often located above the beams, knee braces could be hidden in these walls, those intruding with door-ways or other passages being simply omitted.

Thus in this study knee braces were designed as retrofit for the previously failed specimen 2 to investigate the possible improvement in cyclic behaviour of this type of steel joints, when retrofitted, compared to performance of the original connection.

In the design of the braces, the objective is to maximize the energy dissipation of the knee bracing system. This desired performance must be achieved within the practical constraints normally encountered when operating on actual buildings. Some of these are described following.

a) Braces must be long enough to be connected properly to both beams and its adjacent column (i.e. workability condition). In other words, there should be enough space available for the required welding, gusset plates, etc., at both ends of the brace. On the other hand, if the braces are too long, a larger area of building walls will need to be removed for connecting knee braces to the building steel frame, and/or the braces will be more intrusive. Judgment must be exercised to determine a reasonable range of brace lengths.

b) Applied moments on knee braces connecting a beam to a column causes tension in one brace and compression in the other. Obviously, the capacity and energy absorption capacity of a member in compression is a function of its effective length. Therefore, to maximize capacity and energy absorbtion of the compressive member, its slenderness ratio should be kept as low as possible. In other words, the C_r/T_r ratio for the member must be as close as possible to 1.0.

c) To have an efficient energy dissipating knee bracing system, it is desirable to have all plastic hinges in the buckling compression member form in the member itself, not in the gusset plates or other parts. This allows the dissipation of more hysteretic energy than if out-of-plane buckling occurred with hinging in the gusset plate, and also protects walls against out-of-plane induced damage when braces are embedded in walls. Therefore, bracing sections are chosen such that buckling of the member occurs in the plane of the beam and column. Also, the chosen section should be checked to avoid local buckling or torsional buckling prior to formation of the hinges in the compression member.

d) The braces, in a practical situation, should act as a weak link, i.e. they should yield and dissipate energy. If overly strong braces are used, there would be risk of forming plastic hinges in the connected columns.

Considering the above requirements and assumptions, the knee braces were chosen to be standard double angles 25x25x6.4 mm (1"x1"x1/4"). The knee braces were then designed to develop their failure mechanism when subjected to a moment of 189 kN·m, which is comparable to the range of failure loads for the other connections. They were also checked to be not susceptible to individual buckling and torsional buckling. Then, the required spacing of batten plates, the size of gusset plate and welds were determined. Design calculation for the bracing are in Appendix B.

Obviously, since the previously damaged specimen 2 was to be reused for specimen 3, before installing the knee braces on the specimen, the beams and the columns were realigned to their original right angle position. For efficiency and expediency the knee braces were assembled and

welded to the beams and the column instead of bolted. Bolt holes in bracing members is highly undesirable as it would reduce the section area of the members in tension, specially for small size sections similar to those used in this test, and would cause the section to fail at the net area rather than by yielding over the entire member length. Also, for the compressive knee brace, the end plastic hinges could also occur at the net section with lesser plastic moment capacity than the other sections. Although, on site welding is not encouraged in Canada, the welds on the specimen were performed using standard SMAW (shield metal arc welding) with E70 electrodes, and behaved satisfactory. It is noteworthy that an alternative welded detail but with bolted connections to the beams and columns could easily be designed, allowing all welded operations to be done in shop. This detail would be also useful for non-weldable existing steel beams and columns.

For this specimen additional strain gages were attached to different parts of the bracing angles. The specimen and its instruments are shown in Fig. 3.11.

3.3.5 Specimen 4

Whenever an existing steel structure is found to be of a weldable steel type, it appears logical to attempt enhancing at the cyclic behaviour of the connection by welding. Converting a semi-rigid connection into a fully rigid one seems to be very ideal. However, this approach may have some shortcomings. The weld preparation is difficult (back-up plates, cleanup, etc.), the amount of deposited material is considerable, particularly in the gap almost always present between the column face and end of the beam, the working area is congested and the weld-design can be very complex, in some cases nearly impossible welding, for example where columns are made of built-up sections, as is the case for specimen 4. Moreover, since the columns in old steel buildings were never designed to resist earthquake and are relatively more flexible than the beams, assuming that the conversion to fully fixity was possible, it would create a very dangerous situation by inducing plastic hinges in the column (weak column/strong beam failure mode).

Yet, based on the better understanding of the cyclic performance of semi-rigid connection that resulted from testing the previous specimens, a more judicious application of welding technique is possible which could greatly enhance the performance of the existing connections, by eliminating known weaknesses while keeping those inherently good energy dissipating mechanisms already present. It is noteworthy that in the new proposed "selective welding" approach to the retrofit of semi-rigid connections, weld preparation is limited to the cleaning of surfaces to be welded. It is also believed that the method to improve the behaviour of these connections is easily applicable to the connections of existing buildings having similar type of connections.

The objective of the proposed retrofit, is to minimise the amount of required changes while increasing the connection energy dissipation and capacity. To achieve this in a short time and at low costs, it is important to minimize any changes or replacements to the main parts of the connection. For this new specimen,having the beam-to-column connection detail 2, the connection was retrofitted (i.e. not tested in its existing condition) by replacing only four rivets with high strength bolts and performing selective welding; Calculations are given in Appendix A. To prepare specimen 4, the four rivets connecting the top angles to the column flange were first removed and replaced with high strength bolts. To achieve this, one head of head of each rivet was ground, then from the headless side of the rivets the remaining part of the rivets were hammered out of the holes. Finally high strength bolts, of the same 20 mm (3/4 inch) diameter as the rivets were installed and tightened. To accomplish selective welding on some parts of top and bottom angles as well as stiffener angles, it was necessary to access the stiffened seat angles, therefore the column concrete cover was removed. Then, as shown in Fig. 3.12, the leg of the top and bottom angles in contact with the beam flange were welded, as was part of the stiffener of the seat angles. Explanations of the logic behind this selective retrofit approach are given in the next chapters as they are best understood in the perspective of test results for the first specimen.

It is noteworthy that columns were also shorted for the same reason indicated for the first specimen. However neither holes nor threaded rods were needed as lateral bracing here, since

the concrete cover on this specimen added sufficient weight to overcome the possible lifting forces. After positioning the specimen, the instruments were installed as shown in Fig. 3.13

3.4 Set-up Description

For the purpose of this study a new set-up was designed to perform the experiments horizontally. It was found to be easier to design a simpler reaction set-up and use the strong floor (thickness of 915 mm) to support the specimens, set-up and loading system, rather than using a more complex reaction frame.

The set-up mainly consists of four supports anchored to the floor. Two of those provide hinge supports for the beams and each of the other two is intended to support one hydraulic jack loading the specimens. As described in Section 3.3.1, the moment for each connection is obtained by cantilever action of each beam. Due to symmetry of the specimens, the beams work as a double cantilever system connected to the middle column. Therefore, the load from the jacks applied to the end of the column is balanced by reactions at the end of each cantilever which consequently produces moments at the connections to be tested. To simplify detailing of the test set-up and reaction supports, one way acting hydraulic jacks were chosen. To be able to conduct cyclic tests, two jacks (one at each column end) with their support were provided, to be used alternatively.

As shown in Fig. 3.8 a typical hydraulic jack reaction support is made of a short stub column, standing inside a channel. The channel itself is connected to the floor by a 70mm diameter bolt inserted in one of the story floor holes and fixed in place by nuts.

When applying load to the end of the columns using the hydraulic jacks, special care was taken to reduce the possibility of any shear or load eccentricity with respect to the column axis. To achieve this, two steel plates with notches sandwiching a steel bar were placed between each hydraulic jack and its support to act as a hinge. Then, the position of each jack and hinge was

horizontally and vertically adjusted to aligned the jack ram with the axis of the column. To hold the jacks in-plane, a pair of threaded rods and nuts were used to connect the jacks to their supports.

Beam supports, which act as nearly perfect hinge supports, each consists of a 70mm diameter bolt installed through a floor hole. Each bolts has four nuts. Two nuts were used to anchor the bolts to the floor, one was located underneath the beam web to support the weight of the beam and keep the reaction point at a certain level, and the last one was placed on the beam web to both provide a lateral support for the beam and prevent it from uplifting. To minimize friction between the bolt and beam at the joints and protect the bolts threads, special rings with inside threads were made for each bolt and put at the contact points.

Since the specimens were to be tested horizontally, two roller supports were built and located underneath the specimens on the floor so that the specimens could move back and forth without developing friction forces.

3.5. Instrumentation

In each experiment a variety of instruments were installed to measure and control behaviour of different components of the connections under loading. Measurements were to be taken on load, rotation, displacement and strain at a number of points. Each of these are reviewed following.

3.5.1 Measuring Angles of Rotation

To establish moment-rotation relationship for the connections in each experiments, angle of rotation between the axes of the beam and the column of a connection must be measured. Because each specimen contains two connections,one each side of its column, the angle of rotation of each was measured separately. For this purpose four Linear Voltage Displacement Transducers (LVDTs) were used. The LVDTs used are of the model SGDT-5000, made by Inter

Technology, with range of 125 mm and accuracy of 0.1 mm. Two LVDTs were installed in each side of the connections as shown in Fig. 3.9, such that distance between two fixed points on the column and their corresponding points on an angle clamped to the beams were measured by the LVDTs. Therefore, having values of displacements and position of the LVDTs, the following equations were used to determine the connections rotation on each side of the column;

$$\theta_R = \frac{(d_1 - d_2)}{(h + h_1 + h_2)} \tag{3.1}$$

$$\theta_L = \frac{(d_3 - d_4)}{(h + h_3 + h_4)} \tag{3.2}$$

where $d_1, d_2, d_3, d_4, h_1, h_2, h_3$ and h_4 are the displacements and distances graphically defined in Fig. 3.9. The LVDTs on each side of the column were positioned as far as reasonably possible from each other to obtain maximum accuracy in determining the rotations.

3.5.2 Measuring Strains

Strain and stress levels at number of selected locations on the specimens were measured using Micro-Measurements strain gages model EP-08-250BG-120 which have a strain range of 4% and accuracy of $3.8\ 10^{-6}$. The number of strain gages and their positions on each specimen varies. The position of strain gages for each specimen are shown in Figs. 3.9, 3.11 and 3.13.

3.5.2 Measuring Displacements and Elongations

One LVDT was positioned to measure deformation of the column flange at the connection point of the top angle. . For specimen 3, in which column flange were almost under no stresses, this LVDT was not used.

To measure force or stress level in a connection fastener, one way is to measure strain inside the fastener and then determine stress by using stress-strain relationship of the fastener material. But to apply this method to the rivets of the specimen's connections, difficulty arose due to the fact that there was no access to the rivet shanks, thus no way to attach any strain gages. Therefore, clip gages were used to measure strain in the rivets. Special clip gages were designed for this purpose. A review of the existing literature indicates that this innovative use of clip gages, i.e. to measure strain in the rivets, has not been attempted before. The method is based on measuring elongation of the rivets under stress and comparing change in elongation with the original length of the rivet, consequently determining the value of strain. Since the two heads of each rivet move with respect to each other as the rivet shank elongates, this elongation in the shank can be equated to the change in distance between the two heads as measured by the clip gages. An example of this measurement procedure is shown in Fig. 3.14 for a rivet.

The clip gage itself resembles a portal frame in which a strain gage is attached to the beam top. If the columns in this portal are chosen to be much stiffer than the beam, they behave rigidly compared to the beam, any changes in distance between the supports result in changes in curvature and, consequently, variation of strain at the top fibre of the beam. If the stresses in the beam remain within the elastic range, a linear relationship can be developed between the change in the distance and strain at the beam top fibre. Therefore, utilizing very thin steel stripe and some other attachments, a number of these clip gages were produced in sizes such that they act linearly within the expected range of measurements. Each gage was separately calibrated and attached to the head of selected rivets.

3.5.3 Measuring Loads

The load applied to each specimen was provided by hydraulic jacks. To determine the load, knowing the effective area of the piston of the jacks, it was only necessary to measure the pressure in each jack and multiply this value by the effective area. For this purpose, one pressure transducer was connected to each jack. The type of Inter Technology pressure transducers used

in the experiments have a range of 69 MPa and accuracy of $3.5x10^{-3}$ Mpa.

3.6 Control and Recording Measurements

A data acquisition system Model 200 made by Scimetric Instruments was used. All data was recorded automatically at an interval of five seconds. The system could also continuously report the measured moments and rotations during the tests to determine the progress of the experiments.

Oil pressure in the hydraulic jacks in the set-up were supplied by electric pumps and was monitored during the tests. Pressure inside the jacks was controlled by manually switching the oil pumps.

To achieve cyclic tests with the existing set-up, the hydraulic jacks were used alternatively. Every loading stage was conducted very gradually to allow close monitoring. Therefore, the oil pump had to be turned on and off a considerable number of times. In the process, relaxation of the specimen occurred causing the pressure to fluctuate. At every cycle, the loading continued until the measured rotation at the connections was found to have reached pre-determined or other judged acceptable values, then the specimen was unloaded. To unload, pressure in the jacks could be released by opening the oil valve. This action causes sudden drop in the pressure and only a few data points of unloading could be recorded. The next half cycle was conducted in the same manner using the other jack.

CHAPTER 4

Experimental Results

Description of the experiments conducted with Specimens 1 to 4, important observations, hysteretic curves and the measured data are presented in the following sections. Results of additional but secondary measurements made during the tests are provided in Appendix C. In preparing all figures and results, the sign convention illustrated in Fig.4.1 was used. According to this convention, positive moments apply tensile force on top angles and compressive force on seat angles, while negative moments produce tension in the seat angles and compression in top angles. In each experiment, an enormous number of data points (around 4000) was recorded, owing to the short time interval of data recording and relatively long duration of each test (almost 6 hours). Therefore, a computer program was used to smoothen the original data and drastically reduce the numbers of data points to approximately 130 to 400 depending on the case. For comparison, an example of the results obtained by using the data reduction program versus the original data is given in Appendix D.

The M-θ relationship of the connections is the most important information obtained by these tests. To allow easy cross-reference between all plots, all other data is expressed as a function of moments. Due to importance of moment values, they were measured by two independent methods. One method relied on using values of the measured load, i.e. values from the pressure transducers times the area of piston of the hydraulic jacks multiplied by lever arm (distance between the hinge support and the column face). The other method was by measuring strains at two different points on the beam flanges at a across-section near the connections and using the linear moment-strain relationship of beams and statics to obtain the corresponding moment applied to the connections. Comparison of the results from these measurements showed that the moments calculated based on the first method correlated well with those from the second method,

but were generally more consistent and accurate. Therefore, they were used in plotting the results.

4.1 Experiment 1

The M-θ relationship of the two connections obtained from the test results of Specimen 1 are shown in Figs. 4.2 and 4.3. Due to similarity of the connections, the results of average rotation are also plotted and shown in Fig. 4.4. In these figures, severe pinching of the hysteretic loops, even in the early stages of loading, is clearly observed. This specimen experienced a maximum positive moment (M^{+}_{max}) of 81.1 kN·m and corresponding maximum rotation (θ^{+}_{max}) of 21.28×10^{-3} radian (all values being the average for the connections on both sides of the column). After 6 cycles, failure occurred due to shear failure of a rivet in the seat angle at M^{-}_{max} of -139 kN·m, corresponding to rotation (θ^{-}_{max}) of -27.9×10^{-3} radian.

A first elastic load cycle was conducted by applying load to produce positive bending until M= 17.5 kN·m, corresponding to $\theta = 3.26 \times 10^{-3}$ radian, then load was reversed until M= -24 kN·m, corresponding to $\theta = -3.69 \times 10^{-3}$ radian. Pinching and non-linearity of the M-θ were observed while the top and seat angles remained elastic. For the second elastic cycle, the specimen was loaded in positive bending until M= 29 kN·m, corresponding to $\theta = 4 \times 10^{-3}$ radian. Small gaps between the heel of top angles and column face became visible. Then, the load was reversed until M= -42.6 kN·m and rotation reached $\theta = -3.77 \times 10^{-3}$ radian; while the gaps at the top totally closed, yet no gap was observed in the seat angles. Non-linearity and pinching in M-θ curve was observed again at the zero-crossing, but some linearity was noticed at higher values of moment.

In the third cycle, load was gradually applied in positive bending until M= 52 kN·m, corresponding to $\theta = 6.15 \times 10^{-3}$ radian, and yielding was noticed. This point roughly defines the positive yielding rotation (θ_y). As the moment-strain relationships (Figs. 4.5 and 4.6) indicate, strain gages (10 and 11) located on the vertical legs of the top angles confirmed that the onset

of yielding occurred at approximately M= 40 kN·m. Size of the gaps in the top angles increased and top angle deformations were more pronounced. The specimen was then loaded in negative bending until moment reached M= -62.7 kN·m, corresponding to $\theta = -4.42 \times 10^{-3}$ radian. Small gaps between the seat angles and the column face became visible but still there was no sign of yielding. Also, the gaps between the heel and column face in the top angles closed but new gaps between the toe of the vertical legs of the top angles and the column face was noticed. In the fourth cycle, the specimen was loaded until moment reached M=61 kN·m, corresponding to rotation of $\theta = 8.66 \times 10^{-3}$ radian. It was observed that plastic hinges formed near the rivet heads in the vertical legs and adjacent to the fillet of the horizontal legs of the top angles, resulting in even larger gaps. This was also accompanied by a change in slope of the M-θ relatively at a moment of roughly 55 kN·m. In negative bending, the specimen was loaded until M= -90.8 kN·m and rotation of $\theta = -9.3 \times 10^{-3}$ were obtained. Clear inelastic M-θ behaviour was observed and deformations in the legs of seat angles were noticed, indicating formation of hinges adjacent to the fillet of the legs. The gaps in the seat angles also became more visible and a negative yielding rotation of nearly -6×10^{-3} radian was noted.

To better understand and visually observe deformations of the seat angles and stiffener angles, the specimen was unloaded and immediately reloaded in negative bending until moment reached M= -100.1 kN·m, developing $\theta = -11.87 \times 10^{-3}$ radian, almost twice as much as the yielding rotation. Deformation of the seat angles became more pronounced, and the development of a (still very small) gap between the back-to-back legs of the stiffener double-angles was also observed on both sides, indicating evidence of local buckling of these stiffeners. Strain gages located on the stiffener angles also detected the yielding and formation of hinge mechanism in the stiffener angles at the level of the second row of the rivets under seat angles. The clip gage d_{15} (identified in Fig. 3.9, showing the instruments for the first specimen) detected tensile yielding of the first row of rivets under seat angles at around -95 kN·m.

For the fifth cycle the specimen was loaded in positive bending until rotation reached the value of $\theta = 15.68 \times 10^{-3}$ radian, almost two and half as much as the positive yielding rotation. This corresponded to a moment of M= 76.4 kN·m. As the load increased in the positive bending, the

top angles deformed, their gaps opened up, and gradually the gap between the seat angle and column face closed. However, deformation and yielding of the stiffener angles remained unchanged and did not seem to be recoverable. Therefore, some gaps between the stiffener angles and seat angles were noticed. At M= 65 kN·m, tensile yielding of the rivets in the top angles was observed and detected by the clip gage located on one of those rivets (clip gage d_{12} as identified in Fig. 3.9). Upon unloading, moment reached M= -115 kN·m, corresponding to a rotation of $\theta = -20 \times 10^{-3}$, more than three times as much as the negative yielding rotation. As the negative moment increased, the gaps between the heel of the top angles closed. By this time, as the vertical leg of the top angle has adopted a somewhat curve shape, convex away from the face of the column, under negative moment the gaps above and below the rivets in these top angles respectively opened and closed. This aspect of the top angle's behaviour is shown in Fig. 4.7. Also, by the time the negative peak moment was attained, the gaps between the seat angles heel and column face re-appeared while the other gaps between the stiffener angles and vertical leg of the seat angles became smaller. Gradually, the vertical leg of the seat angles touched the stiffener angles and both moved forward.

The specimen was loaded for sixth cycle, first in positive bending, until large deformations of the rivets in the top angles indicated signs of impending tensile failure. Loading was stopped at $M^{+}_{max} = 81.1$ kN·m, for a rotation of $\theta^{+}_{max} = 21.28 \times 10^{-3}$ radian. The gaps between the heel and column face and the top angles, corresponding to the highest positive moment, were 8.2 mm and 10.2 mm respectively for the right and left side connections. Maximum column flange deformations due to tensile force from the rivets in the top angle were measured to be only 0.4 mm. The severe top angle deformations at the maximum positive moment are well illustrated in Fig. 4.8. Then, the specimen was unloaded; resulting residual rotation of $\theta = 15 \times 10^{-3}$ radian and residual gap openings of 6.2 mm (right side) and 8.0 mm (left side) were measured in the top angles. Negative moment was applied to the specimen until failure occurred. Shear failure of one rivet located in the seat angle of the left side connection occurred when the moment reached $M^{-}_{max} = -139$ kN·m, corresponding to rotation of $\theta^{-}_{max} = -27.9 \times 10^{-3}$ radian. The maximum gap sizes, measured prior to failure, between the seat angles and the column face on the right and left side were respectively 10.5 mm and 12.5 mm. The shear failure of the rivet and residual

deformation of the seat angle and stiffener angles are shown in Fig. 4.9.

4.2 Experiment 2

To conduct the test on Specimen 2, after replacing the rivets with the high strength bolts, all the instruments were checked and all of the measurement readings were re-zeroed. The test mainly aimed at investigating the effect of replacing rivets and the behaviour of the stiffened seat angles under higher negative moment than that reached in the first experiment. Positive moments were also applied to the connections to see effect of reversed cyclic loading on the seat connections, but to conduct this test on the specimen, having already highly deformed rivets and angles in the top part of the connections, and to prevent the possible failure in the top angles, the positive moment was kept below 47 kN·m. In this test, fairly high negative moments were applied to develop considerable rotations and deformation of the seat and stiffener angles.

The M-θ relationship of the connections in both sides of the column are shown in Fig. 4.10 and 4.11. The average results of the two plots is also given in Fig. 4.12. Pinching of the hysteretic loops in these figures is similar to that observed during the first experiment. The connections resisted maximum moment (M^-_{max}) of -160 kN·m, corresponding to a rotation (θ^-_{max}) of -46×10^{-3} radian. During the third cycle, the connection located on the right side failed due to bearing failure adjacent to the hole of one of the high strength bolts in the seat angle.

First cycle started by applying loads to produce negative bending. Non-linearity was observed in the M-θ curve in the early stages of loading. The seat angles deformations were clearly noticable and increased until they came into contact with the stiffener angles. Yielding was noticed at M= -125 kN·m and rotation of $\theta= -16\times10^{-3}$. Yielding of the rivets in tension located immediately under seat angles was also detected by clip gages, d_{14} and d_{15} (positioned on the rivets as shown in Fig. 3.9). The load was increased until M= -141 kN·m, corresponding to rotation of $\theta= -24.6\times10^{-3}$. Strain gages 16 and 17 (located on the stiffener angles) also indicated yielding. Formation of a plastic hinge mechanism occurred in the stiffener angles at the same

position as in the first experiment, when the moment reached M= -135 kN·m. (Figs. 4.13 and 4.14). Local buckling in the leg of the back-to-back leg of stiffener angles was also clearly noticed, as shown in Fig. 4.15. At this load level, even yielding of the second row of the rivets under the seat angles was detected by clip gage d_{24} (positioned on the rivet under d_{15} as identified in Fig. 3.9). The specimen was then unloaded and gradually loaded in positive bending. Similarly to what happened in the previous test, as the positive moments increased, the residual deformation of the stiffener angles remained unchanged but the seat angles moved back toward the column face; i.e. the size of the gaps between the seat angles and column reduced while that of other gaps between the stiffeners and the seat angles increased. The load was increased until positive moments reached M= 42.2 kN·m, developing a rotation of $\theta = 22.3 \times 10^{-3}$. Thus, the gaps between the seat angles and the column face were not completely closed.

In the second cycle, the specimen was loaded in negative bending until M= -155.1 kN·m which corresponded to rotation of $\theta = -34 \times 10^{-3}$ radian. During the course of re-loading both connections, as for the first cycle, the seat angles gradually moved forward until they touched the stiffener angles, closing the gap between the seat angles and stiffener angles. From then on, both seat angles and stiffener angles moved forward. Behaviour was similar to that observed in the previous cycle, except that larger and more pronounced deformations were noticed. In addition, inelastic deformations and flaking of the mill scales were observed adjacent to the holes of high strength bolts and at the edge of the seat angle legs, indicating the onset of excessive bearing (Fig. 4.16). In positive flexure, the specimen was loaded to M= 47 kN·m, corresponding to rotation of $\theta = 21.6 \times 10^{-3}$. Behaviour was again similar to that of the previous cycle.

In the third cycle, the specimen was loaded until bearing failure occurred adjacent to the hole of the high strength bolts (as shown in Fig. 4.17) at M= -160 kN·m, and a rotation of $\theta = -44.5 \times 10^{-3}$. Fig. 4.18 shows the severe deformation in the stiffener and seat angles; The size of the gaps between the column face and the seat angles prior to failure were 13.2 mm on the right side and 8.5 mm on the left side.

4.3. Experiment 3

The M-θ relationship results for the knee braced Specimen 3, for both sides of the column, are given in Figs. 4.19 and 4.20. Also, the M-θ relationship of the average values is plotted in Fig. 4.21. It is observed that the hysteretic loops are not pinched in the small range of rotation, but slightly pinched at larger rotations. The positive moment convention used for the previous experiments is also used here, i.e. positive moments is assumed to cause tension in the top knee braces and compression in the bottom knee braces. The specimen in this test reached maximum moment (M_{max}) of 197 kN·m and developed maximum rotation (θ_{max}) of 29.8×10^{-3} radian. The experiment ended after five cycles, when severe buckling deformations of the knee braces and large rotations were observed and continuation of the test would likely not have generated any new information.

The experiment started with a half cycle in the elastic range to a peak load of M= -103 kN·m and linearity was confirmed. Then the specimen was loaded in positive bending until member 4 (located in the bottom-left corner of the joint) buckled, at M= 184 kN·m, developing positive yielding rotation of $\theta = 5.1 \times 10^{-3}$ radian (Fig. 4.22). This was also confirmed by strain gages 17 and 19, both located at the middle of this member, as buckling progressed. The load dropped slightly while the rotation of the buckled side of the specimen increased to $\theta = 6.45 \times 10^{-3}$.

For the second cycle the moment was again first applied in negative flexure. As the applied load increased, tension in the previously buckled member also increased and caused the member to straighten up. Loading continued until member 2 (located in the top-left corner of the joint) buckled, as shown in Fig. 4.23. The measured load at that level was M= -170 kN·m which corresponded to negative yielding rotation of $\theta = -4.5 \times 10^{-3}$. The strain gages on this member (11 and 13, located at the middle and 15 at the end of the member) also detected post yielding strains, indicating buckling of the member. The load dropped but rotations of that left side of the specimen increased to $\theta = -6.6 \times 10^{-3}$ radian. The specimen was then unloaded and loaded in positive flexure. During this stage of loading, member 4 buckled again at about M= 90 kN·m.

When the moment reached M= 184 kN·m, strain gages (10, 12 and 11, 13, respectively at the middle of members 1 and 2) showed yielding in tension of both members 1 and 2 (top-right and top-left corners of the joint). Then, member 3 (bottom-right corner of the joint) buckled at M= 196 kN·m (Fig. 4.24), corresponding to a rotation of $\theta = 9.9 \times 10^{-3}$ radian. An increase in rotation up to $\theta = 16 \times 10^{-3}$ followed, accompanied with a drop in load.

In the third cycle, for negative flexure, member 2 buckled again at M= -100 kN·m, followed by buckling of member 1 at M= -120 kN·m. This was visually observed and confirmed by strain gages on these members (Fig. 4.25). The load increased until M= -172.6 kN·m, corresponding to a rotation of $\theta = -15.9 \times 10^{-3}$, when member 3 and 4 yielded in tension. The specimen was then loaded in positive flexure until M= 197.1 kN·m, corresponding to rotation of $\theta = 22 \times 10^{-3}$. In the fourth cycle, the specimen was similarly loaded until M= -184 kN·m, corresponding to rotation of $\theta = -24.8 \times 10^{-3}$ radian, and then until M= 197 kN·m, developing a rotation of $\theta = 25.5 \times 10^{-3}$. Finally, in the fifth cycle, the load was increased to M= -195.2 kN·m, corresponding to a maximum rotation of $\theta = -29.9 \times 10^{-3}$. The experiment was ended at this stage by unloading to zero, with a residual rotation of $\theta = 24.9 \times 10^{-3}$ radian.

Clearly, as anticipated, in every cycle, a pair of the knee braces, depending on the direction of the applied load, buckled while the other pair of knee braces yielded in tension. Under reverse loading, the buckled members straighten up and yielded in tension, while the previously yielded ones buckled. However, because of member elongations during yielding, buckling occurred progressively sooner during each subsequent cycle, and after a few cycles, all members were in a buckled state when the specimen was at its original zero-rotation position (Fig. 4.26).

4.4 Experiment 4

The M-θ relationship of the connections on both sides of the column in Specimen 4 are plotted in Fig. 4.27 and 4.28. The average values of the rotations is also plotted in Fig. 4.29. The specimen was subjected to cyclic loads up to maximum positive and negative moment of

respectively M^{+}_{max}= 74 kN·m and M^{-}_{max}= -136 kN·m . These loads respectively caused rotations of θ^{+}_{max}= 25.9x10^{-3} and θ^{-}_{max}= -38.8x10^{-3} radian. The experiment ended after 10 cycles when the applied negative moments caused relatively large inelastic deformations in the seat angles as well as formation of plastic hinges and buckling of the stiffener angles. The maximum average residual rotations were also θ= 16x10^{-3} and θ= -25x10^{-3} radian.

In the first cycle, positive moment was gradually applied until M= 43 kN·m, developing a rotation of θ= 3x10^{-3} radian, at which small amount of yielding on the curve was noticed (positive yielding rotation). As the load increased, the top angles moved slightly forward and very small gaps between the heel of the top angles and the column faces appeared. Then, reverse load was applied until M= -40.5 kN·m, accompanied with rotation of θ= -2.7x10^{-3} radian. The gaps in the top angles closed while no sign of yielding deformations in the seat angles was observed as this part of connection apparently remained elastic. The second cycle was conducted by applying moment of M= 46.3 kN·m, corresponding to rotation of θ= 4.9x10^{-3} radian, almost one and a half times yielding rotation. The specimen was then loaded in negative flexure until M= -70.8 kN·m, developing a rotation of θ= -6x10^{-3} radian (negative yielding rotation). The top angles closed again. Very small yielding in negative flexure was observed from the M-θ, but visual evidence was limited to small deformations in the seat angles and a very narrow gap between the column faces and seat angles.

A third cycle was conducted by applying moment of M= 52.3 kN·m, and corresponding to a rotation of θ= 6.8x10^{-3} radian, and reverse moment of M= -80.6 kN·m, with rotation of θ= -7.8x10^{-3} radian. Deformation of the top angles became very visible. More pronounced deformations adjacent to the fillets of the seat angles and larger gap between the seat angle and column face were noticed. In the fourth cycle, the positive moment increased until a rotation of three times the positive yielding rotation (θ= 9x10^{-3} radian) was obtained at M= 56.7 kN·m. Then in negative flexure moment increased until M= -91.85 kN·m, corresponding to rotation of θ= -10.6x10^{-3} radian. In the fifth cycle, moment reached M= 60.5 kN·m, developing rotation of θ= 12.3x10^{-3} radian. Fairly large deformations of the angle legs near the head of high strength bolts and adjacent to the fillet of the top angles were noticed as a sign of development of a

plastic hinge mechanism. At this level of load, formation of the plastic hinges in the top angles was also detected by strain gage 11 (located on the vertical leg of the top angle on the right side), as shown in Fig. 4.30. Out-of-plane deformations of vertical legs of the top angles were also noticed. Then, loading was reversed until moment reached M= -100 kN·m, developing rotation of $\theta = -14.1 \times 10^{-3}$ radian. The top angle deformations were mostly recovered and the gaps in the top closed while the heel of the seat angles clearly separated from the column face, developing plastic hinges in the legs of seat angles (Fig. 4.31). Also, small gaps between the back-to-back legs of the stiffener angles were observed, indicating onset of their local buckling.

In the sixth cycle, increasing moment to M= 63.6 kN·m and rotation to $\theta = 15.5 \times 10^{-3}$ radian, it was noticed that stiffener angles with their connected seat angles moved back toward the column until the gaps in the seat connections became very small, while deformations of the top angles and size of the gaps were more pronounced. Yet, no pinching in the hysteretic loops were observed. The specimen was then loaded in negative flexure until M= -109 kN·m, corresponding to $\theta = -17 \times 10^{-3}$ radian. The seat angles, and connected stiffener angles separated from the column faces. Slightly larger gaps also appeared between the stiffener angles. Furthermore, some separation of the column flanges from the fire-proofing concrete left inside the column was noticed, indicating local yielding deformations of the flange under tension caused by the pulling action of the rivets of the stiffener angles. The seventh cycle was conducted by applying moment of M= 68 kN·m, accompanied with a rotation of $\theta = 17.8 \times 10^{-3}$ radian. Small deformations of the column flanges under tensile force from the high strength bolts in the top angles were detected by the LVDT d_6 (Fig 3.13), which was controlling the displacement of the column flange with respect to a reference point. Also, out-of-plane deformations of the vertical leg of the top angles became more pronounced. As the negative applied load increased, gaps in the top angles closed, but deformations of the column flanges were not totally recovered. By the time moment reached M= -116 kN·m, developing rotation of $\theta = -22 \times 10^{-3}$ radian, formation of a plastic hinge mechanism in the stiffener angles, along with their local buckling, occurred near the level of the second row of the rivets under seat angles; Their yielding at about -110 kN·m was detected by strain gages 17 and 19 (identified in Fig. 3.13), located on the legs of the stiffener angles (Figs.4.32 and 4.33). On the left side, buckling of the stiffeners caused cracking

of the concrete cover which had not been completely removed (Fig. 4.34).

The eight cycle of the test was conducted by applying moment of M= 72.7 kN·m, developing a rotation of $\theta = 23 \times 10^{-3}$ radian and then reverse moment of M= -127.7 kN·m which developed a rotation of θ= -29.5 radian. In the ninth cycle with the load of M= 74 kN·m, corresponding rotation of $\theta = 25.9 \times 10^{-3}$ radian, very large deformations were produced in the top angles. Maximum size of the gaps in the top angles were measured to be 18 mm and 16 mm, respectively on the right and left side. Figs.4.35 and 4.36 show non-uniform inelastic deformations on the vertical leg and plastic hinge on the horizontal leg of the top angles at the positive peak moment of this cycle. Small column flange deformations due to concentrated load from the high strength bolts were measured to be 1.2 mm. No more load was applied to the specimen in that direction since inelastic deformations significantly enlarged the hole of the high strength bolts in the top angles undergoing major yielding; It was felt that higher loads would have caused the bolt heads to pass through these holes. In the next half cycle, the specimen was loaded in negative flexure until M= -132.6 kN·m, corresponding to rotation of $\theta = -36.1 \times 10^{-3}$ radian.

As noticed in each cycle, when the connection was subjected to positive moment, the stiffener angles and seat angles together moved back toward the column and no gap between the top part of the stiffener angles and seat angles was observed (Fig. 4.37).

The specimen was then unloaded and immediately reloaded in the same negative flexure until M= -136 kN·m, accompanied with maximum rotation of $\theta = -38.8 \times 10^{-3}$ radian. The severe deformations of parts of the stiffener angles and seat angles were observed. The gap between the seat angles and the column flanges reached 13 mm on the right side and 12 mm on the left side. Also, at this level of load, the measured column flange deformation near the rivets of the stiffener angles was about 4 mm (Fig. 4.38). Then the experiment ended by conducting a half cycle in positive flexure until M= 41 kN·m, solely to return the specimen to its original un-deformed position. It is noticed that, throughout this experiment the slope of the M-θ curve during reloading is the same as that during unloading.

Although the cyclic part of the experiment ended as described above, after very large rotations developed in the connections, for academic interest it was decided to monotonicaly subject the specimen to increasing negative moment until connection failure occurred. As shown in Figs. 4.39 and 4.40 the connection on the left side failed adjacent to the fillet of its seat angle horizontal leg after a rather extreme level of plastic deformations distributed to various parts of the connection. The measured moment correspond to the failure was -164 kN·m and rotation of -77×10^{-3} radian.

CHAPTER 5

Comparison and Analysis of the Results

5.1 Comparison of the Test Results with the Predicted Capacities

The experimental results and predicted capacity for each of the two types of connections, tested and calculated assuming different failure modes, are compared in the following sections.

5.1.1 Experiment 1

The test results for the connection detail 1 and the predicted values for first three failure modes, when positive moments are applied, are provided in Table 5.1. Since the positive moments were limited to 81 kN·m during this test, no experimental results corresponding to failure modes 4 to 9 were obtained for comparison with the predicted values.

For failure mode 1, there is a good agreement between the prediction and test values. It is noteworthy that the location of plastic hinges to calculate predicted capacity for this failure mode plays a very important role. To calculate the capacity corresponding to this hinge mechanism Kishi et al. (1990) and Lewitt et al.(1966) assumed that two hinges form in the vertical leg of the top angles connections (Figs 2.2 and 2.6) . However, the comparison of the predicted and test results together with observations show that for such a riveted connection, it seems more realistic to assume that in the vertical leg only one plastic hinge forms. Indeed, the head of the rivets in the vertical leg of the top angles are very close to the toe of the fillet in the vertical legs and allow only one hinge to form in the vertical legs of the angles. Obviously, there is another plastic hinge which forms adjacent to the fillet of the horizontal legs to create a plastic mechanism. Fig. 5.1 illustrate the top angle and location of hinges used to calculate this failure

mode. The predicted value of Table 5.1 was obtained based on the above assumptions.

The development of the failure mode 2 was prevented in this test by using stiffener plates as described earlier. However, some small deformations still occurred as a result of tensile force from the rivets since, practically, the stiffeners could not be placed exactly along the rivet axis.

The predicted value for failure mode 3 seems to be almost 18% greater than the experimental one (65 vs 80 kN·m). It was observed, during the experiment that the position of the prying force, assumed to act at the toe of the vertical leg of the top angles for the analytical method used in the prediction, changed as repeated inelastic deformation of the leg developed, particularly after a few cycles as the vertical legs of the top angles became progressively more convex away from the column, as described earlier. Since the position of the prying force (Q, in Fig.5.2) moves to a point closer to the rivet, the lever arm of the prying force becomes shorter and its value increases to satisfy statics. Consequently, this increase in the value of the prying force causes yielding of the rivets to occur at a lower load than expected.

Table 5.2 shows the experimental results and the predicted values for failure mode 1 to 5 when negative moment is applied to the connection. The predicted values are in good agreement with the test results and can be considered as reliable lower bound solutions.

Some improvement are possible in the predicted value for failure mode 1. Indeed, the tabulated value has been calculated assuming that the force F obtained from the couple of forces produced by the moment in the connection acted on the seat angle leg. However, based on test observations and comparison of the predicted and experimental values for failure mode 1, it can be inferred that this horizontal force is actually acting underneath the seat angle at the level of the seat angle fillet, since it is this seat angle fillet which pushes the stiffener angles (as indicated by the free-body diagrams of Fig. 5.3). This slight change in the location of the force, equal to the thickness of the seat angle leg (9.5 mm), reduces the lever arm of that force F required to develop the plastic hinge mechanism in the stiffener angles. By assuming this new position and corresponding higher magnitude of the horizontal force, F, the corresponding failure moment

changes to -109 kN·m, a value which is in much closer agreement with the results indicated in Table 5.2.

Very good agreement between the predicted value and test result for failure mode 2 also confirm that the tension yielding on the first row rivets of the seat angles occur slightly before or nearly at the same time as plastic hinges form in the stiffener angles.

The failure mode 3 did not occur because it was purposely prevented using stiffener plates inside the column as described earlier.

The predicted load for failure mode 4 is in good agreement with that obtained by the experiment, indicating that the rivet's shear capacity was somewhat 12% greater than expected, i.e. in the calculation, shear capacity of the rivets was underestimated. Here, the predicted shear to tension capacity ratio of the rivets was calculated assuming a value of 0.75, which can vary according to the riveting conditions and possibility of shear-tension interaction for a rivet. As reported in existing literature (Kulak et al. 1987) the ratio can go up to 0.83.

The failure mode 5 was not observed simply because, as the result of the next experiment showed, the level of load in this experiment was not high enough to cause such failure.

5.1.2 Experiment 2

It is important to recall that experiment 2 is somewhat a continuation of experiment 1 following the replacement of the rivets which failed (or were about to fail) in shear, by high strength bolts. Hence, self-equilibrating internal stresses remaining from the prior test were already present at the start of this test. For Specimen 2, the experimental results and the predicted values for failure mode 1 to 5 when the connection 1 is subjected to negative moments are provided in Table 5.3.

Good correlation between the predicted and experimentally obtained values for failure modes 1

and 2 was obtained resulted in the first experiment. However, in the second experiment, greater loads corresponding to these failure modes were measured. For failure mode 2, this can be attributed to the fact that the first row of rivets in the seat connection already yielded during the first experiment. The results of the first test showed that yielding of the rivets continued until their strain hardening range. Therefore, because of development of the strain hardened condition of the rivets at the start of this second test, higher load was needed to cause the already elongated rivets to develop new large inelastic deformations detectable by clip gages.

This is also valid to some extent, to explain the increase in reported experimental value of failure mode 1, i.e. strain hardening of the rivets affect the redistribution of stresses in the stiffener angles. In fact, as seen in the free-body-diagram of Fig. 5.3, for a given magnitude of applied load to this connection, a lesser moment is felt at the assumed location of the plastic hinge in the stiffener angle if the first row rivets become capable of resisting higher tensile forces. These tensile forces, by their orientation on a free-body diagram of the stiffener angles, produce moments opposed to that needed to produce the plastic hinge in the stiffener angles. Therefore, to compensate for this reduced moment, higher load is required to develop the plastic hinge mechanism. Still, similarly to what was found in the previous test, but more evidently, yielding of the rivets occurred prior to formation of a plastic hinge mechanism in the stiffener angles.

Failure mode 3 was again prevented due to presence of the stiffeners. Failure mode 4 did not happened either since high strength bolts were used instead of rivets. Although, the rivets subjected to shear in the top angles were not replaced with high strength bolts, they did not fail. As observed during testing, when fairly high negative moments were reached the beams rotated such that their top flange came into contact with the column flange, at which point the compressive force from the top flange of the beam was partly transferred to the column through shear action of the rivets and partly by direct contact with the column. Consequently, the amount of shear force on these rivets was limited and, obviously in this case, lower than expected to cause their failure.

In failure mode 5, the predicted load is 16% smaller than that obtained from the experiment.

Although high strength bolts were used in bearing resistance, some amount of clamping force resulted from the normal pre-tightening of the bolts. Thus, friction forces may add to the bearing forces, partly explaining the additional shear resistance. For example, assuming that the bolts are tight enough to develop just half of their slip critical resistance, this would increase the predicted failure load by 20 kN·m. Therefore, if such an adjustment is made, a very close prediction of the failure load is possible, but difficult to rely-upon without the benefit of test results. The effect of friction forces in bearing resistance of the fasteners has been also reported by others (Kulak et al. 1987)

5.1.3 Experiment 3

The test results form this experiment show that the intended plastic mechanism of the knee bracing occurs when the applied moment is about 183 kN·m. Comparing this value with the predicted value of 189 kN·M (obtained from a design based on the principles presented in Chapter 3), a very good agreement between the two values is found. It is noteworthy that the measured values of the moment applied to connection 1 in this experiment confirmed that the existing connection itself provides almost no contribution to the total resistance; the knee braces are considerably stiffer and effectively resist nearly all the applied moment. Therefore, as done during design of the knee braces for this experiment, capacity of the existing connection can be ignored when knee braces are added as a retrofit.

5.1.4 Experiment 4

Comparison of the predicted value of 59 kN·m (Table 3.4) and the value of 68 kN·m which corresponds to the load at which inelastic deformations of the column flanges were noticed in this experiment, shows that failure mode 1 can be fairly well predicted. However, the expected value is 13% smaller than the test result, probably because the column flange was assumed of uniform thickness in the calculations whereas it is actually thicker in the vicinity of the column web. Therefore, in some cases such as here, the predicted value for this failure mode can be

considered conservative.

Comparison of the results for failure mode 2 shows that the predicted value of 72 kN·m is 16.6% greater than the experimental result of 60 kN·m, which means that the prediction method used does not yield an accurate or even a conservative solution. This is because the high strength bolts which fix the vertical leg of each top angle to the column are not closely spaced compared to the length of the angle. It is normally assumed for the calculation of the load corresponding to the plastic hinge mechanism of a top angle that two straight yield lines in the vertical leg of the top angle are present: One line is located adjacent to the fillet of the vertical leg and the other one in the vicinity of the head of the high strength bolts, both parallel to the longitudinal axis of the top angle. However, this was not the case here, as deformations in the vertical legs of the top angles illustrated. It was observed that a more complex yield line pattern developed across the vertical legs and around the location of the high strength bolts. If a new yield line pattern, as shown in Fig.5.4, is assumed for the calculations, the corresponding predicted moment becomes 60.2 kN·m, which is very close to the experimental result. This shows that when dealing with fairly long angles having few number of fasteners not closely located over the length of the angle, the proposed yield line pattern, or perhaps even more complex ones if additional accuracy is sought, should be considered since the aforementioned traditional assumption could produce a significant discrepancy and un-conservative predictions (Appendix E).

When the connection is subjected to negative moments, the experimentally obtained value corresponding to failure mode 1 is -110 kN·m, which is different from the predicted value of -86 kN·m as presented in Table 3.5. From test observations, and based on a proposed yield line pattern in the seat angles similar to that used for the top angle, a new model for the failure mechanism in the seat connection can be established, as shown in Fig.5.5. The calculation shows that the failure load to develop such a mechanism is -116.2 kN·m, which better agrees with the test result. Therefore, the influence of the length of the seat angles and relative location of its fasteners on the aspect of failure mechanism is confirmed as it was for the top angle.

Since the specimen was not loaded to the expected level needed to trigger the other failure

modes, no other experimental result was obtained to allow comparisons, except for failure mode 5 which was reached in the final separate test to failure in negative flexure. Failure of the connection occurred at -164 kN·m whereas the predicted moment corresponding to this failure mode 5 was -270 kN·m (Table 3.5). Carefully examination of the fracture point revealed that it was located exactly where plastic hinges adjacent to fillet of the horizontal leg of seat angle legs had formed. This indicates that in determining the failure load of such a seat angle type of connection, the interaction of bending and tension must be considered instead of pure tension in the gross section of the seat angle leg.

5.2. Hysteretic Response of the Connections

In this section, general behaviour of the connections under cyclic loads and causes for the shape of the hysteretic loops are reviewed.

5.2.1 Connection Detail 1

The M-θ relationship of the connection detail 1 shows a distinct pinching of the hysteretic loops. Since the area under the curves reflects the absorbed energy in each cycle, the presence of highly pinched curves means that the energy absorbed by the connection is lower than optimum and reduced by some factors. The main causes of this pinching can be categorized as follows.

a) Slippage at the rivet holes

The slippage at the rivet holes appears to be resulted from the contribution of two factors. One is the lack of tight fit inherent to riveting practices in the past. The standard riveting practice required the holes to be made with clearance of 1/16 inch (1.6 mm), but specially in the case of field riveting, centre of the rivet holes were not always well matched. In addition, diametric shrinkage after the cooling of hot driven rivets caused small gaps to develop between each rivet's shank and its the edge of its hole, particularly as the grip length of a rivet increases (Kulak et

al. 1987). The other factor is that the clamping force due to the pre-tensioning force of the rivets after cooling is not high enough to prevent slippage by frictional resistance between the connected plates. This is especially true for the rivets driven in the field for which the clamping force appears to be very low, since riveting of such rivets is conducted with different tools from those used in shop riveting (Kulak et al. 1987).

Therefore, some slippage in the holes of the field driven rivets of this connection under a low shear value produced by the moment on the connection, can cause the pinching observed in the very early stages of loading in both positive and negative flexure. However, as the load increases, considerable shear resistance can be developed at the riveted connections through bearing action.

b) Rocking of the top angles

As stated earlier, by observation of the moment-strain relationship of the top angles (Figs.4.5 and 4.6), it can be inferred that response of the top angles to the reversing force applied to their horizontal leg can also be responsible for pinching in the hysteretic curves.

When a positive moment is applied to the connection, it results in a tensile force acting on the top angle horizontal leg which increasingly causes plastic hinging and tensile yielding of the rivets to occur. This is the major source of resistance of the top angle, but when the load is reversed, instead of a tensile force, a compressive force is applied to the horizontal leg which mainly causes the hinge deformations of the horizontal leg to reverse. However, the plastic hinge mechanism in the vertical leg is not as effective, since the already elongated rivet has lost its ability to provide, by clamping-force, a fixed support for the vertical leg of the angle. Moreover, the connection has no natural means of reversing deformation of the already yielded rivet; rivets can not be compressed by the plates they connect. As a result of this, without any considerable resistance, the vertical leg rocks over the column flange, i.e. the deformed vertical leg rotates about the hinge in the horizontal leg and the toe of the vertical leg gradually separates from the column face. This continues until the heel of the angle touches the column flange, at which point

the compressive load is directly transferred to the column. Therefore, in every cycle, rocking of the angle occurs and causes some pinching in the M-θ curve. Different stages of response of the top angle are illustrated in Fig.5.6.

c) Lack of integrity of the stiffened seat connection

The observations and results from the experiment 1 show that the stiffened seat connection developed a consistently pinched hysteretic loops. In fact one cause of this pinching is separation of the seat angle from stiffener angles when the connection is subjected to a positive moment, after negative moments have produced inelastic deformations of both the seat and stiffener angles, i.e. the stiffener angles do not contribute in resisting the horizontal force applied to the seat connection subjected to positive moments since there are no mechanism present in this connection to force them back under this reversed moment, particularly if the rivets joining the stiffener angles to the columns have yielded in the prior negative moment cycle, as would often be the case. Therefore, the capacity of the seat connection for loading in that direction is considerably reduced until the seat angles bear anew on the column.

In negative flexure, the stiffener angles and the first row of rivets, when already yielded and inelastically deformed, do not provide any resistance until the seat angle deforms sufficiently to touch the stiffener angles, and this can only happen when rotations developed at the connection approximately reach the negative residual rotation obtained in the previous cycle. Therefore, before that value of rotation is reached, no contribution from the stiffener angles is made to the connection resistance.

5.2.2 Connection Detail 2

Hysteretic curves for connection detail 2 indicate relatively low pinching and, consequently, good energy dissipation of the connection. This is mainly due to a number of changes made to the connection, described as follows.

a) Welding on parts of the top and seat angles

The absence of visible yielding or crack propagation of the welds selectively made to retrofit the connection showed that these welds can effectively prevent slippage at the holes of the rivets due to shear force produced by the moment at the connection. In addition to this, the welds increases the connection shear capacity, and thus moment capacity, of the connection.

b) Effect of replacing high strength bolts

As expected in experiment 4, no considerable deformation at the toe of the top angles was observed. This means that the high strength bolts provides a sufficiently large clamping force to prevent rocking of the vertical legs observed in experiment 1.

c) Integrity in the stiffened seat connection

As very clearly observed during the test, welding of the stiffener angles to the leg of the seat angles caused these two parts to move together. Therefore, they both contribute to the flexural resistance, whether the connection is subjected to positive or negative moments.

Although the pinching of this connection is greatly reduced by welding and use of high strength bolts, some small amount of pinching still exists which is, in this particular case, due to inelastic deformations of the column flanges under point loads from the fasteners. Locating stiffener plates near the position of these fasteners, as done for connection detail 1, would minimize the remaining pinching to a great extent.

5.2.3 Knee Bracing

The hysteretic loops of the knee braces show a small amount of pinching when large rotations at the joint are developed. This is due to the fact that once a knee brace buckles, its residual

deformation and out-of-straightness can not be completely eliminated when subjected to tension in the next half cycle. Moreover, tensile load causes the member to yield and elongate; after each yielding excursion, the stress-free elongated member is longer, and has to buckle just to be able to fit back into the original distance between its supports (gusset plates) connected to fixed points on the beams and the column. Therefore, in every new cycle of this test, buckling occurs sooner than in the previous cycle, because in every new cycle the member is longer than before when unloaded.

As the M-θ hysteretic curve of the knee bracing test shows, pinching occurs in the form of a progressively lower slope for the ascending branch of the curve. At the onset of a given cycle, as the load increases, a pair of knee braces which were already buckled are now undergoing tension, but cannot develop their full yield resistance until they become straight "un-buckled" member again. It only requires small amount of load to overcome the plastic moments in these members and straightened them up. Also, the two other members, which were already deformed and elongated in tension, are now undergoing compression; they can obviously resist some loads before and while they buckle. However, as stated earlier, the buckling of these members occur relatively fast. Consequently, over some range of rotations all members can be buckled when the specimen is returned at its original position, and in that case, the capacity of the knee braces is provided mostly by the compressive members. It is noteworthy that the capacity of these members can be increased if the ratio of C_r/T_r is chosen as close as possible to 1 (recall that C_r and T_r are respectively the compressive resistance and tensile resistance of a member), but practically it is sometimes practically difficult to achieve this, as in this experiment where C_r/T_r ratio was 0.8.

If knee braces cannot be provided with a C_r/T_r ratio of close to 1.0, an alternative solution to minimize pinching is to use special frictional type of fasteners in the connection of the member to the gusset plates. Use of friction bolted fastener to efficiently dissipate energy in the connections have been studied by researchers (Tremblay and Stiemer, 1993, Grigorian et al. 1992). Advantage of this type of energy dissipating system is that it is designed to ensure that the friction mechanism is activated prior to buckling of yielding of the braces. Hence, it

virtually eliminates damage to braces and the possible need for repairs following an earthquake.

CHAPTER 6

Conclusion and Practical Recommendations

6.i Conclusions

Based on the experimental results and predicted analytical values on the behaviour of existing stiffened-seat angle connections, it can be concluded that:

- Although these connections were not originally designed to resist moments they can develop considerable amount of capacity and ductility.

- The negative moment capacity of the existing stiffened-seat angle connections is considerably greater than their positive moment capacity. The actual capacity in each direction varies as a function of the geometry and size of the angles, as well as arrangement and resistance of the rivets.

- The existing stiffened-seat angle connections can dissipate some amount of energy when subjected to cyclic loads, however, their hysteretic curves are pinched, even within the elastic range of stresses produced in these connections. The pinching is caused by different factors, such as; tensile yielding of rivets, slippage in the holes of rivets and separation of stiffener angles from seat angles.

- The use of selective welding on the connections and selective replacement of rivets with high strength bolts, as described in this study as a retrofitting technique can increase moment capacity and considerably improve energy dissipation in these connections.

- The addition of knee bracing system as a retrofit solution for these steel joints is seen to be effective in developing large moment capacities dissipating considerable energy, in both positive and negative flexure.

Owing to the presence of a quantifiable potential capacity and ductility for these connections, the hysteretic moment-rotation response obtained from the experiments can be mathematically modeled and used to express the realistic characteristics of a joint (if panel zone effect in adjacent column is ignored). Such model can then be implemented in a nonlinear analysis program for frames, and used to analyze buildings having these connections (retrofitted or not) and subjected to earthquake excitations. Results of such analyses can be then interpreted in terms of level of probable damage, reliability of the existing connections, and need to retrofit.

6.2 Practical Recommendation

Results of the experiments on the existing connections, show that to consider these connections as reliable resisting elements, one has to ensure that under expected applied moment, they do not behave in a very highly pinched and/or brittle failure mode. Therefore, a structural engineer can find the failure loads corresponding to tension and shear yielding of the rivets, and development of plastic hinge mechanism in the connections, by using the methods proposed in this study, and compare them with those expected to be applied to the connections during probable earthquakes.

As the experimental results show, the retrofitting techniques used for the joints with existing connections are very efficient and therefore recommendable for practical purposes. First method is selective-welding and selective rivet-replacement on parts of existing connections. The second method is to connect knee braces to the members of a joint without any changes made to the existing condition of their connections. Choosing either of the two methods depends on costs, labour efficiency (access and site constraints on constructability) and demands of each case. It is noteworthy that use of the second method may be preferred where higher risk of severe earthquake exists, since knee braces can be designed for fairly large positive and negative

moment capacity and are very good energy dissipation. The first method, however, seems to be of lower costs while probably better suited to low and/or medium seismic regions since these connections do not enhance the resistance as significantly as knee bracing; moreover, larger storey drifts are expected as results of using these connections.

6.2.1 Selective Retrofitting of the Existing Connections

This suggested retrofitting technique, applicable to existing stiffened seat connections of the type studied here, entails the following procedure.

- Replacing rivets located in vertical leg of top angles with high strength bolts tightened to the 70% of their tensile capacity.

- Welding to connect the horizontal leg of top and seat angles to the flanges of connecting beams. These welds alone should have enough shear resistance to transmit all of the axial force produced in the beam flange to the angles without relying on any contribution from the existing rivet in shear until the expected moment capacity of connection is reached.

- Welding to connect the horizontal seat angle legs to the end of stiffener angles along their legs which are parallel to the longitudinal axis of the seat angle.

- Addition of stiffener plates at the location of the concentrated loads on column flanges. These stiffeners in the compressive region should be positioned near the beam flanges, and in the tension regions should be as practically close as possible to the axis of rivets.

6.2.2 Use of Knee bracing

Use of knee bracing as a retrofit of joints is not only limited to beam-to-column joints where the particular type of semi-rigid connections tested here are present. In fact, even if a connection

is damaged or not capable of resisting any moment, this retrofitting technique can be used. In practice, to optimize energy dissipation, depending on the magnitude of the expected applied moments, knee braces are designed such that they yield in their gross section when subjected to maximum tension and they reach a capacity as closely as possible to compression yielding when subjected to compression forces. Therefore, the following conditions should be met;

- Slenderness ratio of the knee braces should be kept as low as possible.

- Out of plane buckling of the knee braces should be avoided, and plastic hinges should be allowed to occur in the knee braces instead of in gusset plates, for more energy dissipation.

- Moment capacity of the knee bracing system should be kept lower than that which would produce hinging in the columns, to avoid the risk of localized storey plastic collapse mechanism.

Preferably, knee braces can be welded in shop to their gusset plates, and welded or bolted (if steel is not weldable) on site to the beams and columns. A symmetric configuration of four knee-braces per beam-column joint is also advocated.

6.3 Areas for Further Investigations

There are number of old buildings with steel frames having this type of riveted stiffened-seat angle connections. To precisely estimate the level of damage likely to occur in these buildings under various levels of earthquake excitation, further investigation on the behaviour of these connections is required. Further research is particularly needed in the following areas;

- Analytical model to predict hysteretic M-θ relationship of this type of semi-rigid connections.

- Nonlinear analyses of steel frames subjected to different levels of earthquake excitation, using

the analytical developed model to evaluate their resistance and their ductility level.

- Investigation of additional retrofitting strategies, such as replacing top angles with stronger ones, welding rivet heads to their connecting plates, use of frictional bolted fasteners in the connections of knee braces.

- Developing analytical models for the retrofitted connections and nonlinear analysis of the frames subjected to earthquake excitations using these models.

More knowledge on the performance of these frames subjected to earthquakes in different seismic region may translate into demonstrating that only limited retrofitting is needed or even that the buildings are satisfactory in as their existing conditions, instead of expensive retrofits at prohibitive costs which may lead to the alternative decision of demolishing many of these buildings.

References

Ang, K. M., and Morris,G.A. (1984). "Analysis of three-dimensional frame with flexible beam-column connections" *Can. J. Civ. Engrg.*, 11, 245-254.

Astaneh, A., et al. (1989a). "Cyclic behaviour of double angle connections." *J. Struct Div.*, ASCE,115(5), 1101-1118.

Astaneh, A., et al. (1989b). "Experimental Studies of a Single Story Steel Structure with Fixed, Semi-Rigid and Flexible Connections" *Earthquake Engineering Research Centre*, Report No.UCB/EERC-89/15.

Canadian Institute of Steel Construction (1991). *Handbook of Steel Construction (CISC)*, Willowdale, Ont.

Charles, W. R., et al. (1993) " Evaluation of the strength, stiffness and ductility of older steel-framed structures." Structural Engineering Association of North California Research committee, *Research Bulletin Board*, BB93-3, (B-2)-(B-3).

Chen, W. F., and Lui, E. M. (1985). "Columns with end restraint and bending in load and resistance factor design." *AISC Engrg. J.*, 22(4), 105-132.

Chen, W. F., and Lui, E. M. (1991). " Stability Design of Steel Frame. " CRC Press, 244.

Colson, A., et al. (1983). "Connection incidence on the elastic behaviour of steel structures." *Euremech Colloquium*, 174.

FEMA (Federal Emeregency Management Agency) (1992), " NEHRP Handbook for seismic rehabilitation of existing buildings", *FEMA*-172/June 1992.

Fry, M. J., and Morris, G. A. (1976). "Analysis of flexibly connected steel frames." *Can. J. Civ. Engrg.*, 2(3), 280-291.

Grigorian, C. E., Yang, T. -S and Popove, E.P. (1992). "Slotted Bolted Connection Energy Dissipation" *UCB/EERC*, Report 92/10.

Hetchman, R. A.,et al. (1947). "Riveted semi-rigid beam-to-column building connections, progress report no. 1 " AISC Research at Lehigh Univ., Bethlehem, Pa.

Jones, S. W., et al. (1982). "Columns with semirigid joints." *J. Struct. Engrg.*, ASCE, 108(2), 361-372

Ketchum, M. S. (1924). *Structural Engineer's Handbook*, McGraw-Hill Book Company.

Ketchum, M. S. (1932). *The Design of Steel Mill Buildings and the Calculation of Stresses in Framed Structures*, McGraw-Hill Book Company, 613.

Kishi N., and Chen, W. F. (1990). "Moment-rotation relations of semirigid connections with angles." *J. Struct. Engrg.*, ASCE, 116(7), 1813-1834.

Kishi, N., Chen, W. F. (1986). "Data base of steel beam-to -column connections" *Struct. Engrg. Report No. CE-STR-86-26*, School of Civ. Engrg., Purdue Univ., West Lafayette, Ind.

Kulak, G.L., et al. (1987). "Guide to Design Criteria for Bolted and Riveted Joints", Second Edition, John Wiley and Sons, New York, 28,29,30,33,115.

Lewitt, C.W., et al. (1966). "Restraint Characteristics of flexible riveted and bolted beam-to-column connections." *Dept. Civ. Engrg.*, Univ. of Illinois, Urbana, Ill.

Lightfoot, E., et al. (1974). "Elastic analysis of frameworks with elastic connections, *J. Struct. Engrg.*, ASCE, 100(ST6), 1297-1309.

Lui, E. M., Chen W.F. (1983). "Strength of H-columns with small end restraints." *Journal of the Institution of Structural Engineers*, 61.B(1), 17-26.

Lui E. M., et al. (1986). "Analysis and behaviour of flexibly jointed frames." *Engineering Structures*, Butterworth Publishers, Surrey, U.K., 8(2), 107-118.

Marly, M. J., et al. (1982). "Analysis and test of flexibly-connected steel frames." *Report to AISC under Project 199*, AISC, Chicago, Ill.

Maxwell, S. M., et al. (1981). "A realistic approach to the performance and application of semi-rigid joints in steel structures." *Joints in Structural Steel Work*, J. H. Howlett, W. M. Jenkins, and R. Stansby, eds., Pentech Press, 2.71-2.98.

Monforton, A. R., et al. (1963). "Matrix analysis of semi-rigidly connected frames." *J. Srtuct. Engrg.*, ASCE, 87(ST6), 13-42.

Moore, H. F., and Wilson, W. M. (1917). "Tests to determine the rigidity of riveted joints of steel structures." *Engineering Experiment Station, Bulletin No. 104*, Univ. of Illinois, Urbana, Ill.

Radziminski, J. B., and Azizinamini, A. (1986). "Low cyclic fatigue of semi-rigid steel beam-to-column connections" *Proceedings of the third U. S. National conference on Earthquake Engineering*, 1285-1296.

Rathbun, J.C. (1936). "Elastic properties of riveted connections" *Trans.* ASCE, Paper No. 1933, Vol. 101, 524-563.

Richard, R. M., et al. (1980). "The analysis and design of single plate framing connections." ASCE *Engrg. J.*, 2d Quarter, 38-52.

Salmon, C. G., and Johnson, J. E. (1980). *Steel Structures*,Harper & Row, Publishers, New York, second edition, 731-733.

Scott, W. F. (1904). *Structural Designers' Handbook*, The Engineering News Publishing Co.

Stelmack, T. W. (1983). "Analytical and experimental response of flexibly connected steel frames." *Reported to AISI CEAE Dept.*, Univ. of Colorado, Boulder, Colc.

Stelmack, T. W. (1986). "Analysis and tests of flexibly connected steel frames." J. Struct. Engrg., ASCE, 112(7), 1573-1586.

Trapy, T. S., et al. (1981). "Behaviour of semi-rigid beam-to-column end plate connections." Proceedings Conference, *Joints In Structural Steelwork*, J. H. Howlett, W. M. Jenkins and R. Stainsby, eds., Halsted Press, 2.3-2.25.

Tremblay, R. and Stiemer, S.F. (1993)."Energy dissipation through friction bolted connection in concentrically braced steel frames." *Proceedings of ATC-17-1*, Seminar on seismic isolation, passive energy dissipation, and active control, Applied Technology Council, Sanfrancisco, USA

Young, C. R., and Jackson, K. B. (1934). "The relative rigidity of welded and riveted connections." *Canadian Journal of Research*, vol. 11, 62-100.

Youssef-Agha, W., and et al. (1989). "Seismic response of low-rise steel frames." *J. Struct. Engrg.*, ASCE, 115(3), 594-605.

Connection Detail No.	Specimen No.	Experiment No.	Description of Specimen
1	1	1	Connection detail 1 (no retrofit)
1	2	2	Connection detail 1 retrofitted by replacing the failed rivets with high strength bolts
1	3	3	Connection detail 1 retrofitted by adding knee-braces
2	4	4	Connection detail 2 retrofitted by selective welding

Table 3.1 Summarized description of the specimens

No	Failure Mode	Moment (kN·m)
1	Formation of hinge mechanism in top angle	51
2	Yielding in column flange due to concentrated load from rivets (without added stiffener)	67
3	Yielding of top angle rivets in tension	80
4	Bearing failure at rivet holes in the top angle	117
5	Crippling of column web under compressive load from beam flange (without added stiffeners)	122
6	Shear failure of rivets	122
7	Gross section shear failure in leg of top angle	193
8	Net section tensile failure in leg of top angle	230
9	Gross section tensile yielding leg of top angle	309

Table 3.2 Prediction of the positive moment capacity for connection detail 1 (used in specimens 1 and 2)

No	Failure Mode	Moment (kN·m)
1	Formation of plastic hinge mechanism in stiffener	-80
2	Tensile yielding of first row of stiffener rivets under seat angle	-101
3	Crippling of column web under compressive load from beam flange (without adding stiffeners)	-122
4	Shear failure of rivets	-122
5	Bearing failure at the rivet holes	-134
6	Tensile failure of first row of stiffener rivets under seat angle	-149
7	Gross section shear yielding in stiffener angles	-178
8	Net section Tensile failure in leg of seat angle	-230
9	Gross section tensile yielding in leg of seat angle	-309

Table 3.3 Prediction of the negative moment capacity for the connection detail 1 (used in specimens 1 and 2)

No	Failure Mode	Moment (kN·m)
1	Yielding of the column flange due to concentrated load from high strength bolts	59
2	Formation of hinge mechanism in top angle	72
3	Gross section shear failure in leg of top angle	151
4	Shear failure of weld in top angle	222
5	Gross section tensile yielding in leg of top angle	270
6	Net section tensile failure in leg of top angle	409

Table 3.4 Prediction of the positive moment capacity for connection detail 2 (used in specimen 4)

No	Failure Mode	Moment (kN·m)
1	Formation of hinge mechanism in the stiffener angles and the seat angles	-86
2	Gross section shear yielding of stiffener angles	-169
3	Crippling of column web under compressive load from beam flange	-201
4	Shear failure of weld in seat angle	-222
5	Gross section tensile yielding in leg of seat angle	-270
6	Net section tensile failure in leg of seat angle	-409

Table 3.5 Prediction of the negative moment capacity for connection detail 2 (used in specimen 4) .

No	Failure Mode	Predicted Moment (kN·m)	Experimental Moment (kN·m)
1	Formation of hinge mechanism in top angle	51	55
2	Yielding in column flange due to concentrated load from rivets (without adding stiffener)	67	Not observed
3	Yielding of top angle rivets in tension	80	65

Table 5.1 comparison of the experimental and predicted values for positive moment capacity of connection detail 1 (used in specimens 1 and 2)

No	Failure Mode	Predicted Moment (kN·m)	Experimental Moment(kN·m)
1	Formation of plastic hinge mechanism in stiffener	-80	-100
2	Tensile yielding of first row of stiffener rivets under seat angle	-101	-95
3	Crippling of column web under compressive load from beam flange (without adding stiffeners)	-122	Not observed
4	Shear failure of rivets	-122	-139
5	Bearing failure at the rivet holes	-134	Not observed

Table 5.2 Comparison of experimental and predicted values for the negative moment capacity of the connection detail 1 (used in specimen 1)

No	Failure Mode	Predicted Moment (kN·m)	Experimental Moment(kN·m)
1	Formation of plastic hinge mechanism in stiffener	-80	-135
2	Tensile yielding of first row of stiffener rivets under seat angle	-101	-125
3	Crippling of column web under compressive load from beam flange (without adding stiffeners)	-122	Not observed
4	Shear failure of rivets	-122	Not observed
5	Bearing failure at the rivet holes	-134	-160

Table 5.3 Comparison of experimental and predicted values for the negative moment capacity of the connection detail 1 (used in specimen 2)

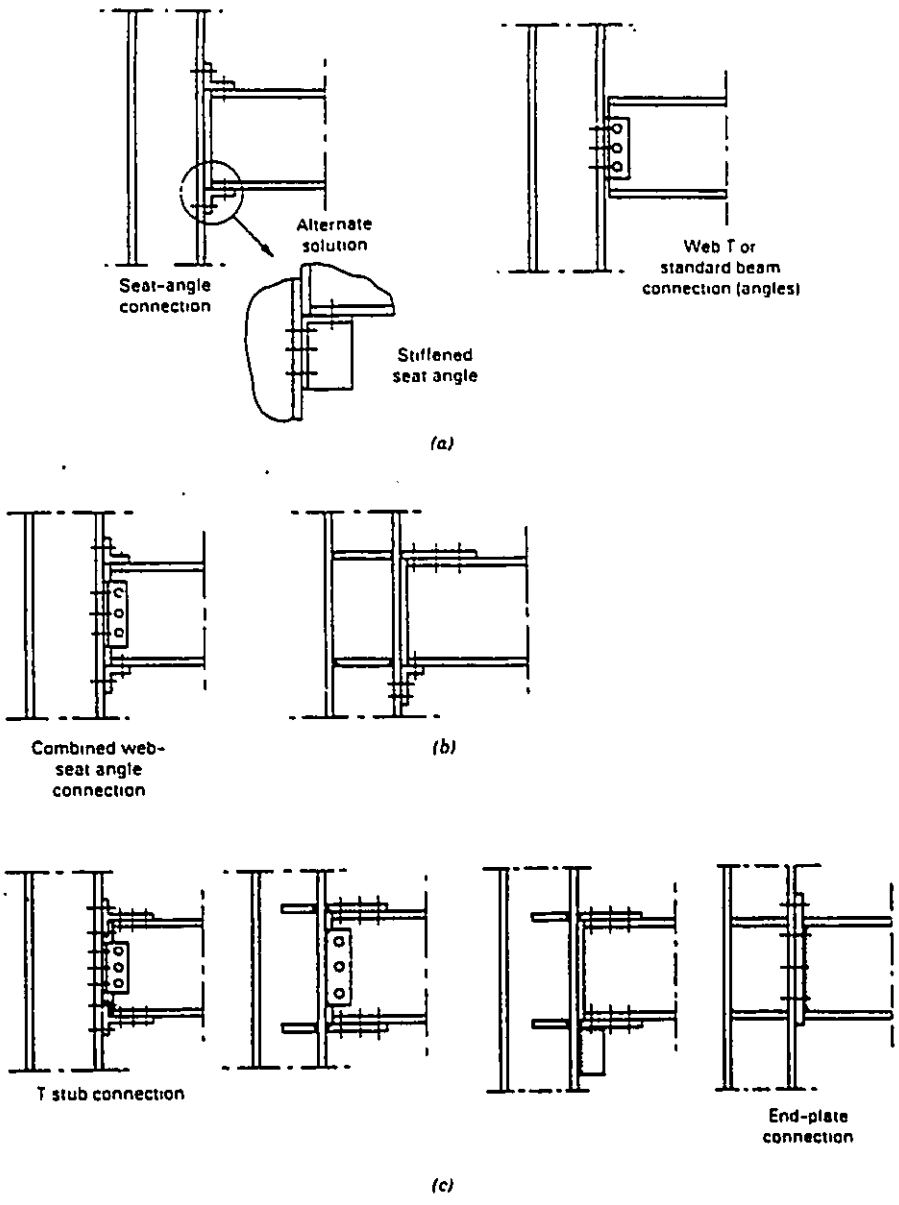

Figure 2.1 (a) Flexible connections. (b) Semi-rigid Connections. (c) Rigid Connections. (Kulak et al. 1987, Chapter 18)

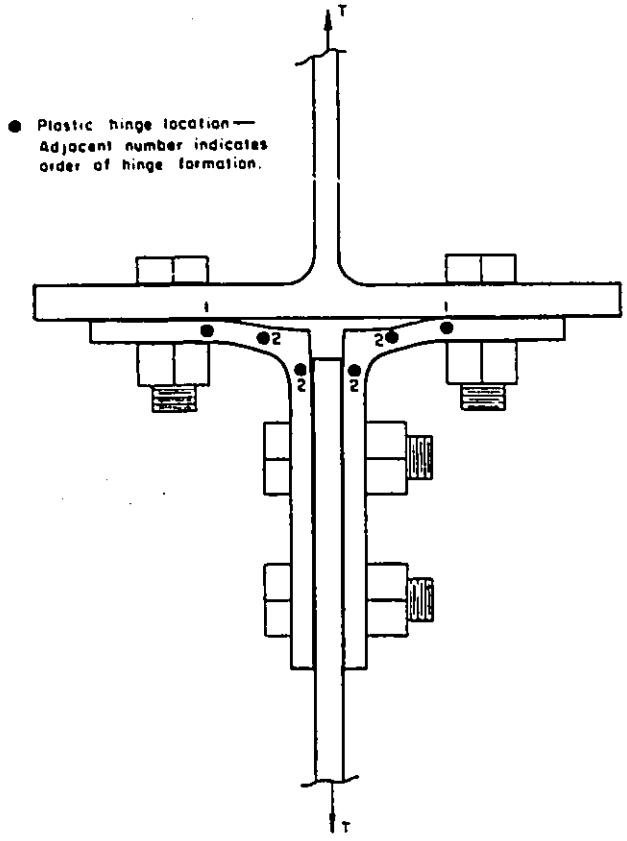

Figure 2.2 Location of plastic hinges in angles under tension (Lewitt et al. 1966)

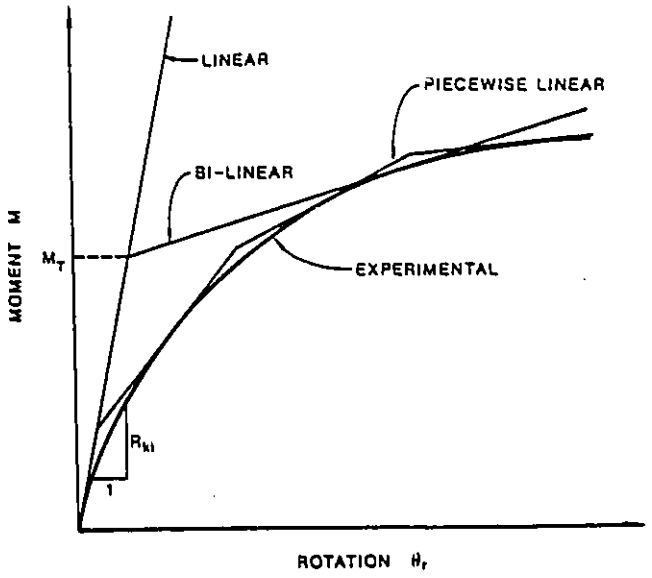

Figure 2.3 Linear M-θ models (Chen and Lui 1991)

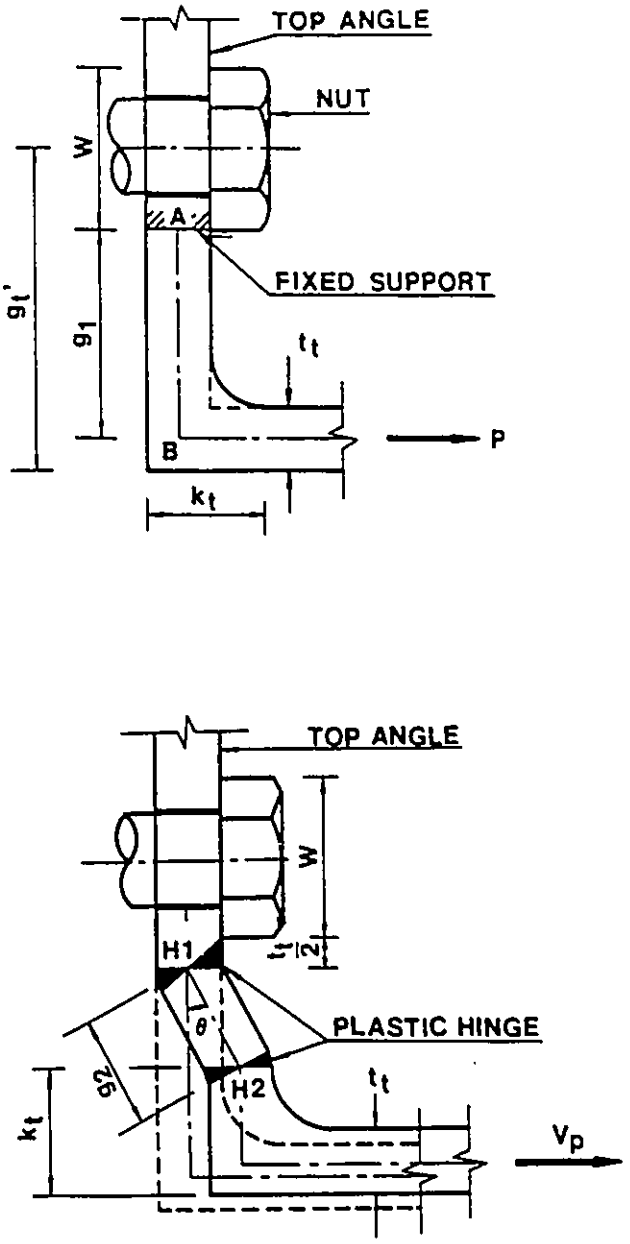

Mechanism of Top Angle at Ultimate Condition

Figure 2.4 Initial and ultimate conditions of top angles used in the model by Kishi and Chen (1990)

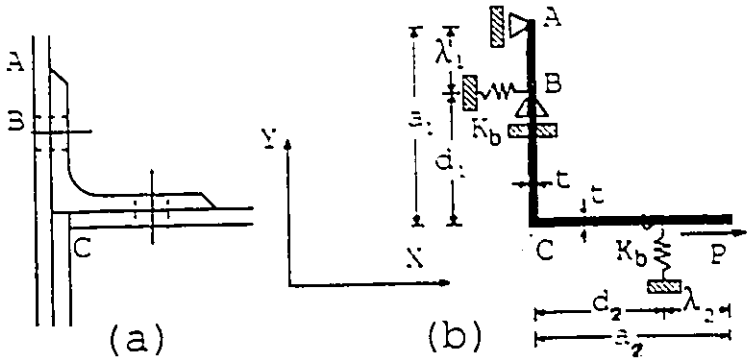

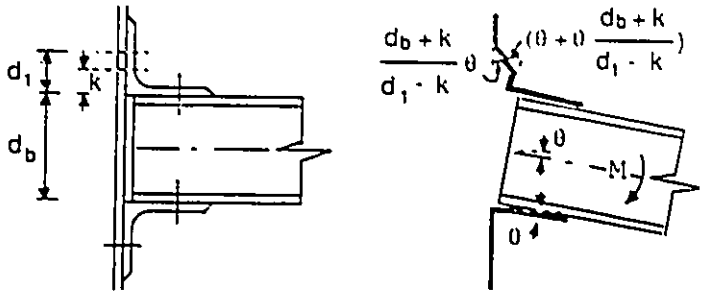

Idealized Yielding Moment for Top and Seat Angle Joint

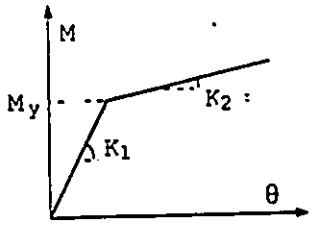

(M–θ) Relation for Analytical Model

Figure 2.5 Physical models of top and seat angle connections for elastic and ultimate conditions with bi-linear M-θ relationship (Youssef-Agha et al. 1989)

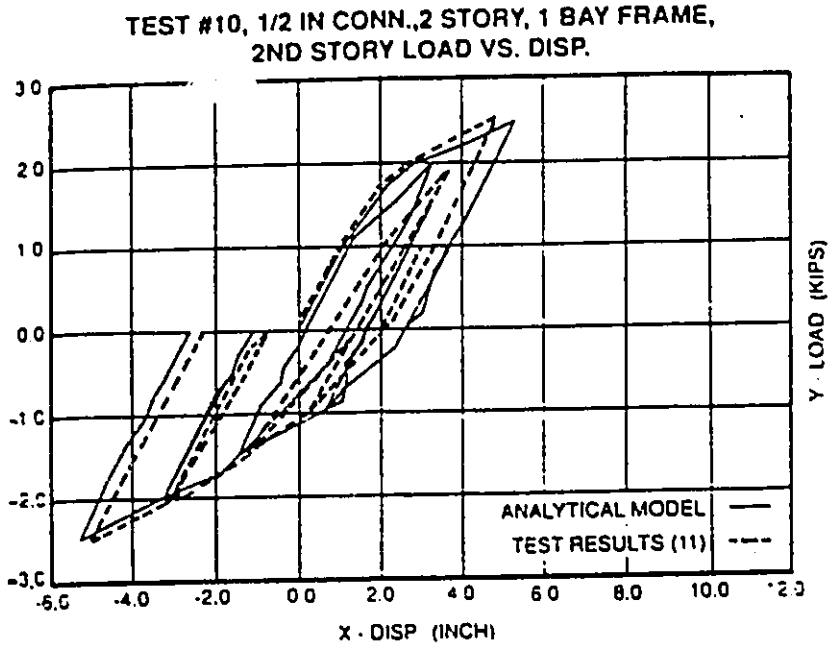

Figure 2.6 Comparison between analytical model and experimental results based on bi-linear model by Youssef-Agha, et al. (1989)

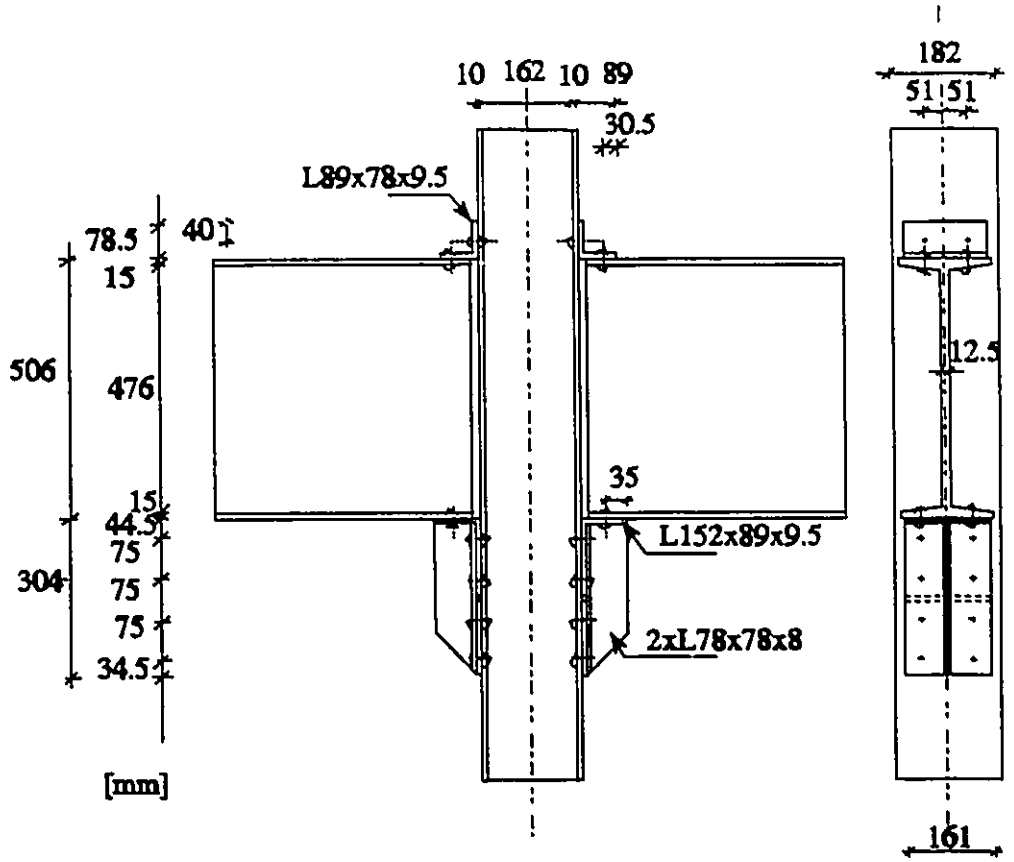

Figure 3.1 (a) Connection Detail 1

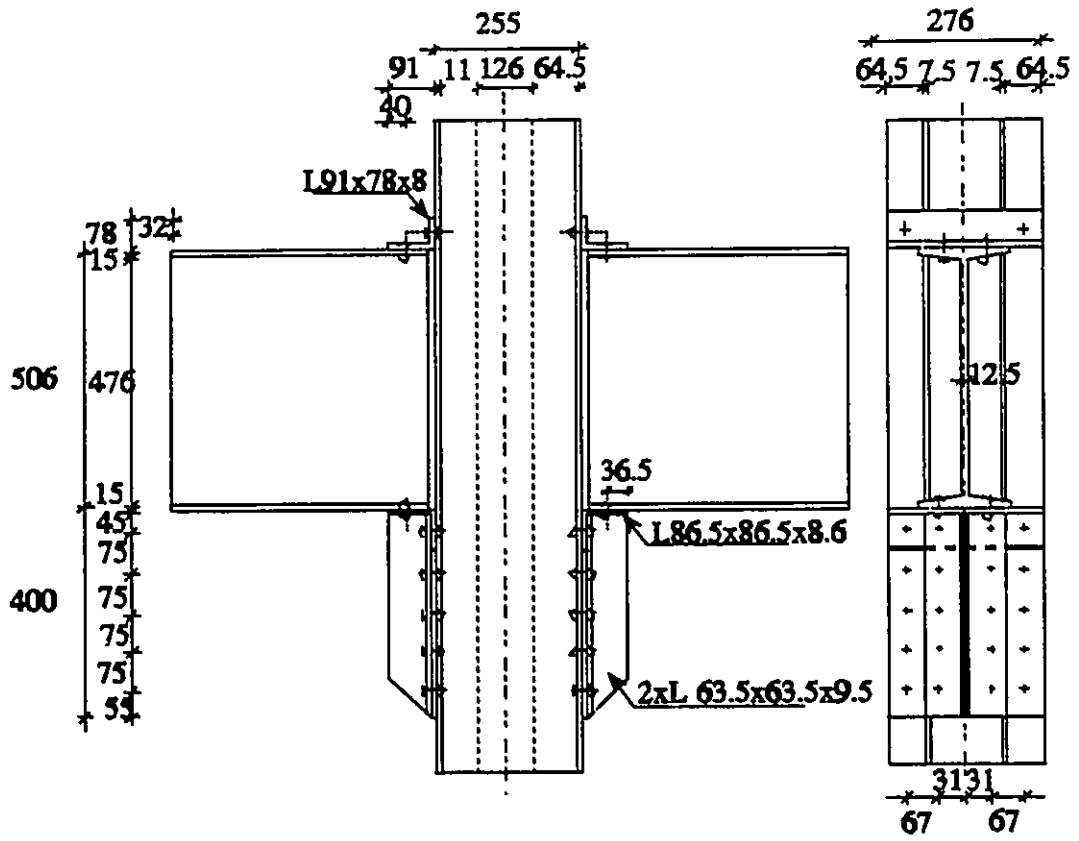

Figure 3.1(b) Connection Detail 2

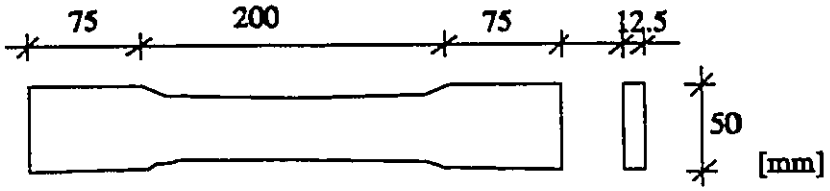

Coupon of steel for standard Tensile Test

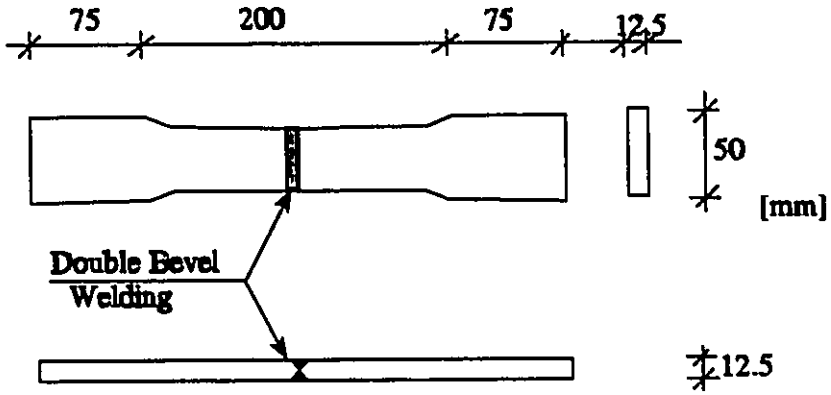

Coupon of Steel Used for Weldability Test

Figure 3.2 Coupons of steel used for tensile and weldability tests

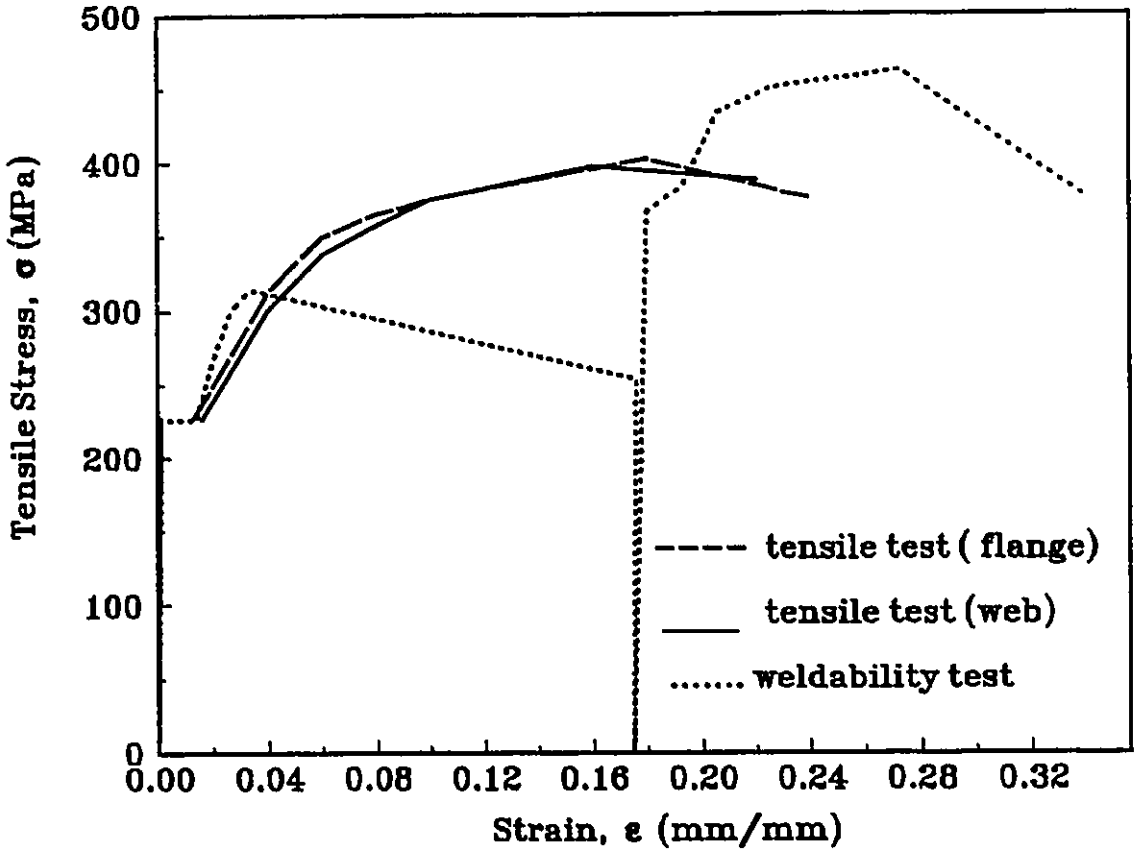

Figure 3.3 Stress-strain relationship for existing steel

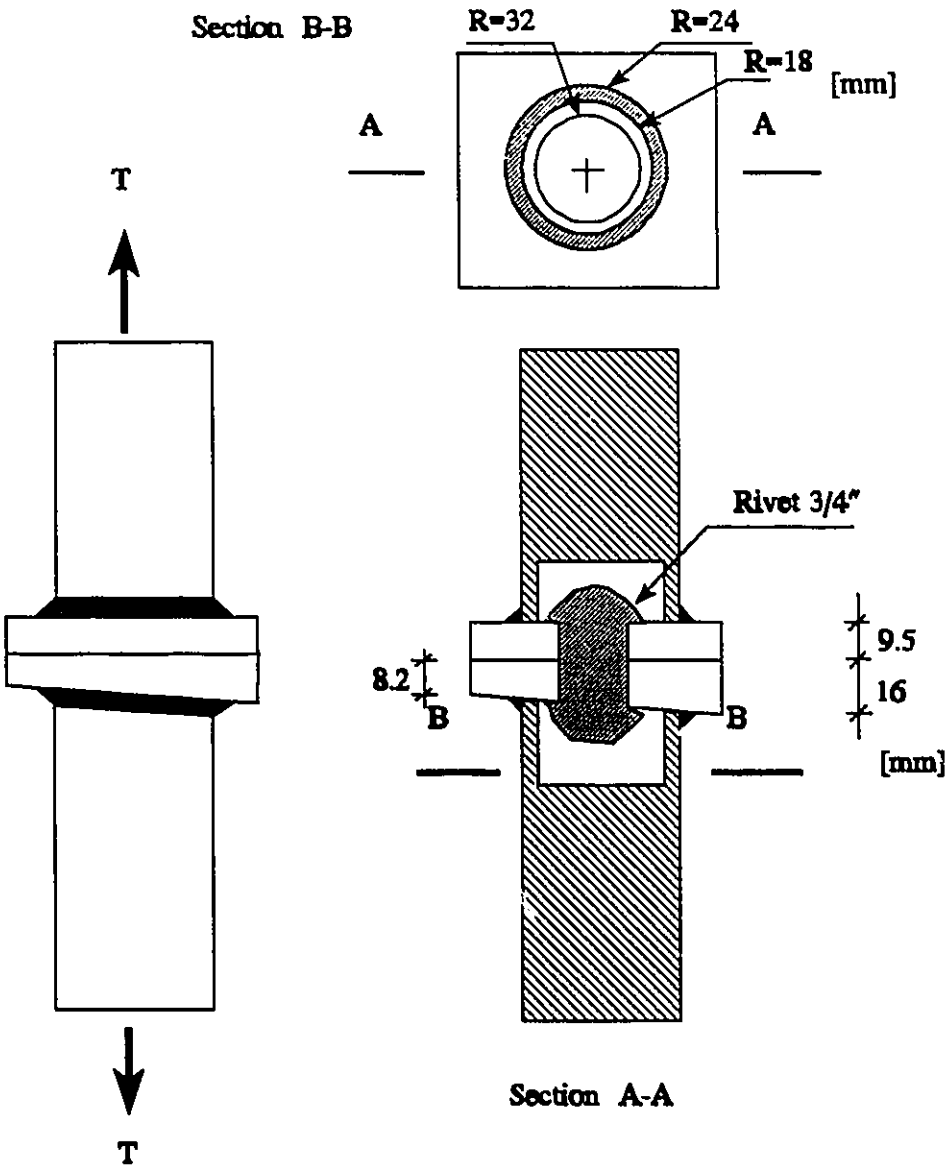

T, tensile force applied by testing machine

Figure 3.4 Detail of the specimen for tensile test of the rivet

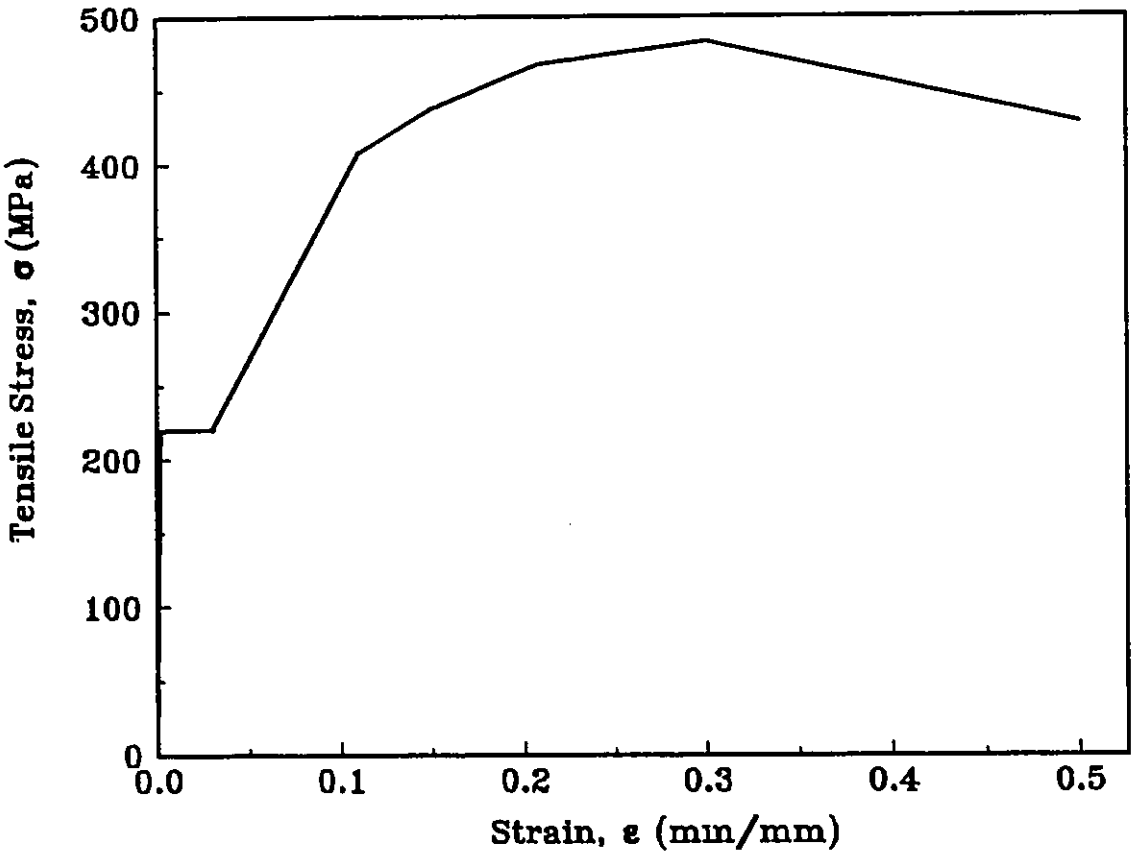

Figure 3.5 Stress-strain relationship obtained from tensile test of rivet of 3/4" diameter

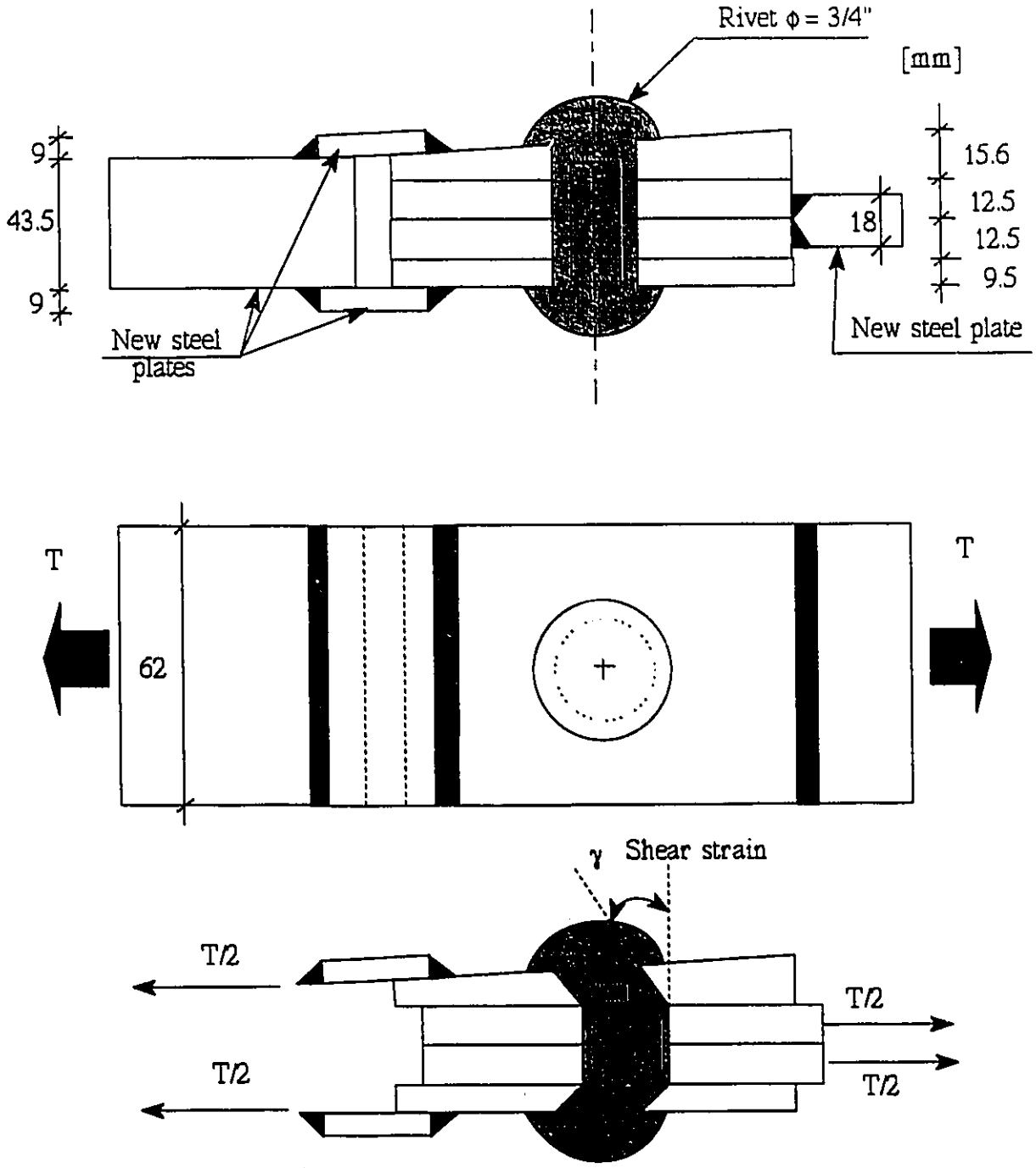

Figure 3.6 Detail of the specimen used for shear test of rivet and model used to calculate shear deformation of rivet

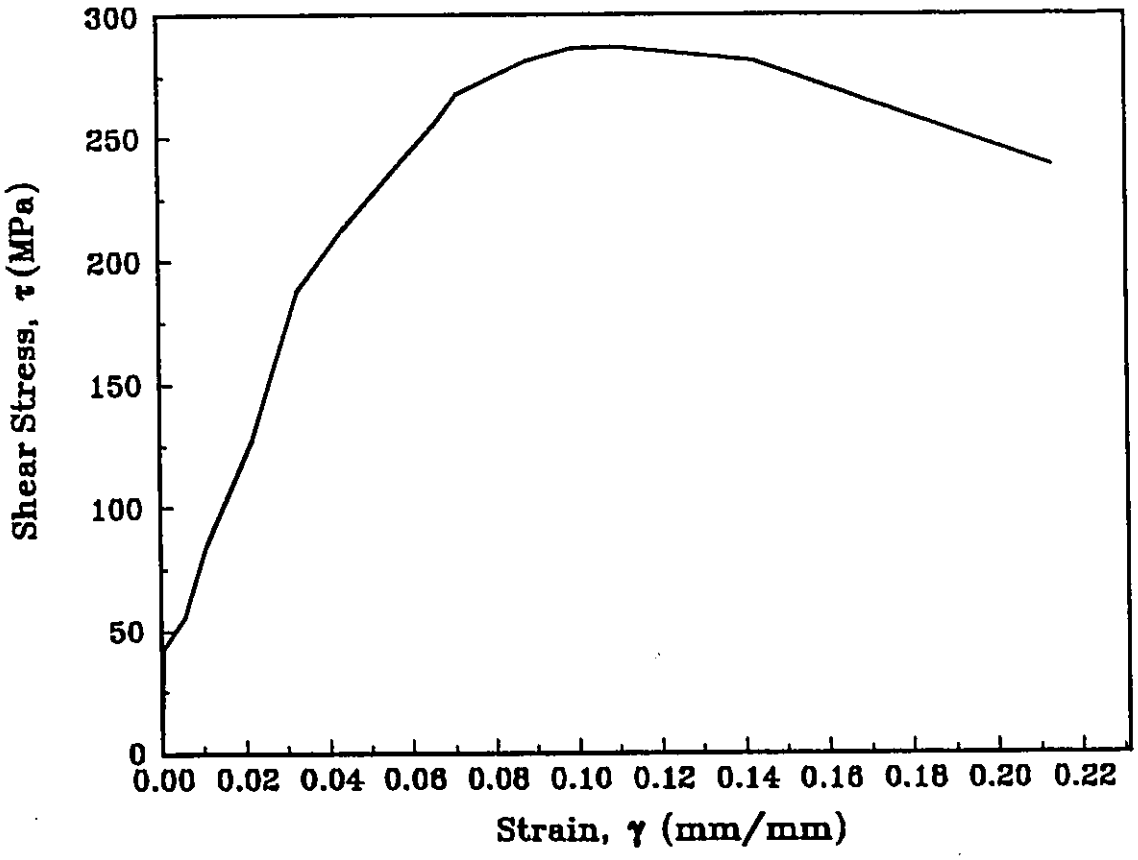

Figure 3.7 Shear stress-strain relationship of the rivet of 3/4" diameter

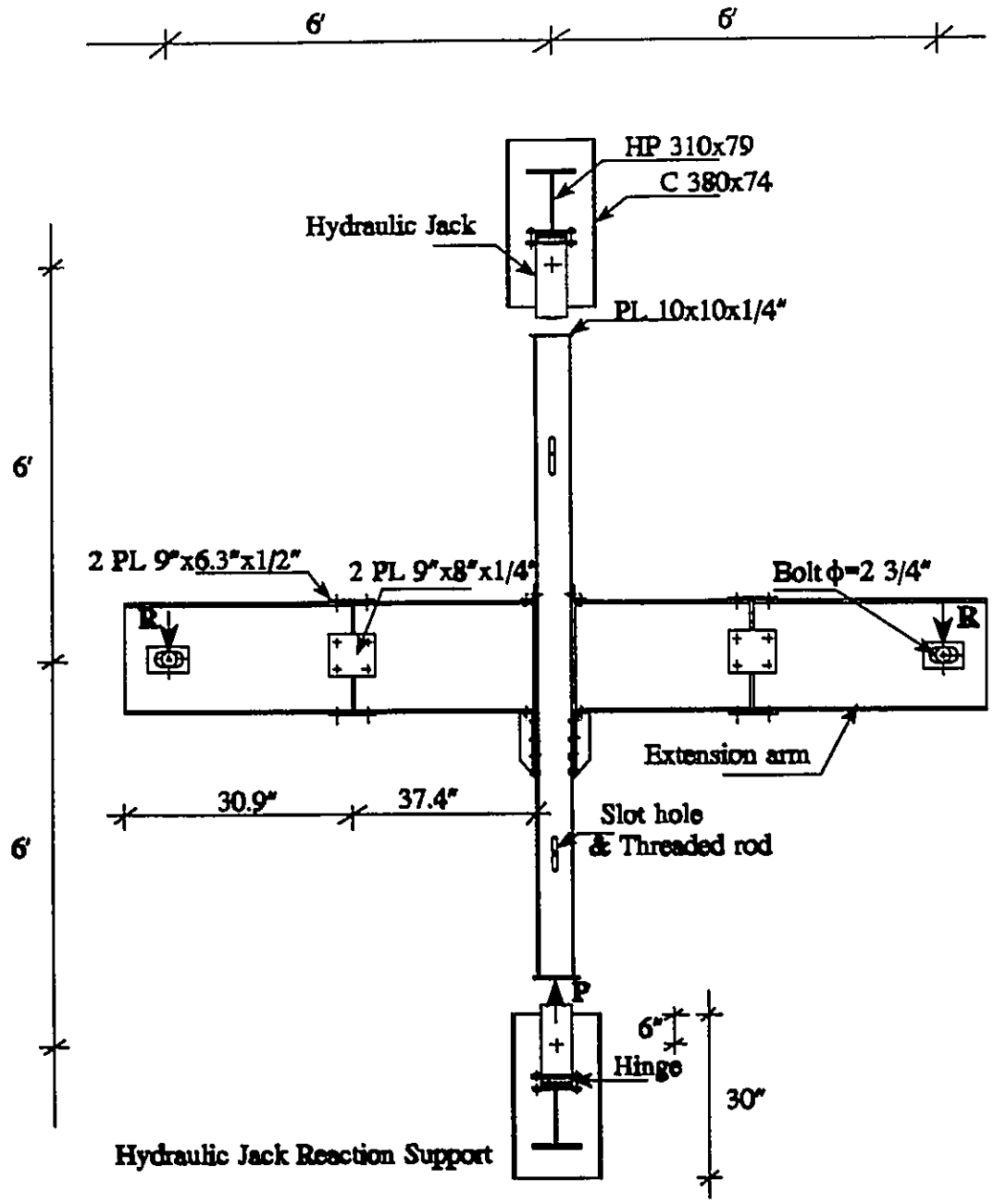

Figure 3.8 Connection detail 1 and the test set-up

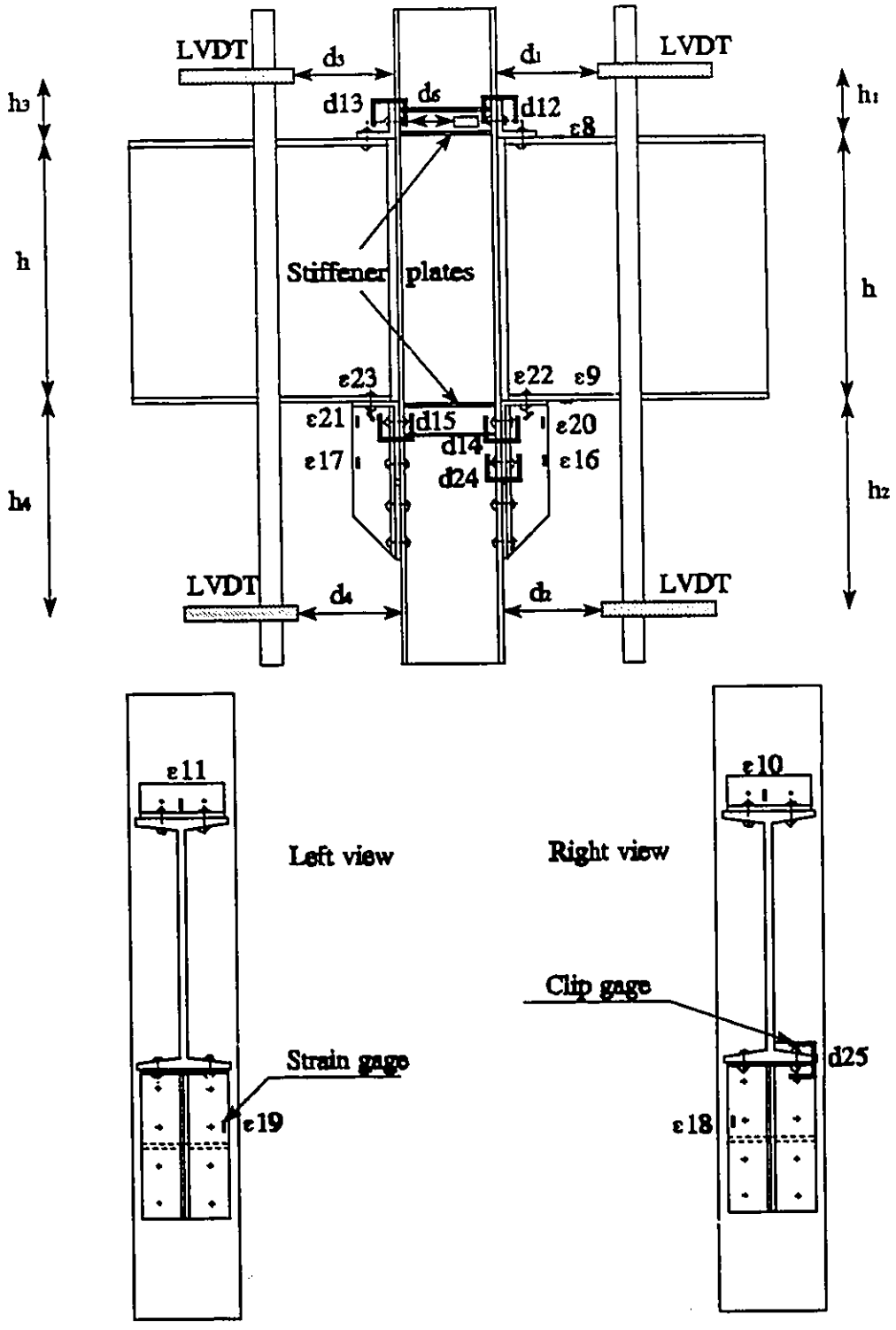

Figure 3.9 Instrumentations in specimen 1 and 2

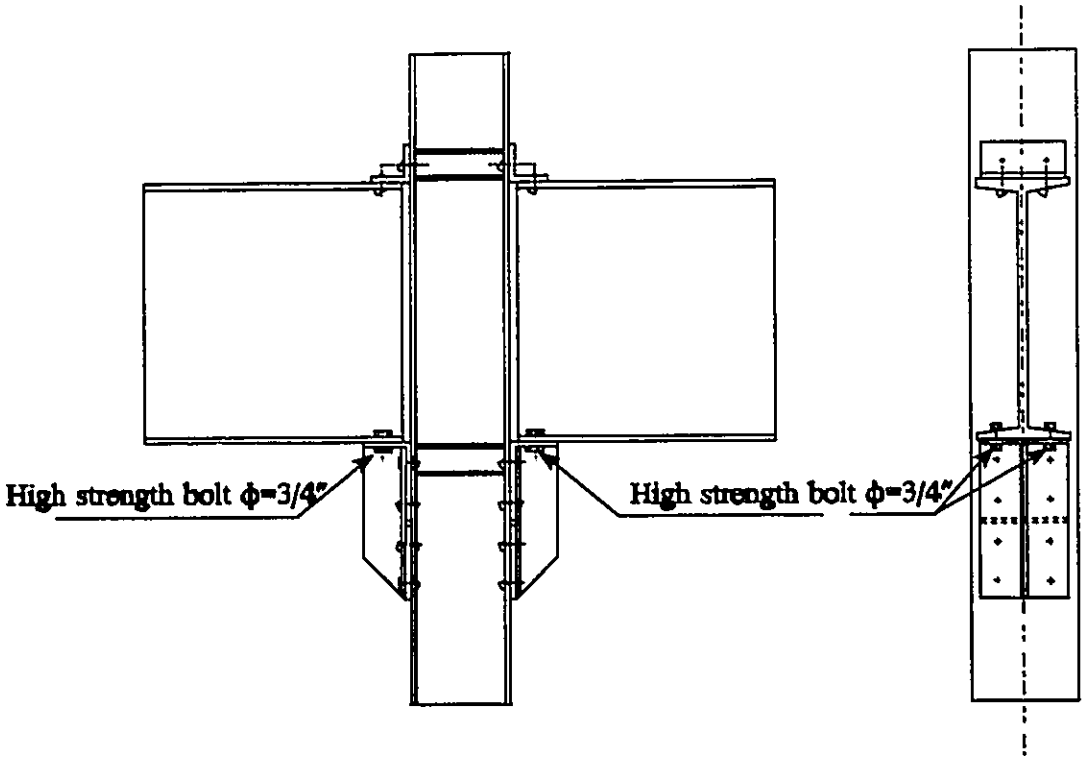

Figure 3.10 Connection detail 1 used for Specimen 2 and location of high strength bolts

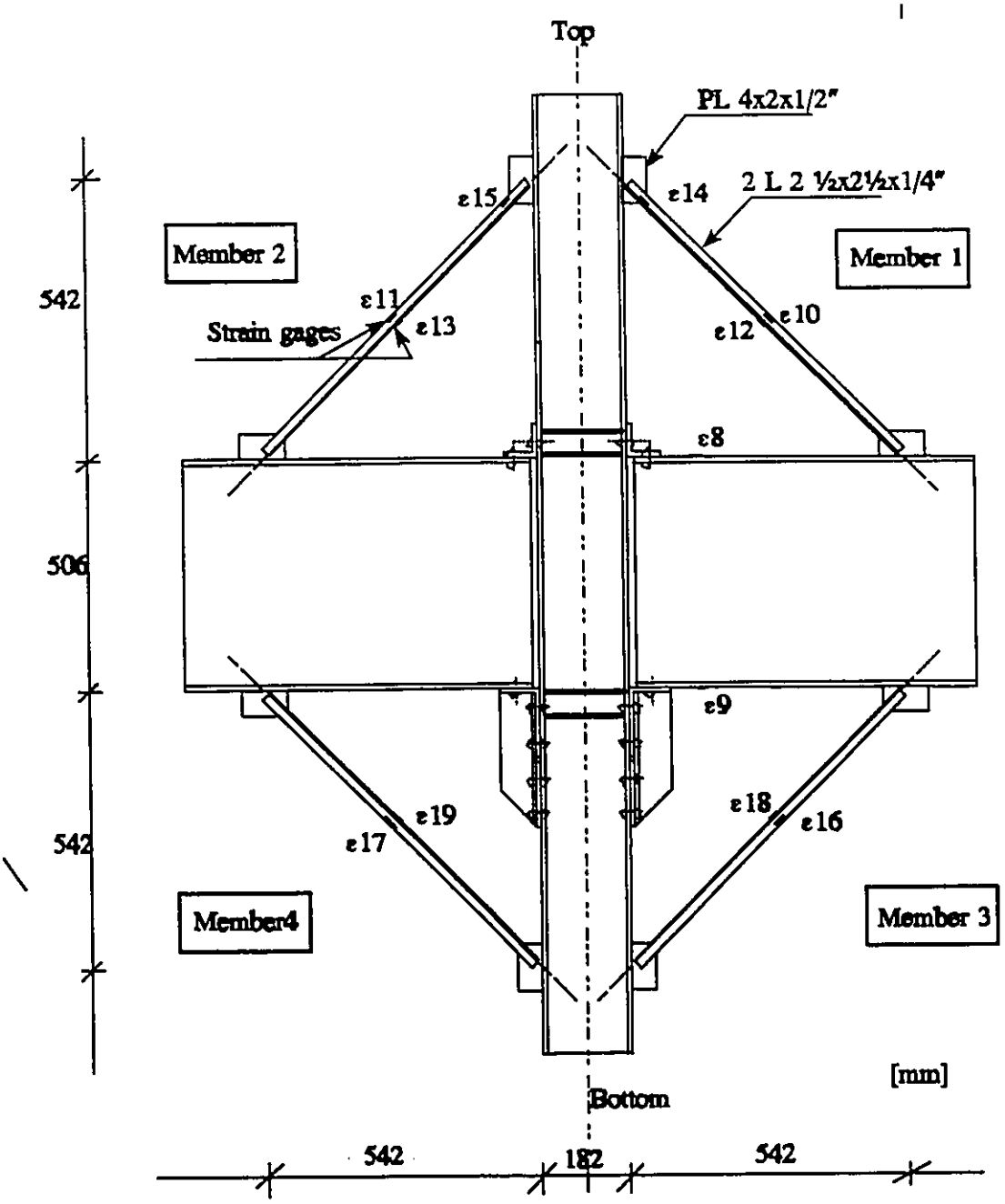

Figure 3.11 Knee braces and location of strain gages

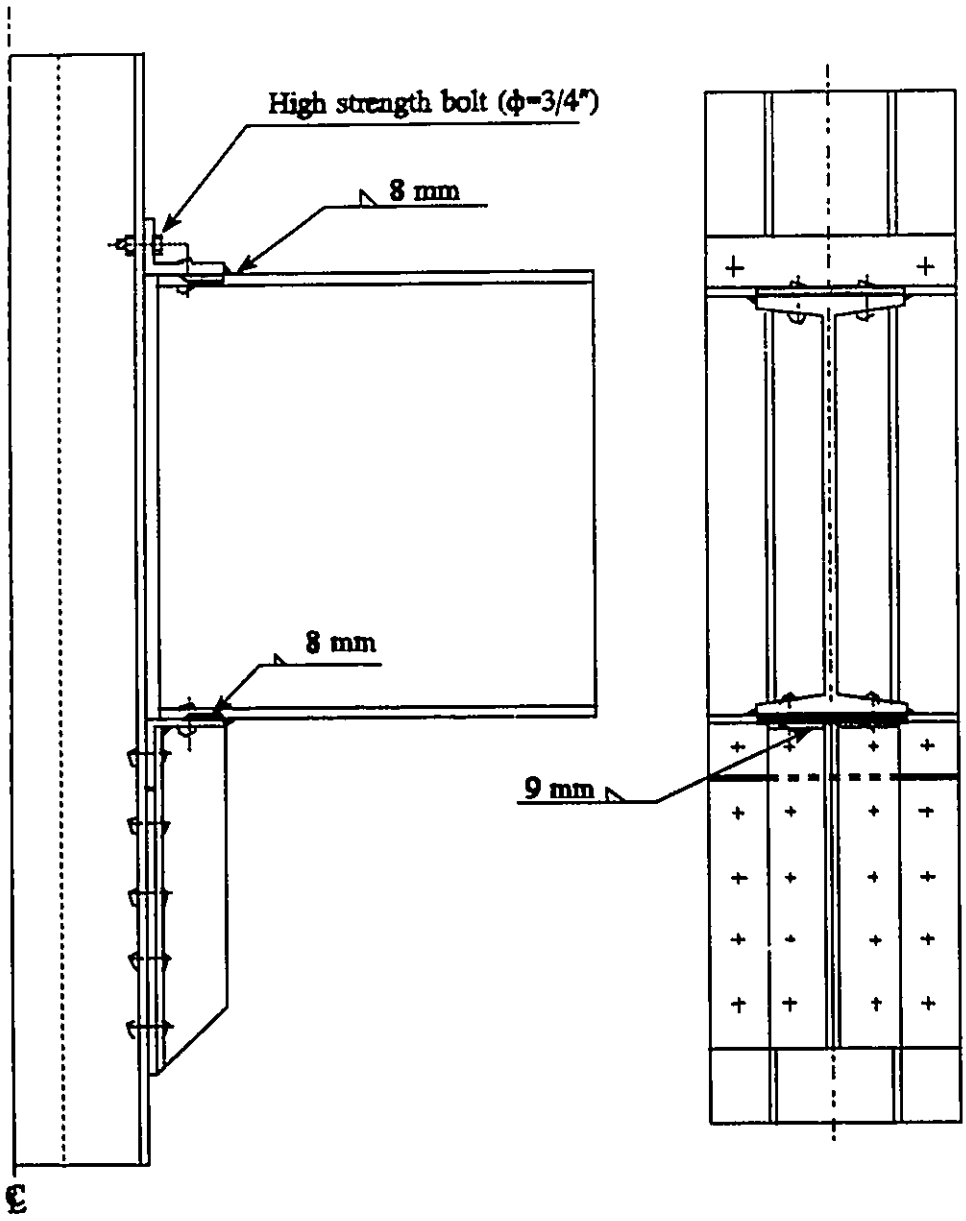

Figure 3.12 Weldings and location of high strength bolts in connection detail 2 used in Specimen 4

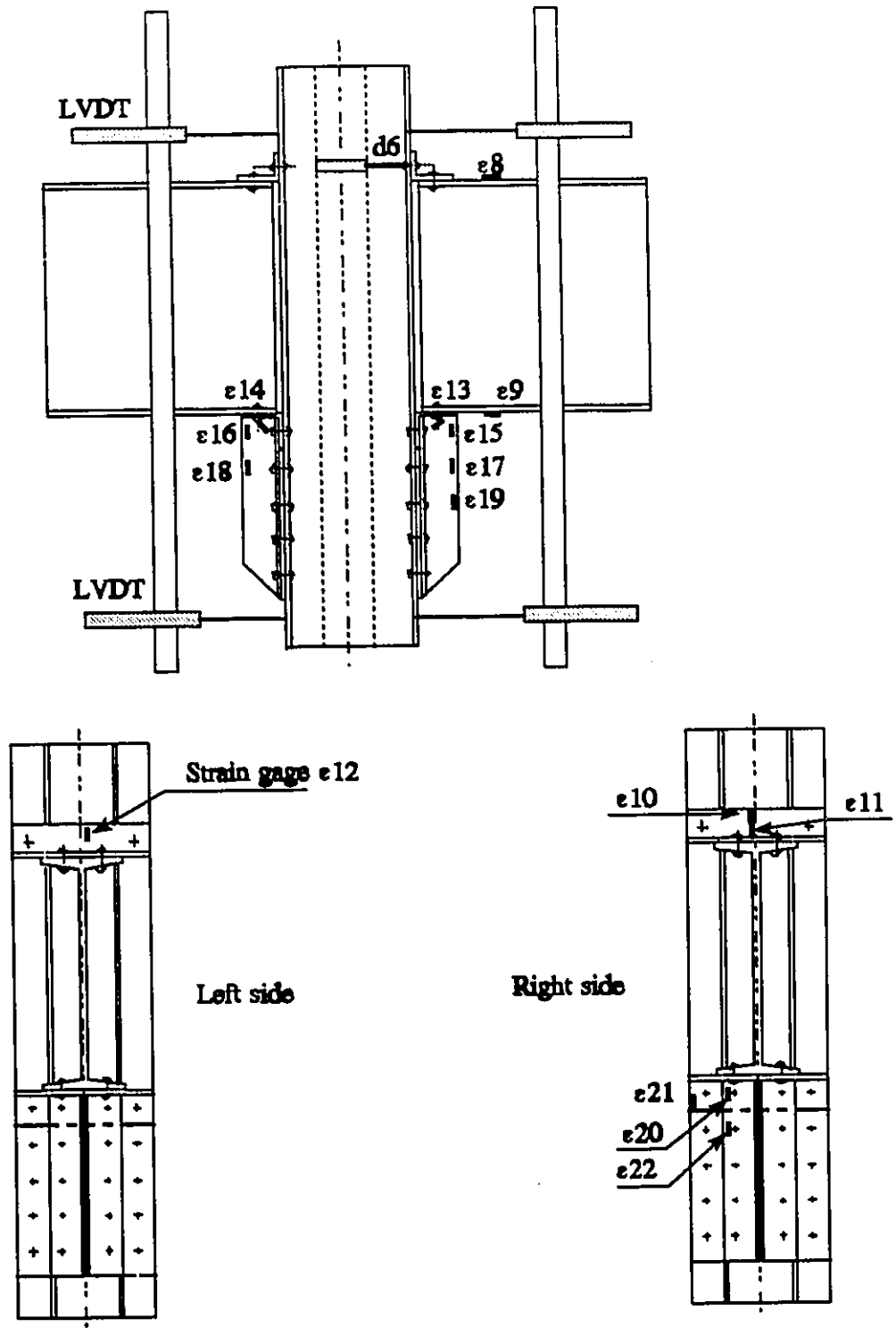

Figure 3.13 Location of strain gages in connection detail 2 (Specimen 4)

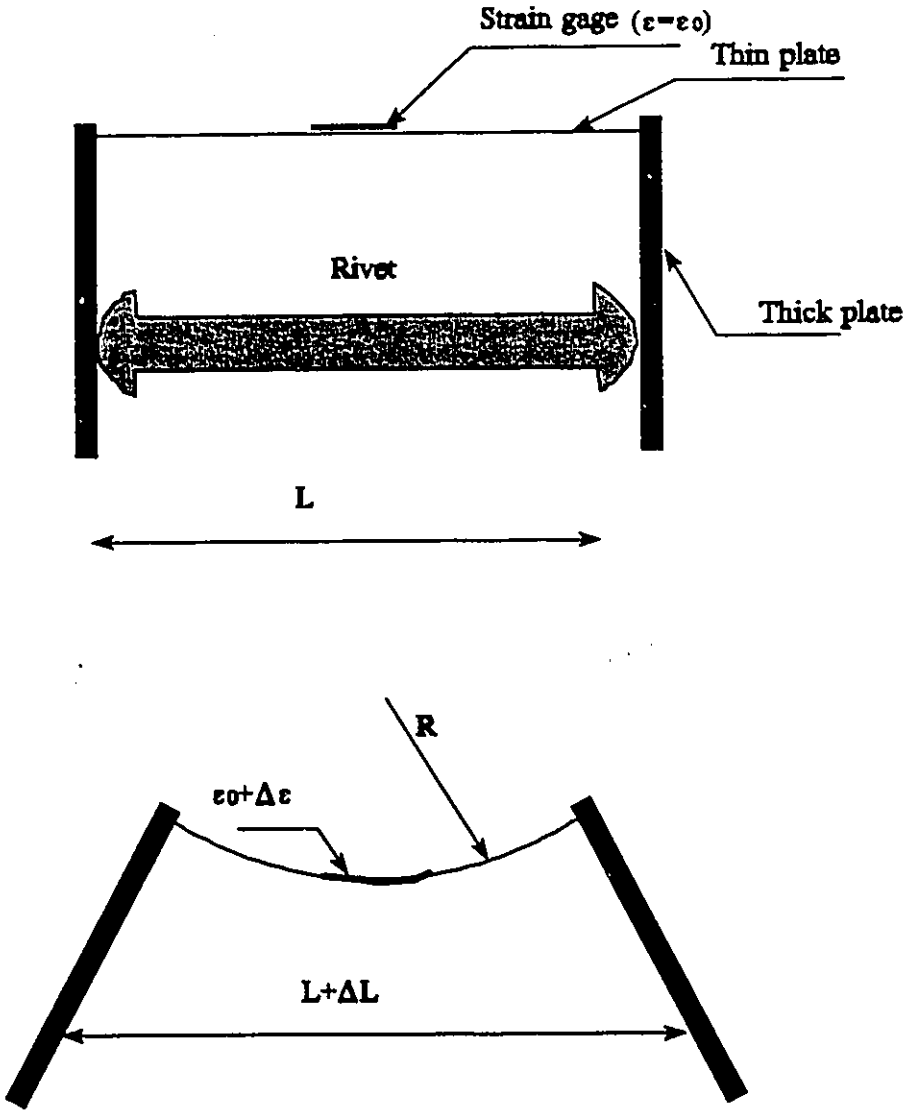

Figure 3.14 Clip gage and measuring elongation of a rivet

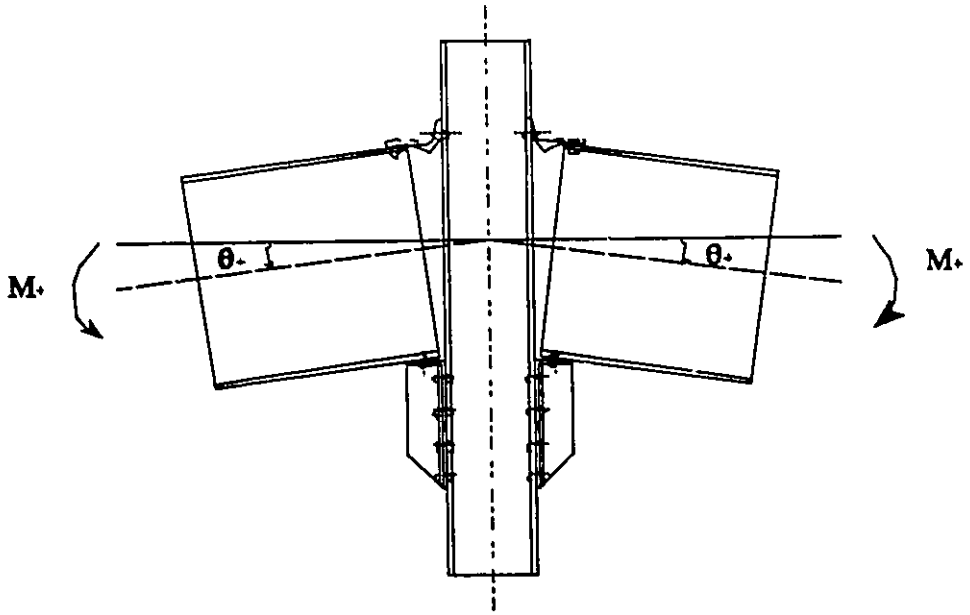

Positive moment and rotation

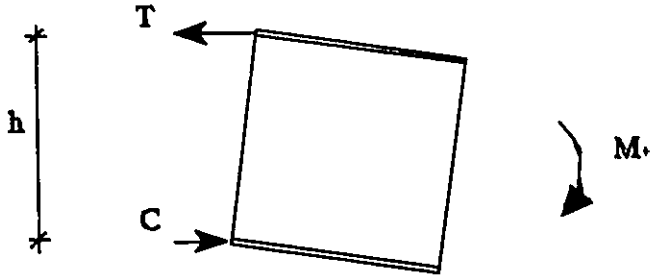

Free body diagram of the beam

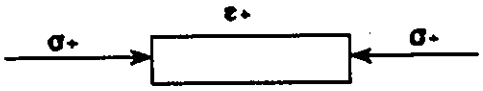

Positive stress and strain

Figure 4.1 Sign conventions

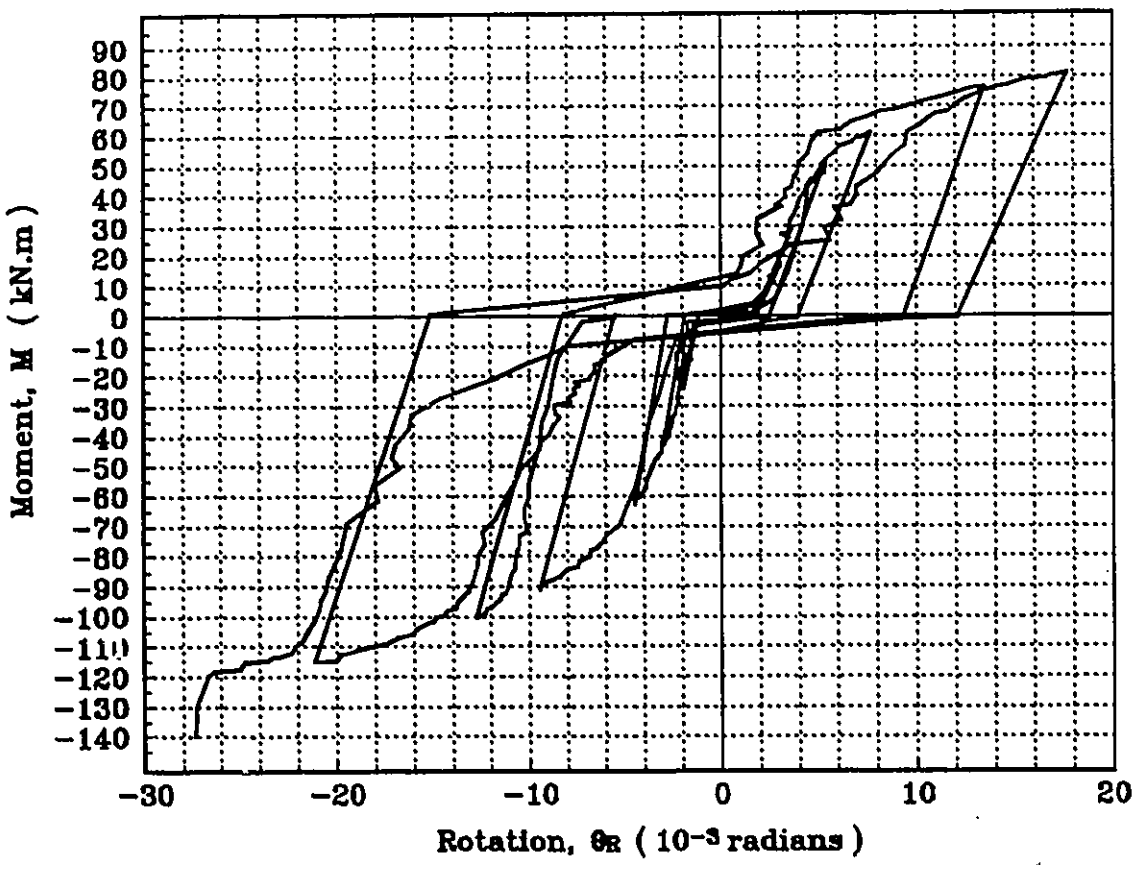

Figure 4.2 M-θ relationship of specimen 1 at the right side

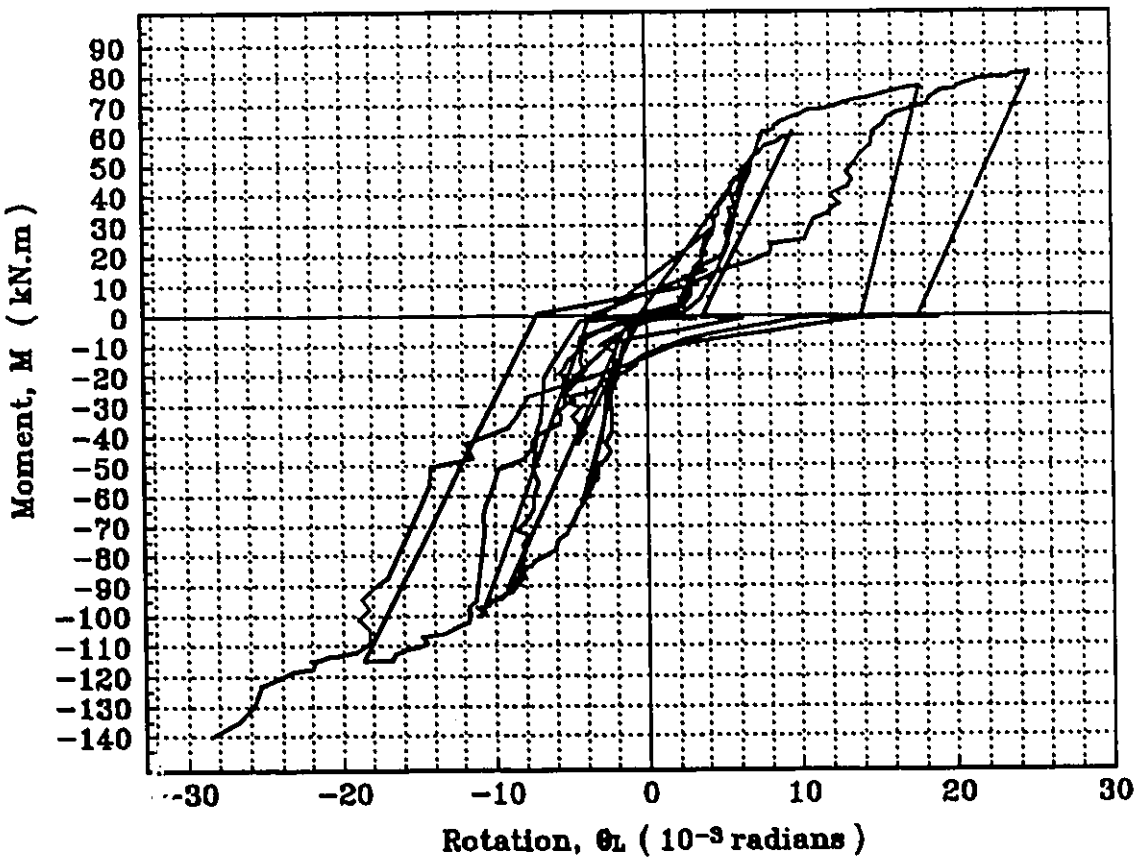

Figure 4.3 M-θ relationship of specimen 1 at the left side

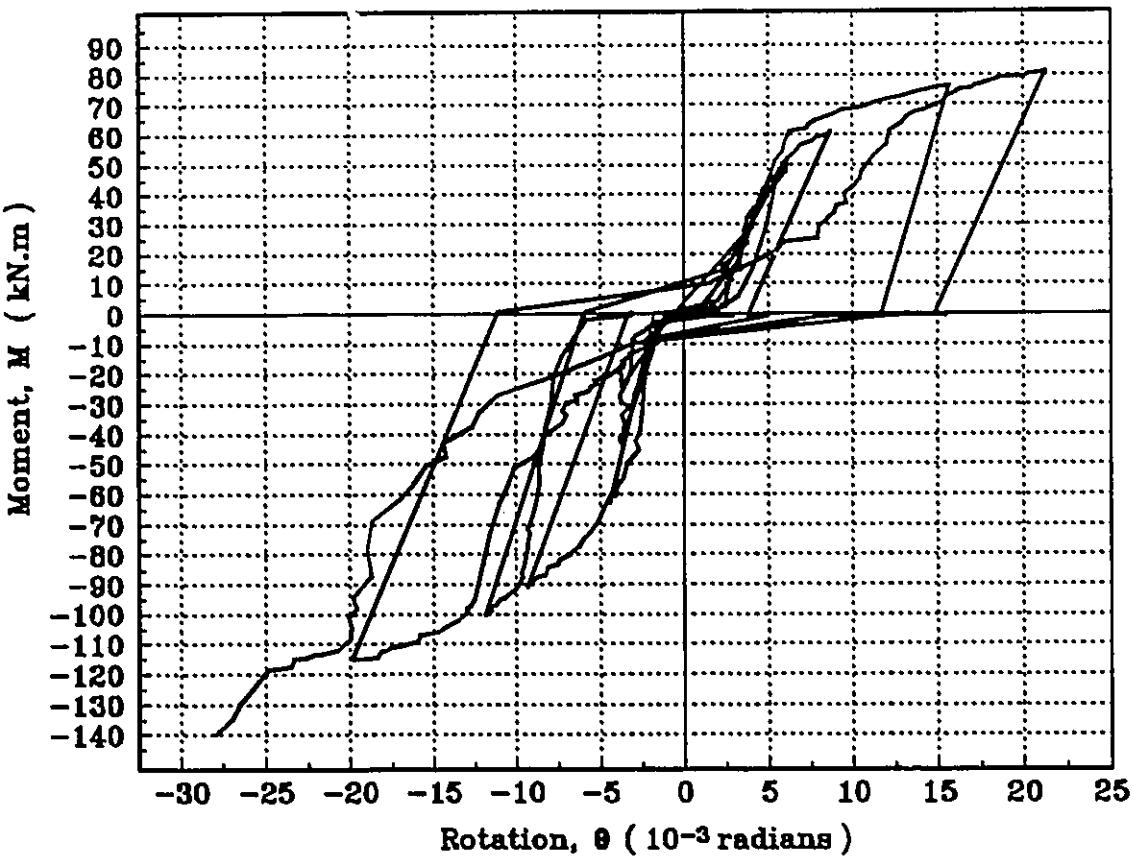

Figure 4.4 M-θ relationship based on average results for connection detail 1, specimen 1

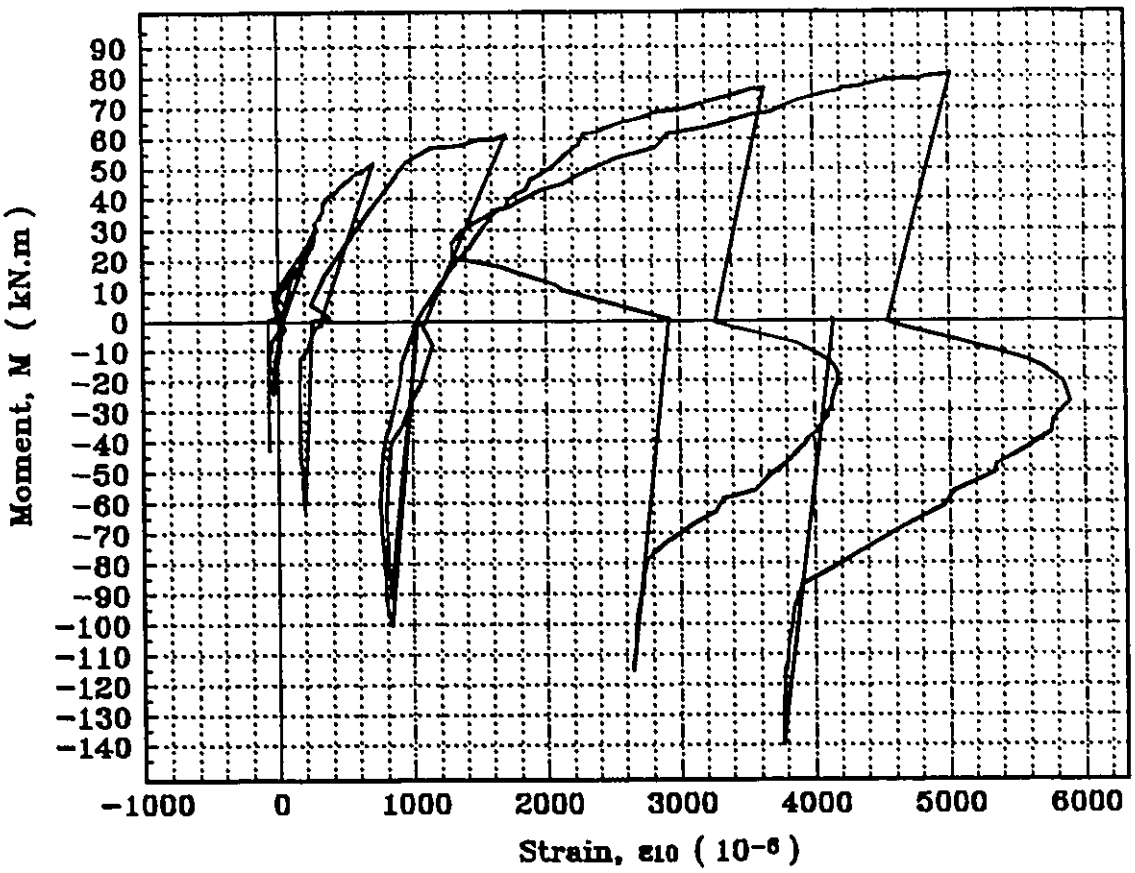

Figure 4.5 Moment-strain relationship for strain gage ε10 of the connection detail 1, specimen 1

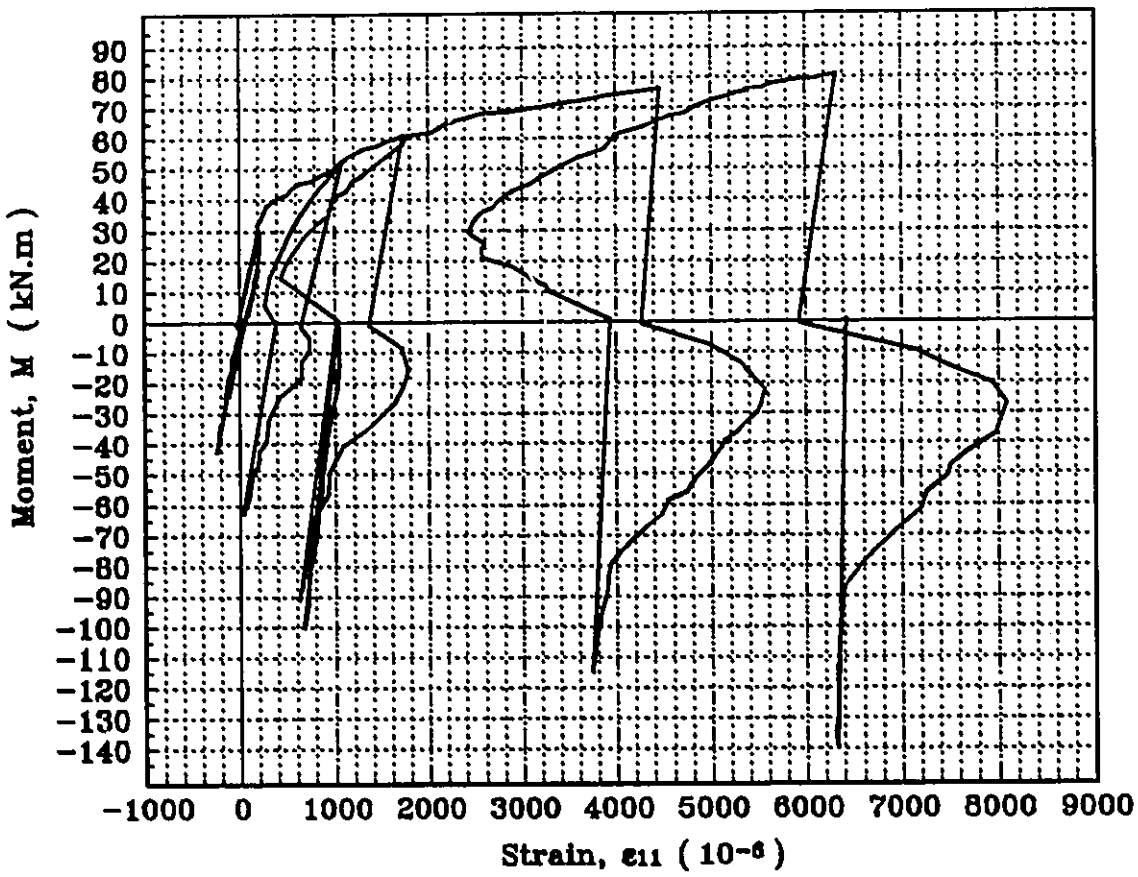

Figure 4.6 Moment-strain relationship for strain gage ε11 of the connection detail 1, specimen 1 .

Figure 4.7 Top angle closes the gap between heel and column face, specimen 1

Figure 4.8 Top angle maximum deformation in experiment 1

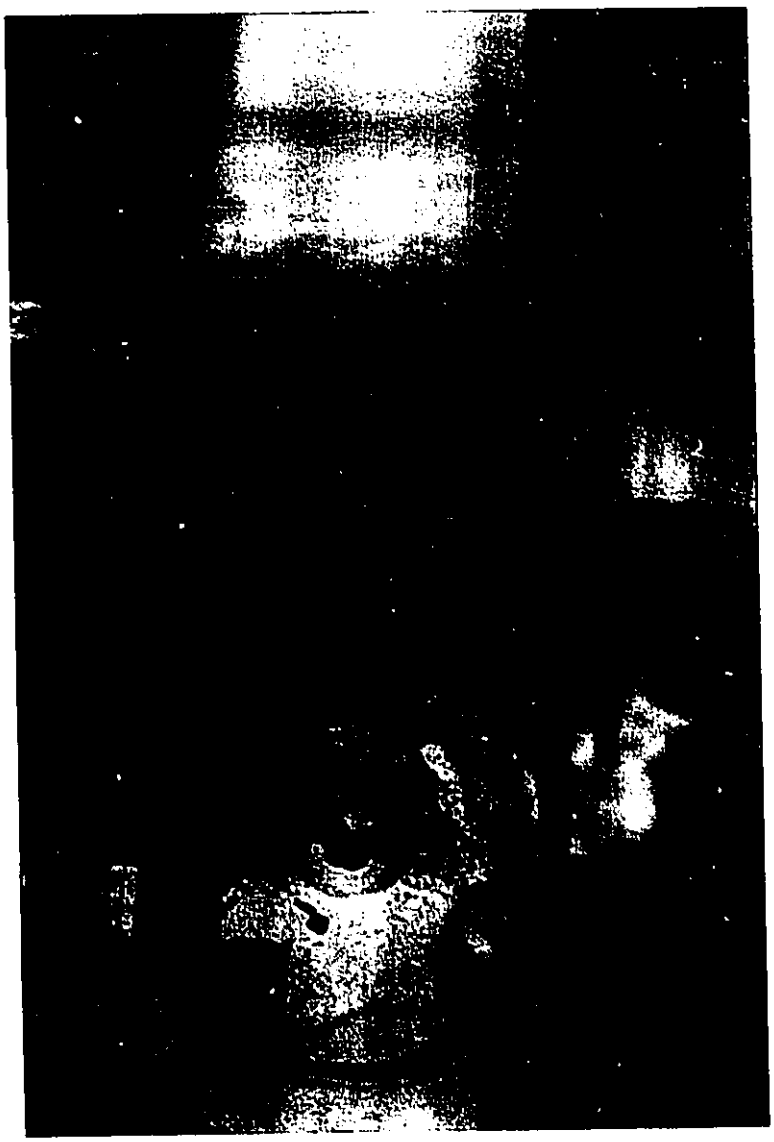

Figure 4.9 Shear failure of rivet and separation of the seat angle from the column face, specimen 1

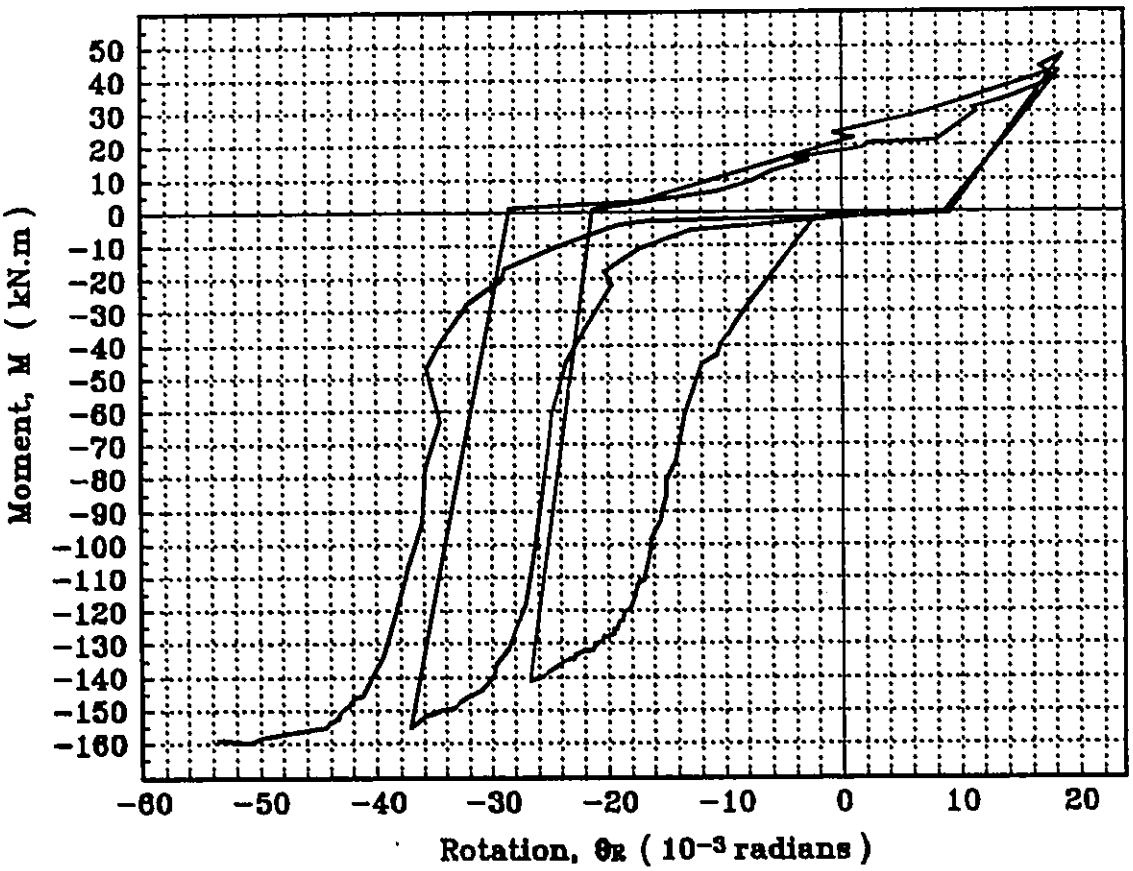

Figure 4.10 M-θ relationship of the connection in the right side the Specimen 2

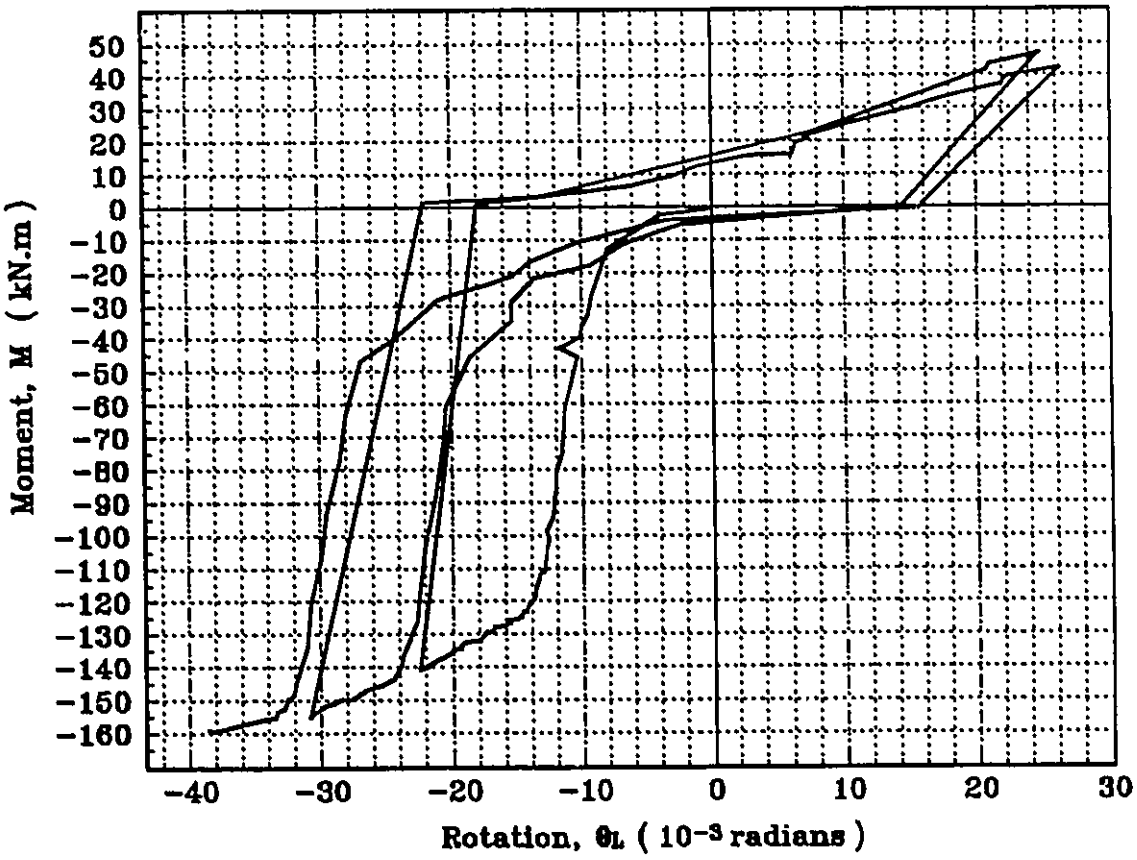

Figure 4.11 M-θ relationship for the connection in the left side of the Specimen 2

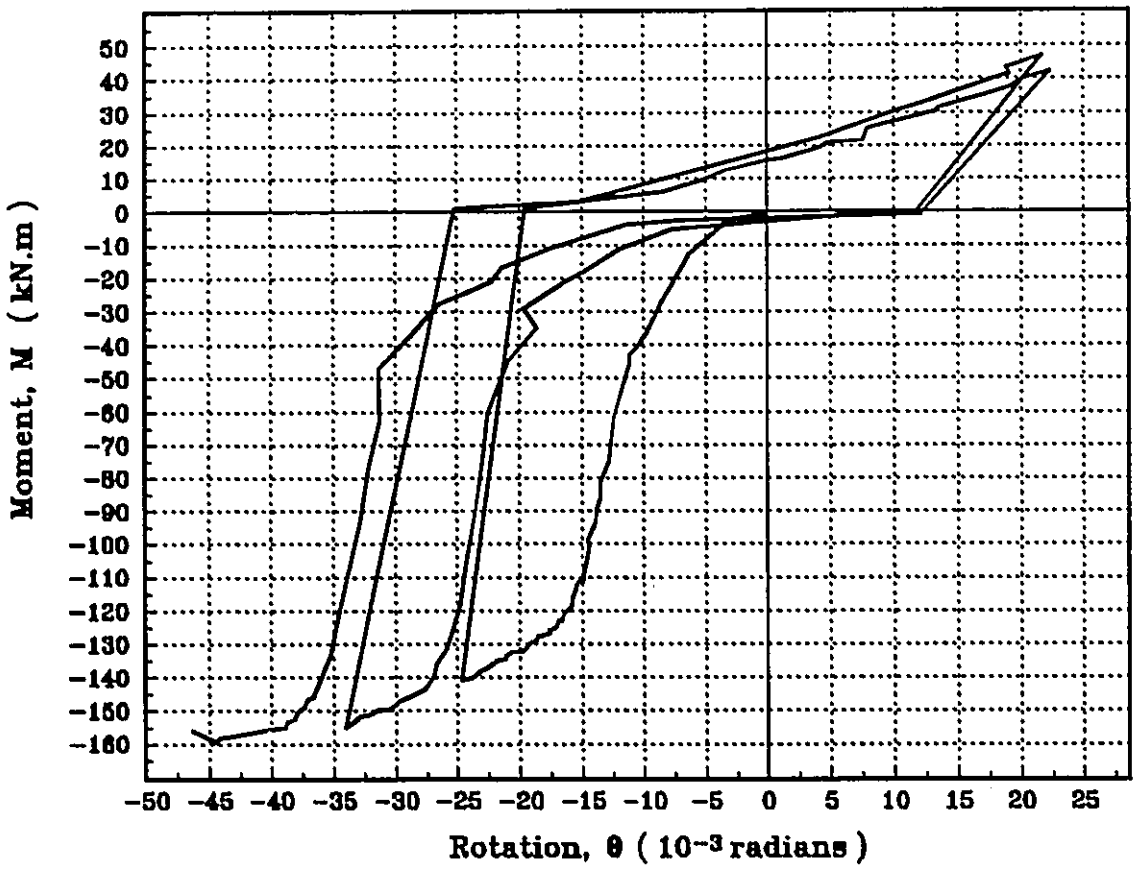

Figure 4.12 Average result of M-θ for Specimen 2

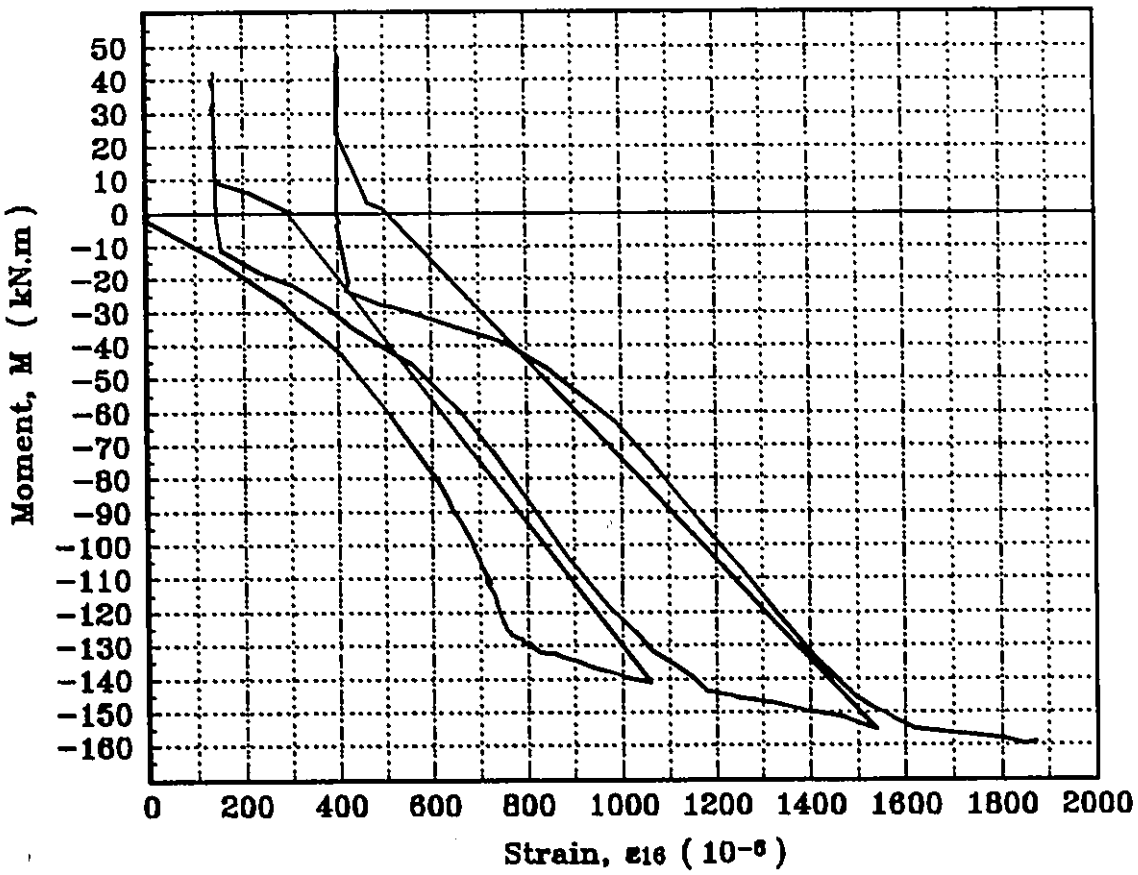

Figure 4.13 Moment-strain relationship of strain gage ε16, specimen 2

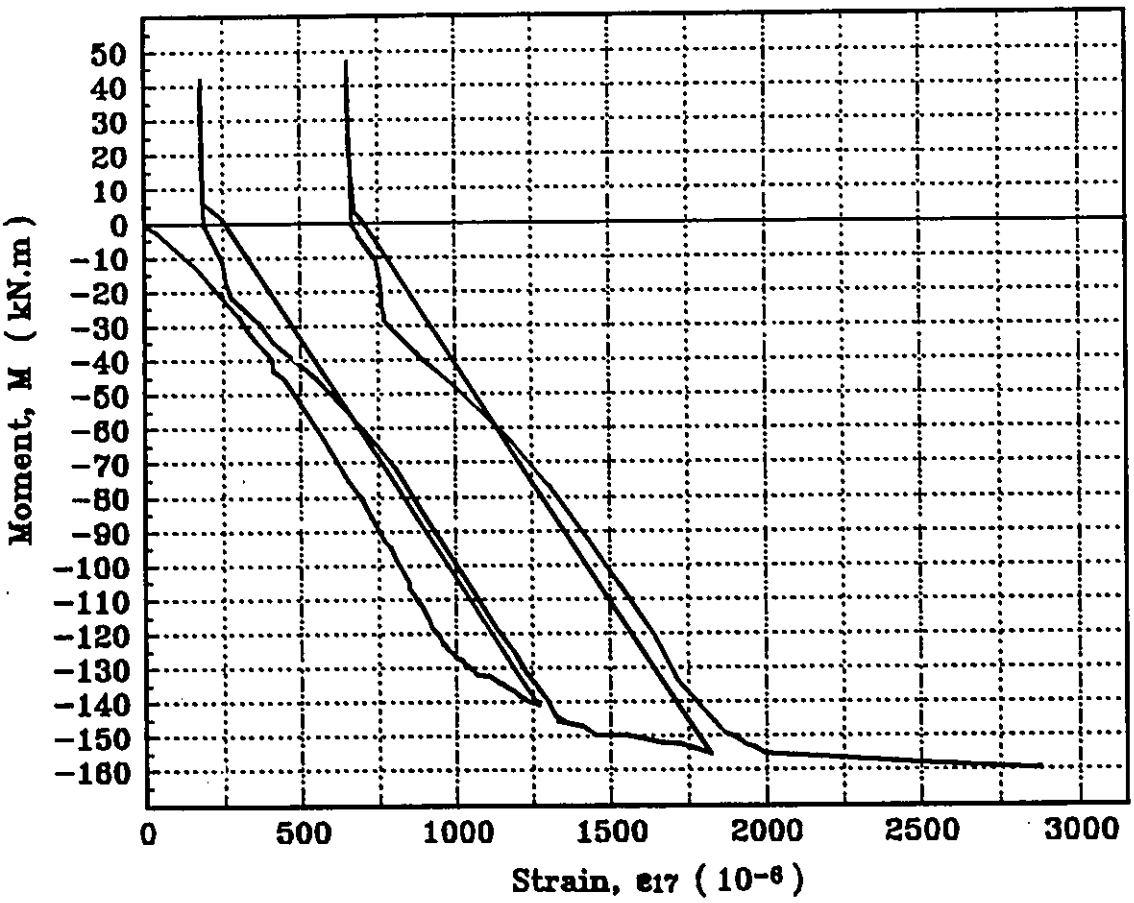

Figure 4.14 Moment-strain relationship of the strain gage ε17, specimen 2

Figure 4.15 Local buckling of the stiffener angles, specimen 2

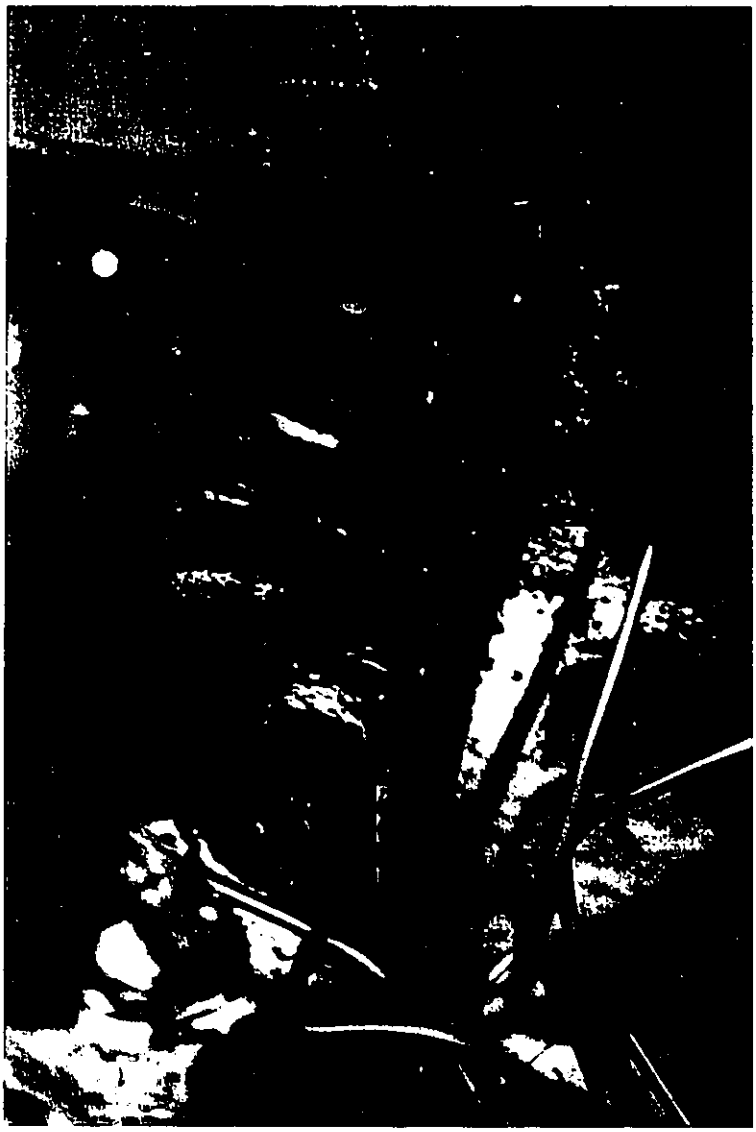

Figure 4.16 Onset of bearing failure, specimen 2

Figure 4.17 Bearing failure, specimen 2

Figure 4.18 Maximum deformation of seat angle and stiffener angles in experiment 2

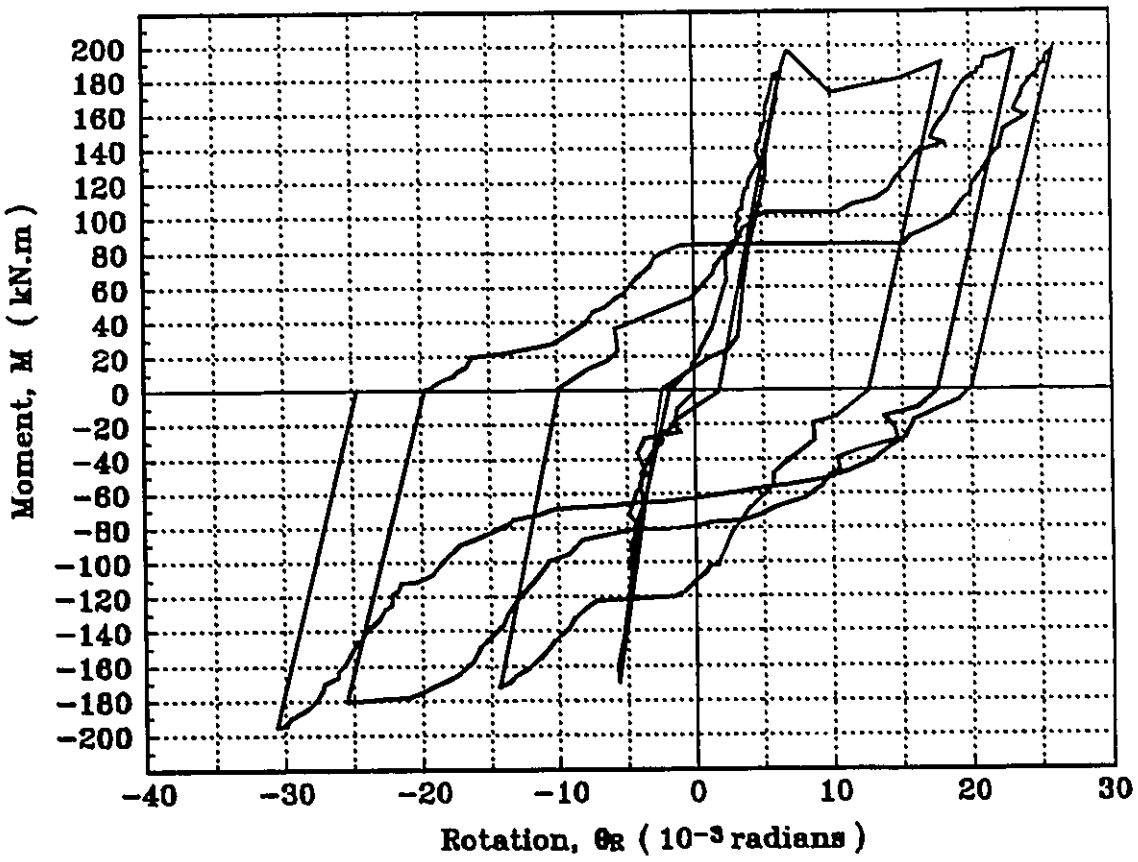

Figure 4.19 M-θ relationship of the knee braces in the right side of the Specimen 3

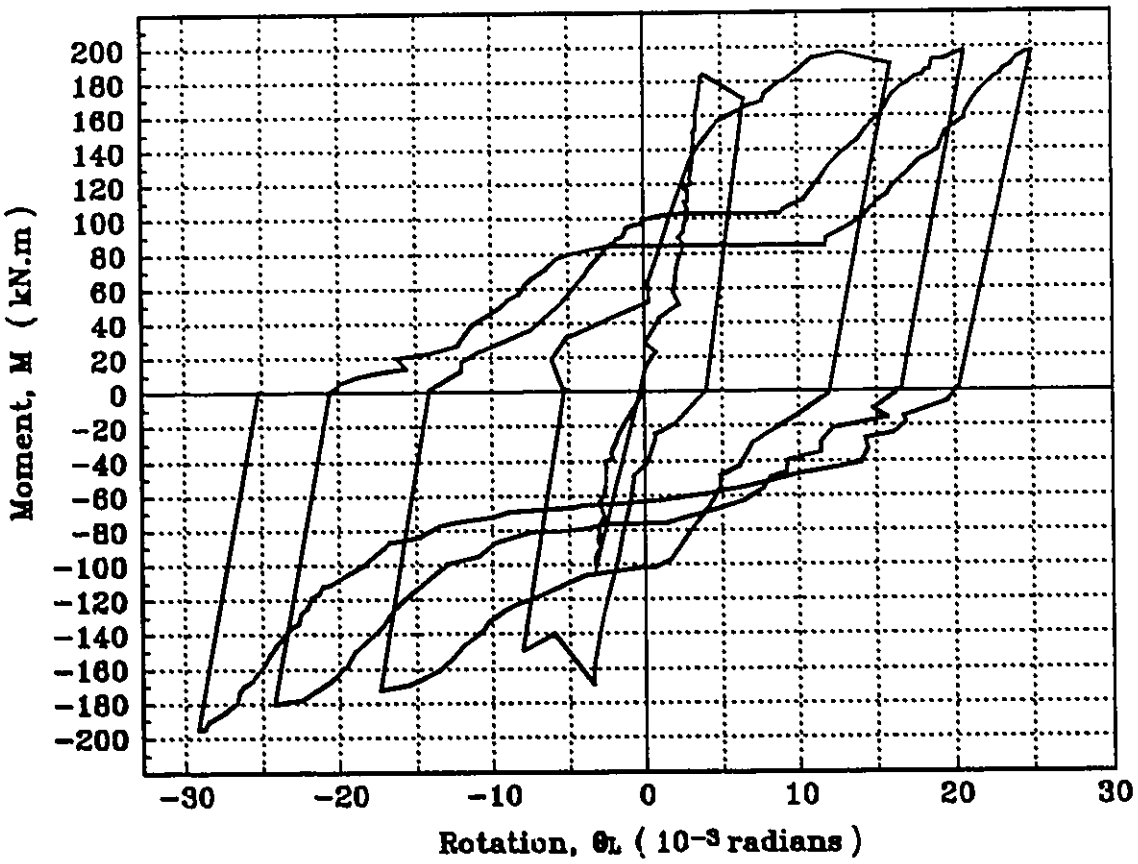

Figure 4.20 M-θ relationship of the knee braces in the left side of the Specimen 3

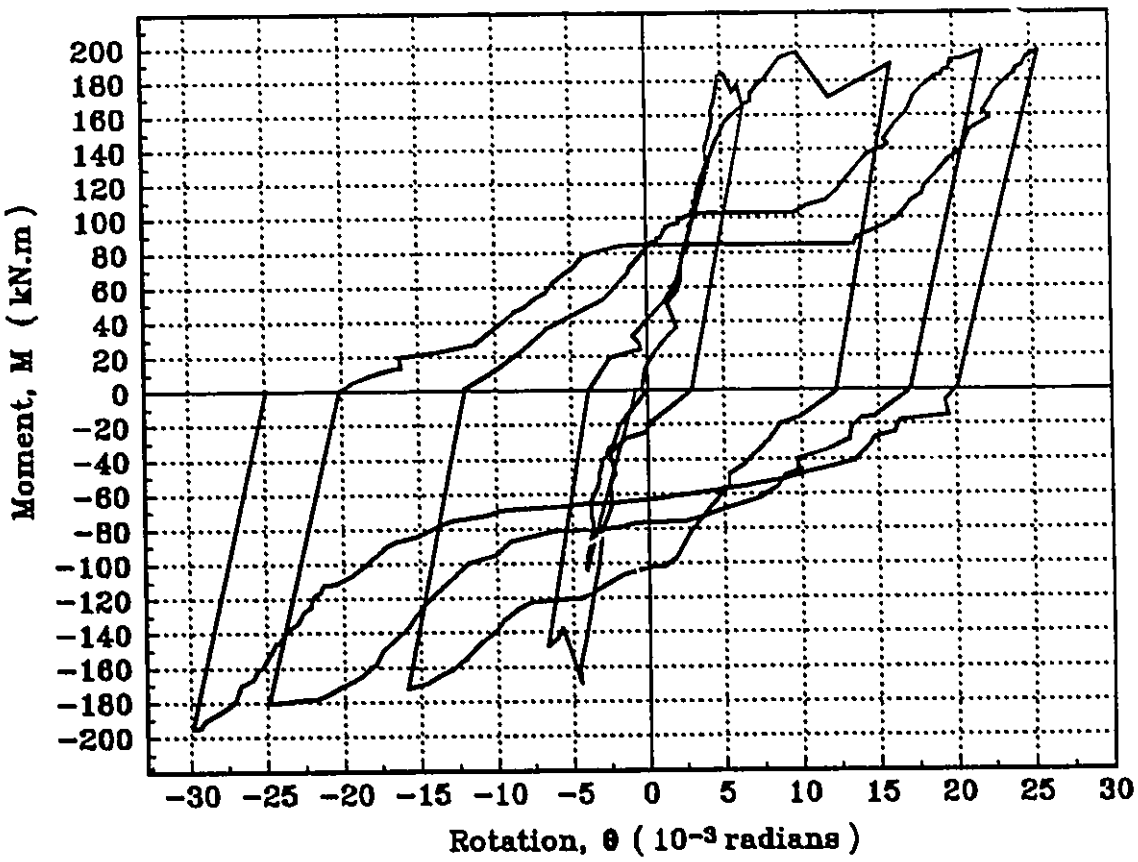

Figure 4.21 Average result of M-θ for knee braces in Specimen 3

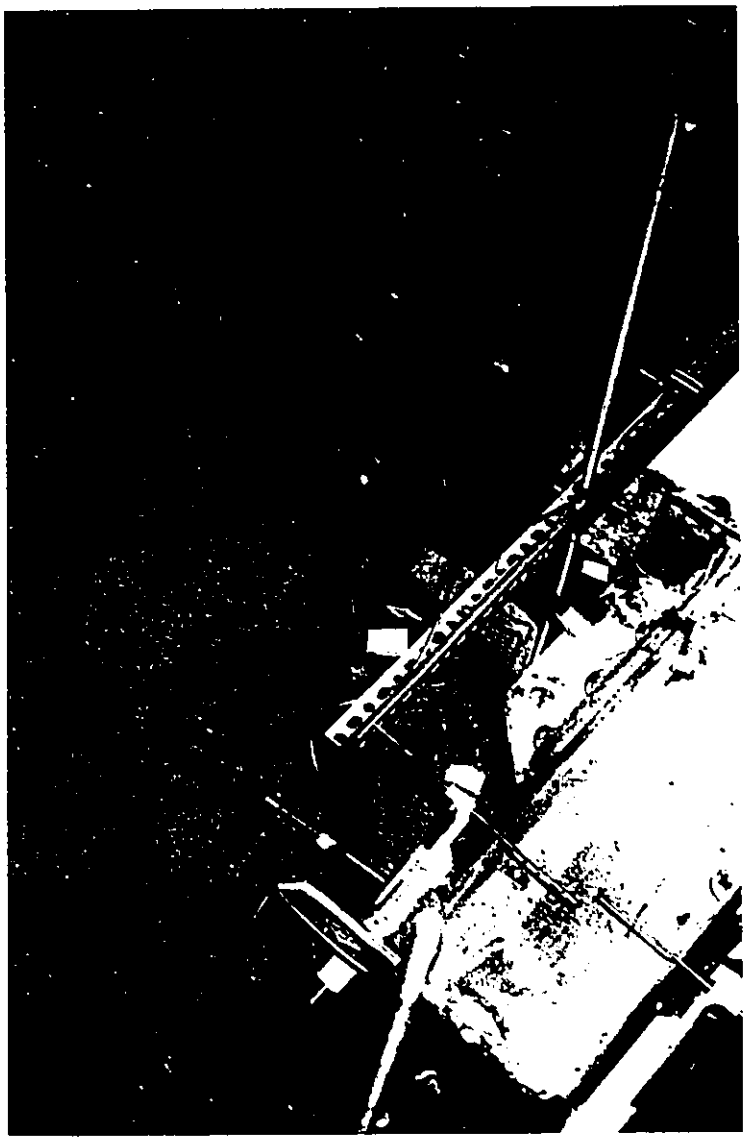

Figure 4.22 Member 4 buckled, specimen 3

Figure 4.23 Member 2 buckled, specimen 3

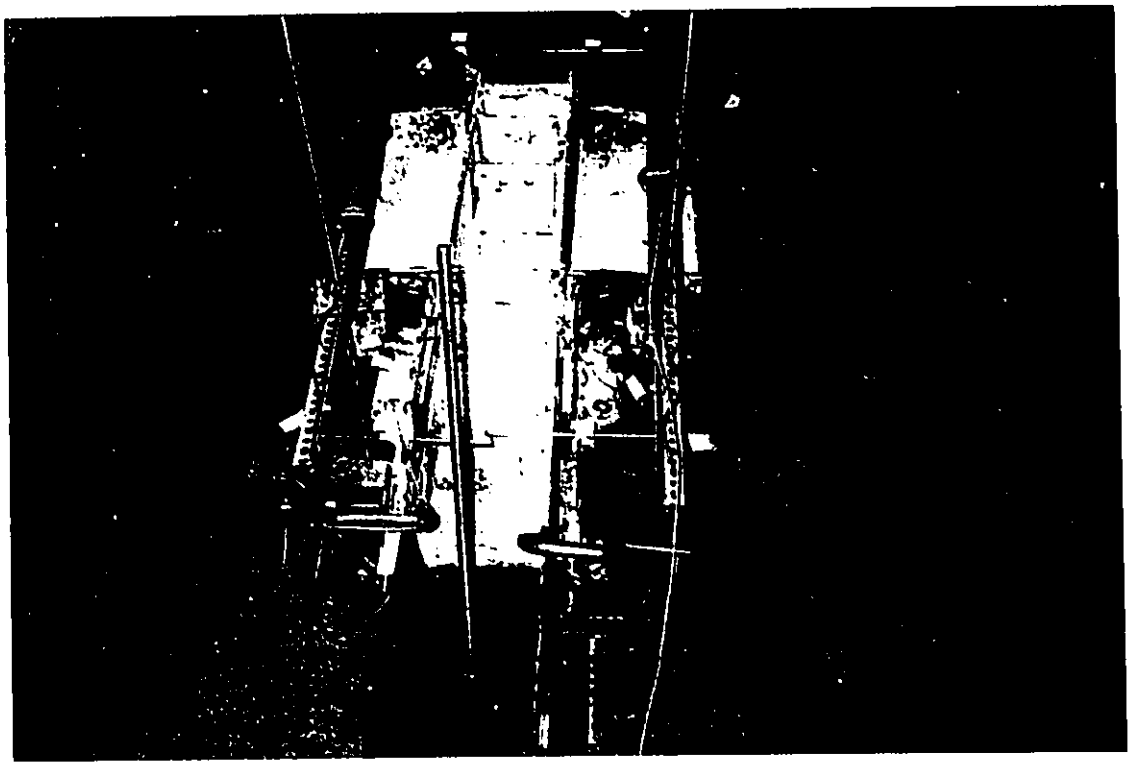

Figure 4.24 Member 3 buckled and Member 4 buckled for the second time, specimen 3

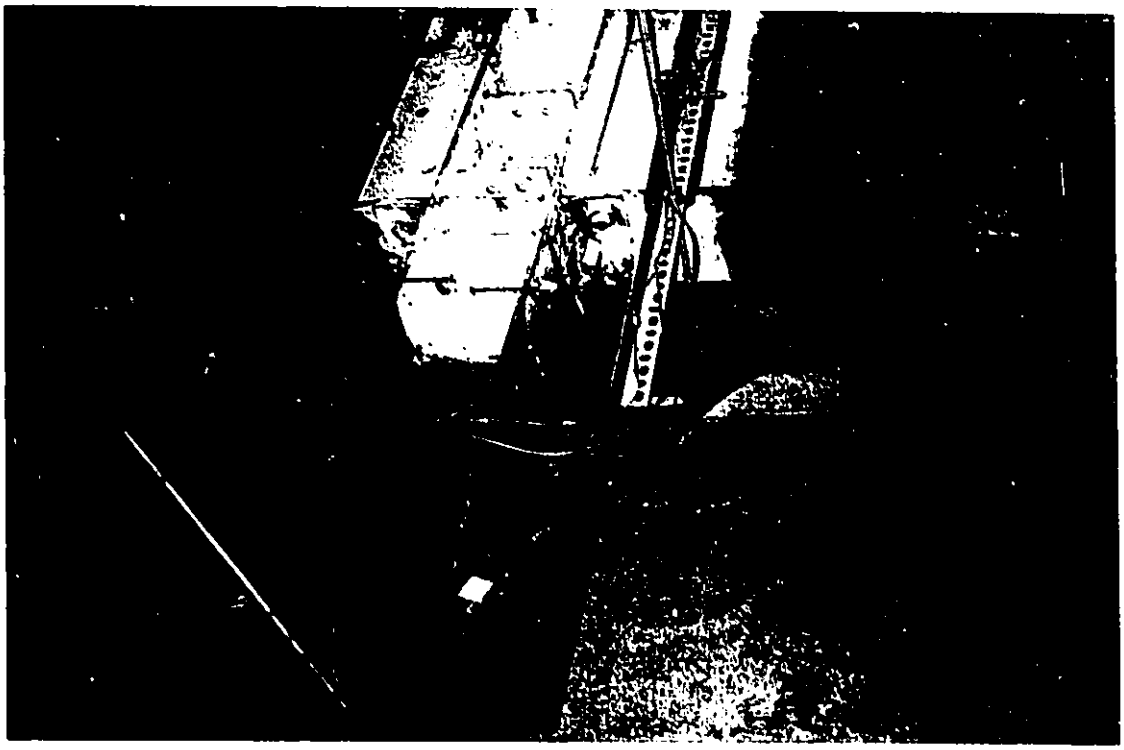

Figure 4.25 Member 1 buckled (first time) and Member 2 buckled (second time), specimen 3

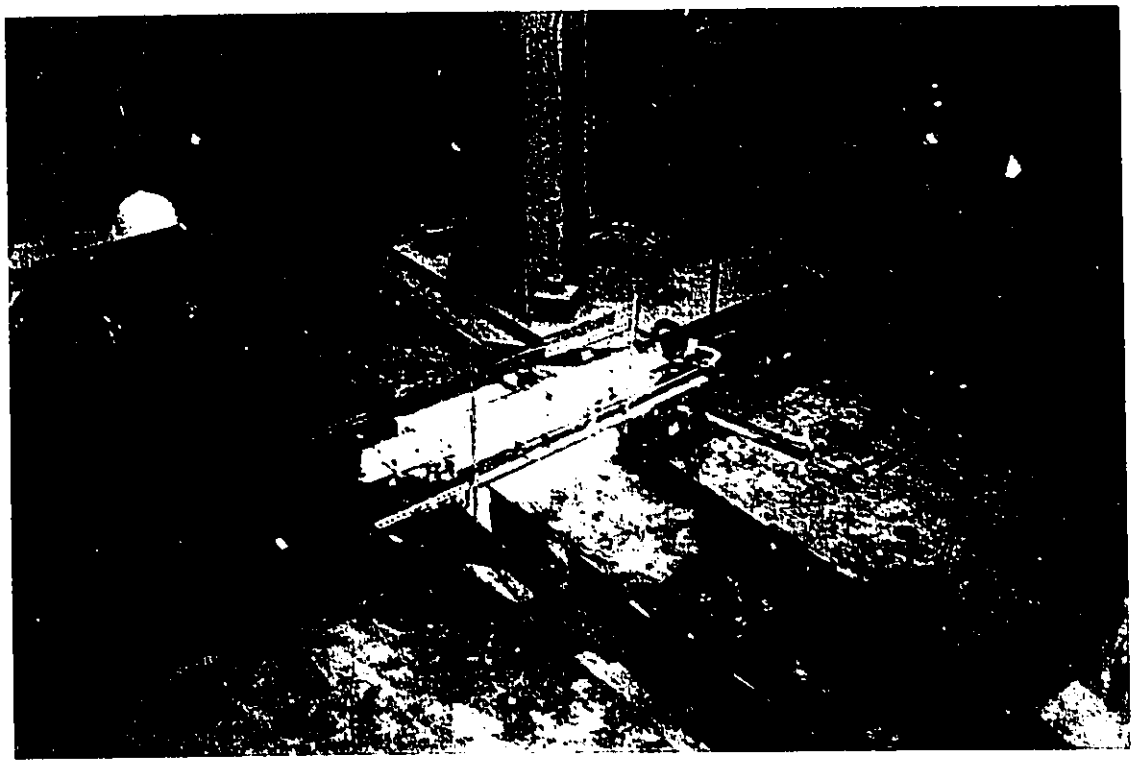

Figure 4.26 All knee braces are in buckled shape while the beams and columns are at their original position, specimen 2

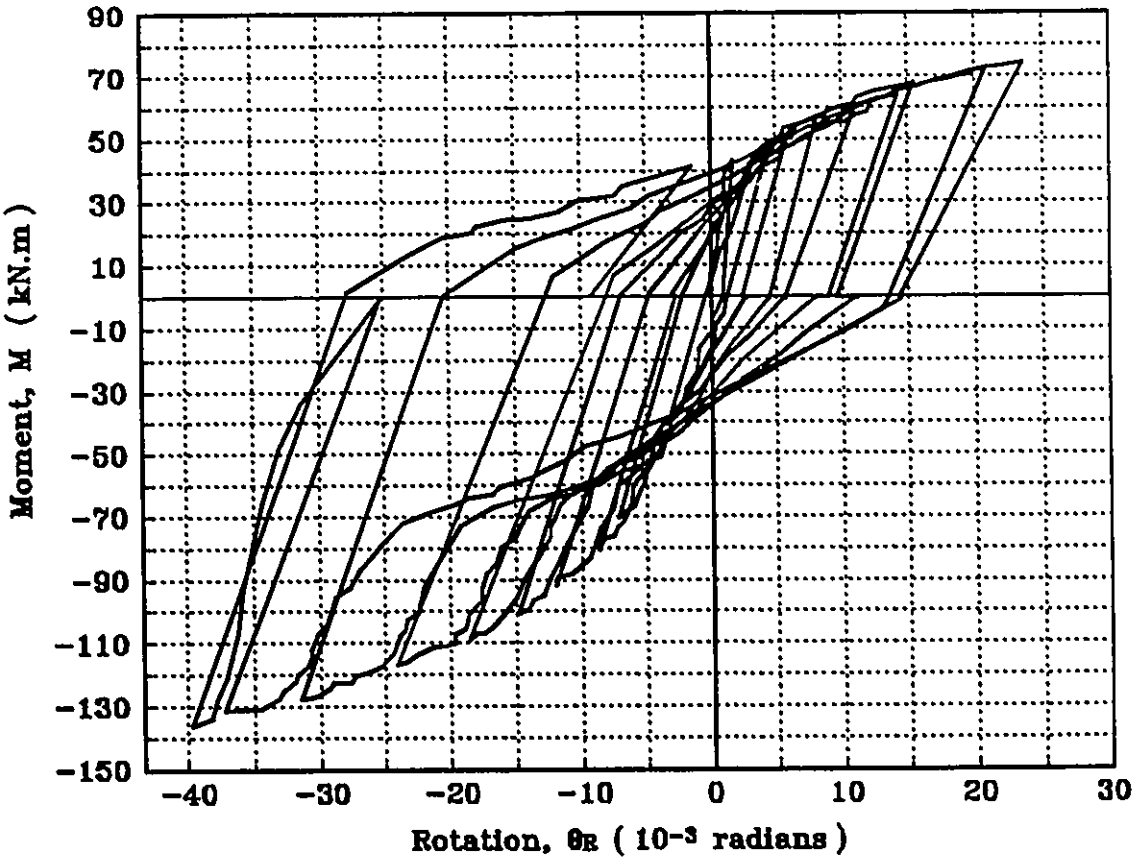

Figure 4.27 M-θ relationship for connection in the right side of the Specimen 4

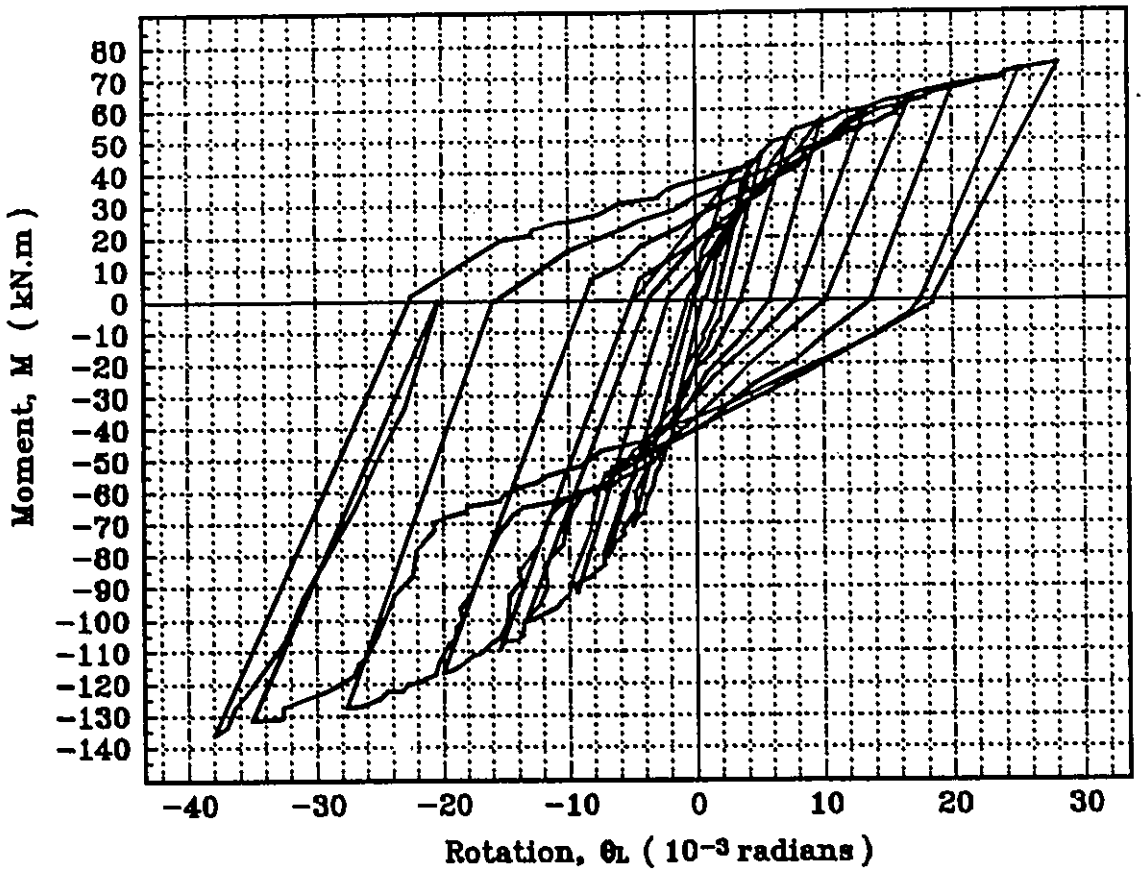

Figure 4.28 M-θ relationship of the connection in the left side of Specimen 4

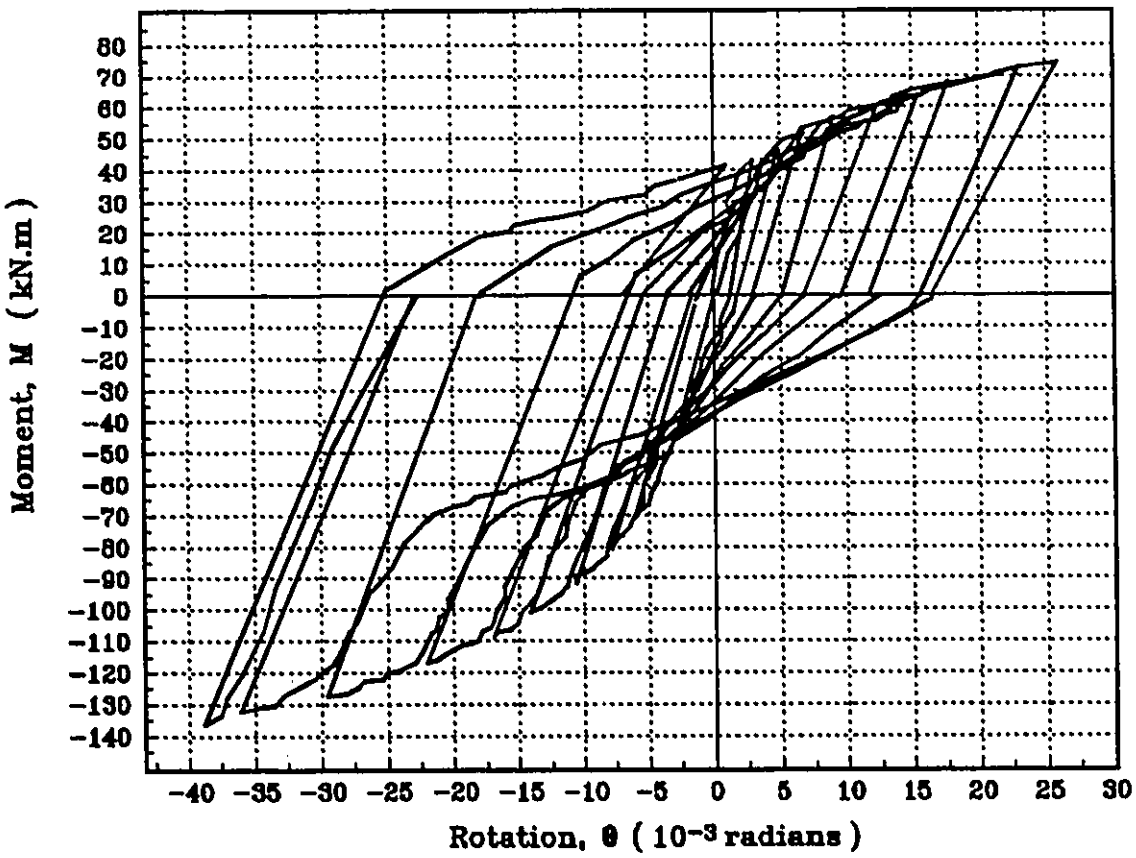

Figure 4.29 Average result of M-θ for connection detail 2, specimen 4

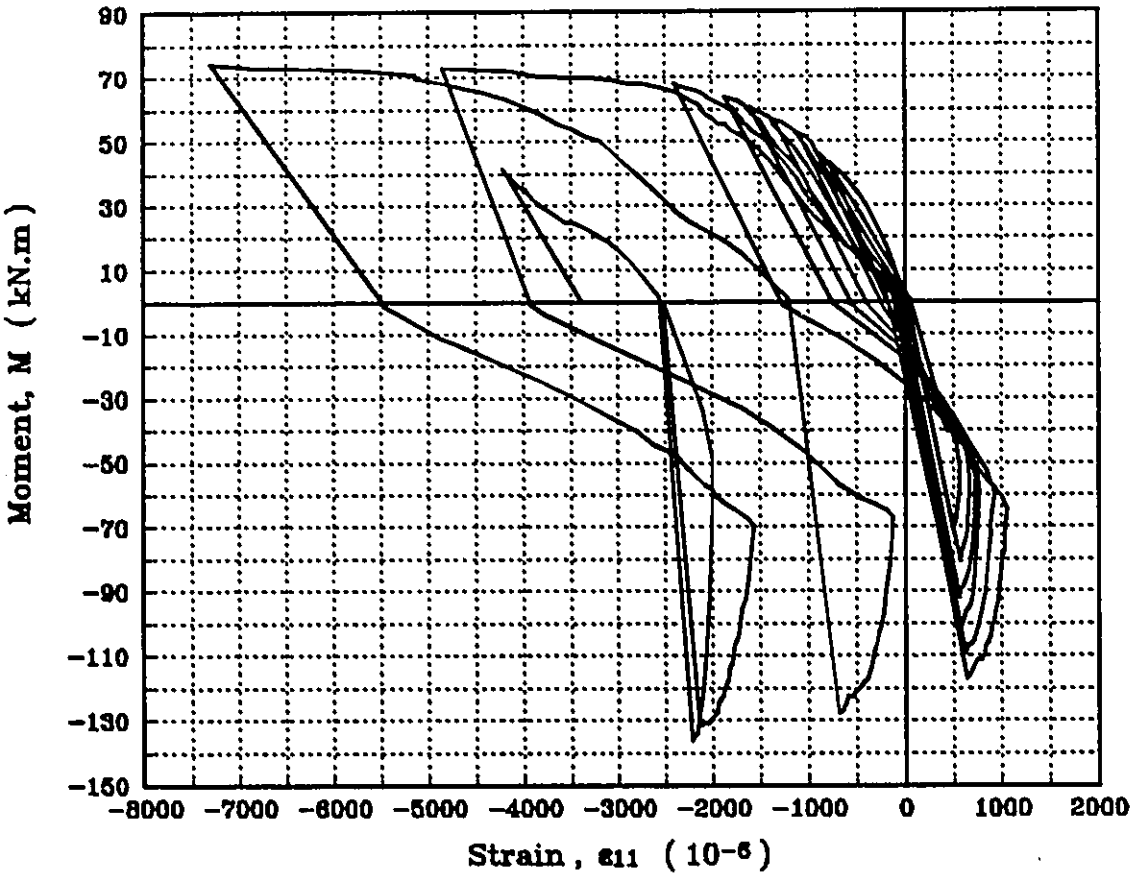

Figure 4.30 Moment-strain relation ship for strain gage ε11, specimen 4

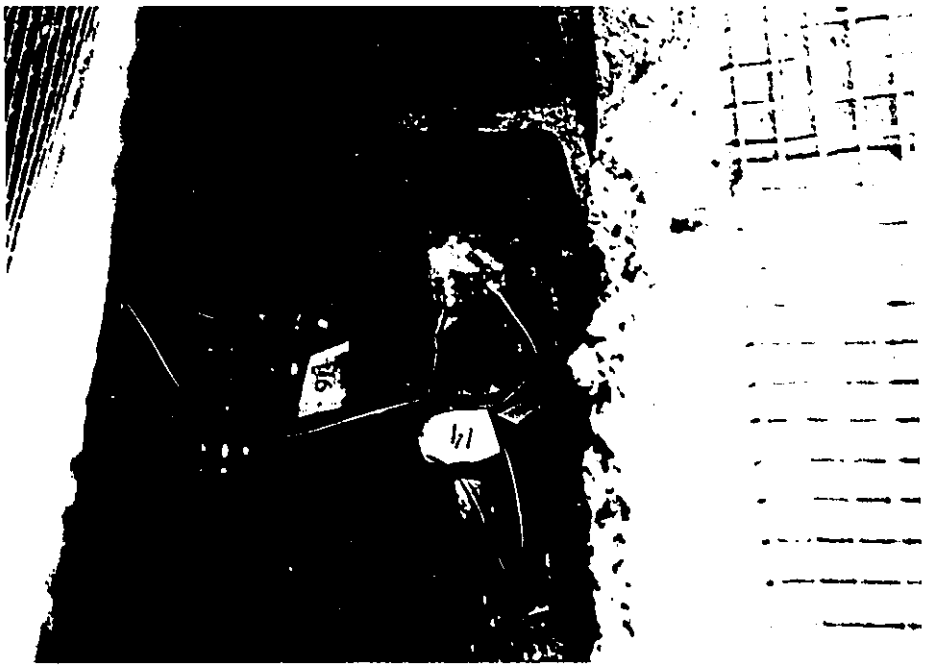

Figure 4.31 Seat angle deformations, specimen 4

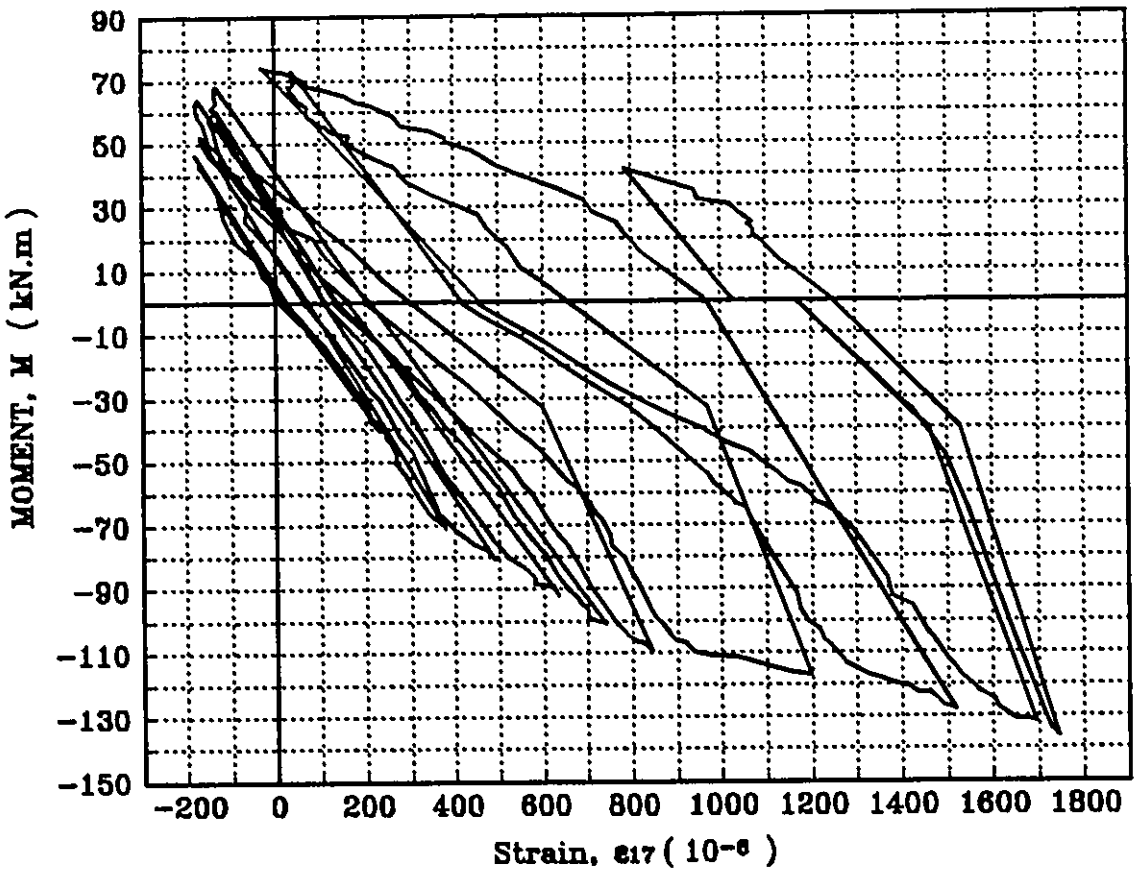

Figure 4.32 Moment-strain relationship for Strain gage ε17, specimen 4

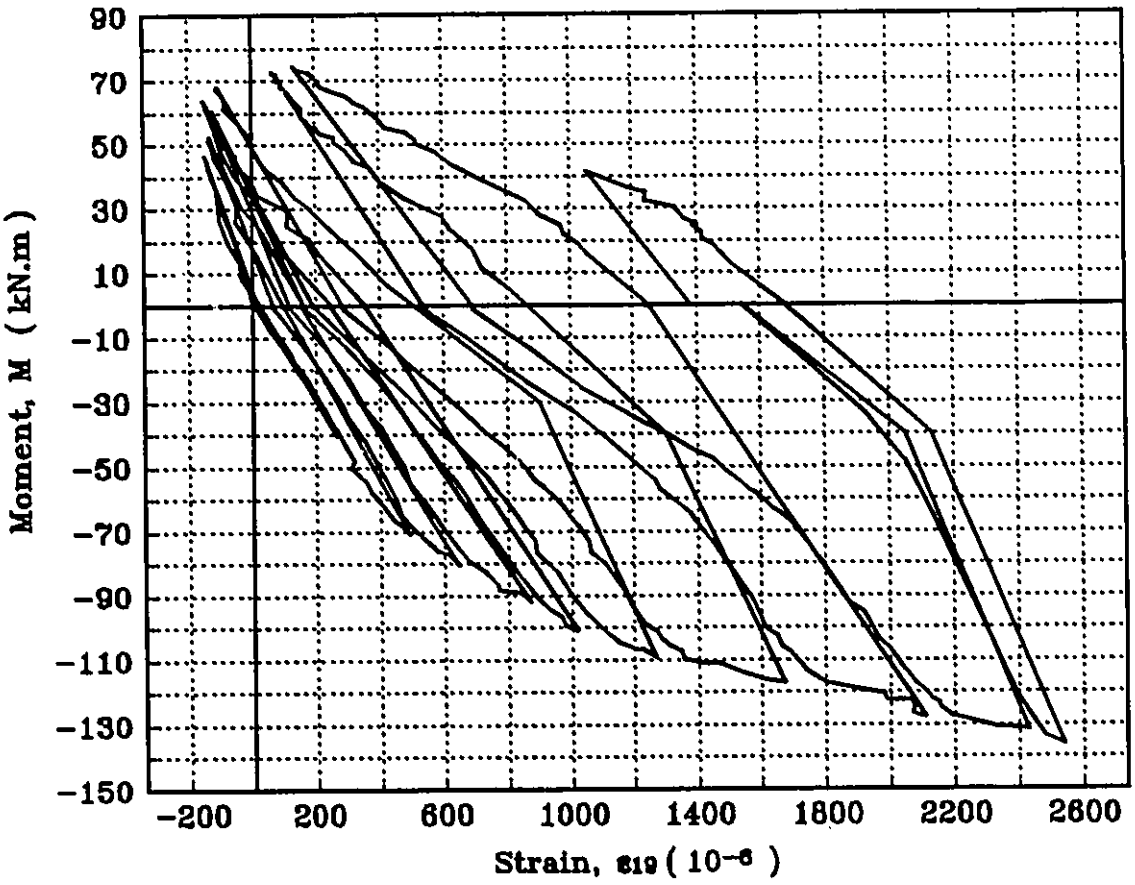

Figure 4.33 Moment-strain relationship for Strain gage ε19, specimen 4

Figure 4.34 Local buckling of stiffener angles and development of cracks in the concrete cover, specimen 4

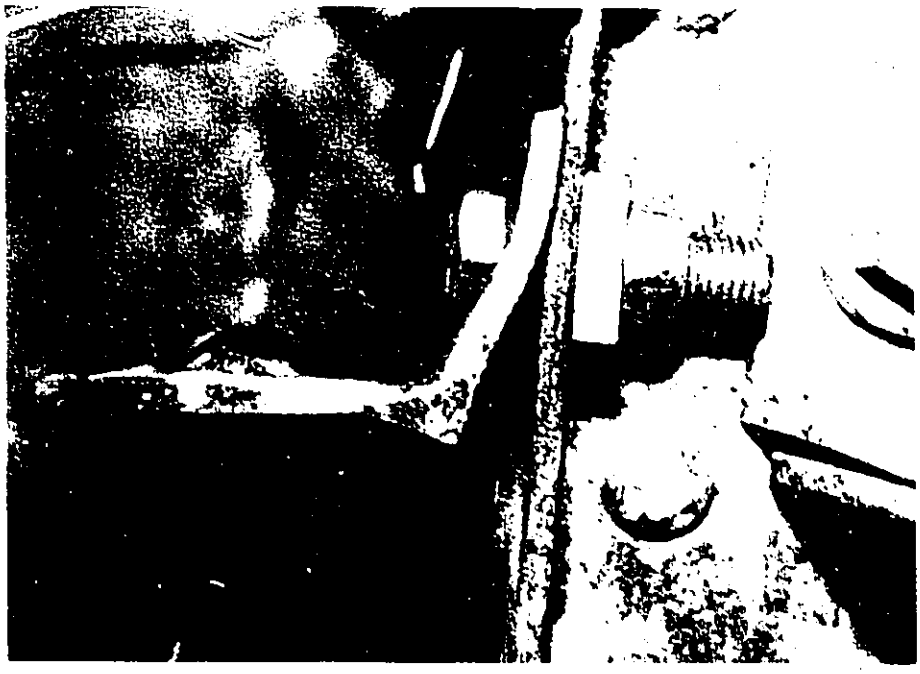

Figure 4.35 Maximum deformation of the top angle, specimen 4

Figure 4.36 Out-of-plane deformation of the top angles, specimen 4

Figure 4.37 Notable absence of separation of stiffener angles from the seat angle, specimen 4

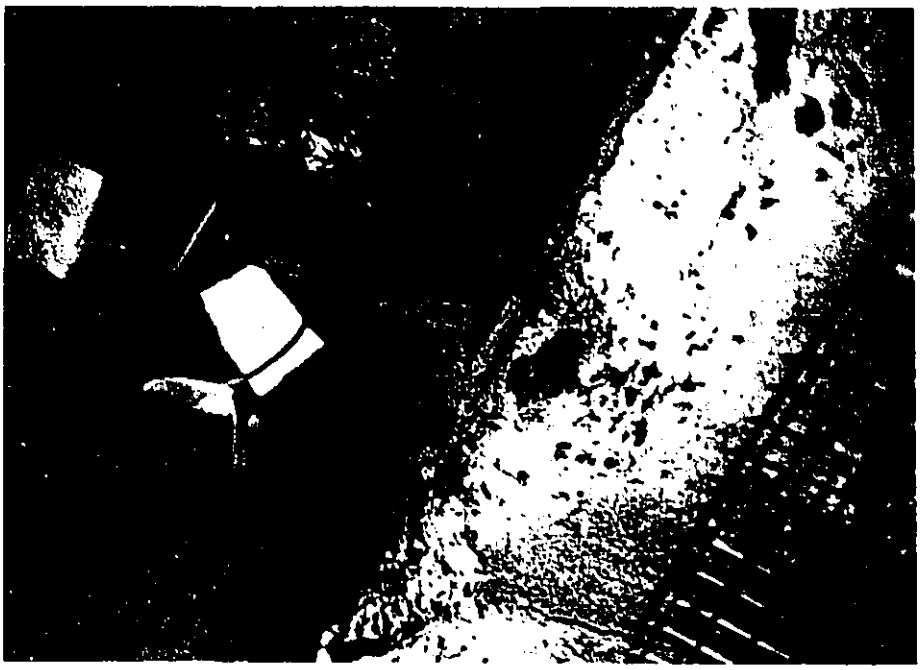

Figure 4.38 Column flange deformation near the first row of the rivets in the seat angles, specimen 4

Figure 4.39 Failure in the seat angle leg, specimen 4

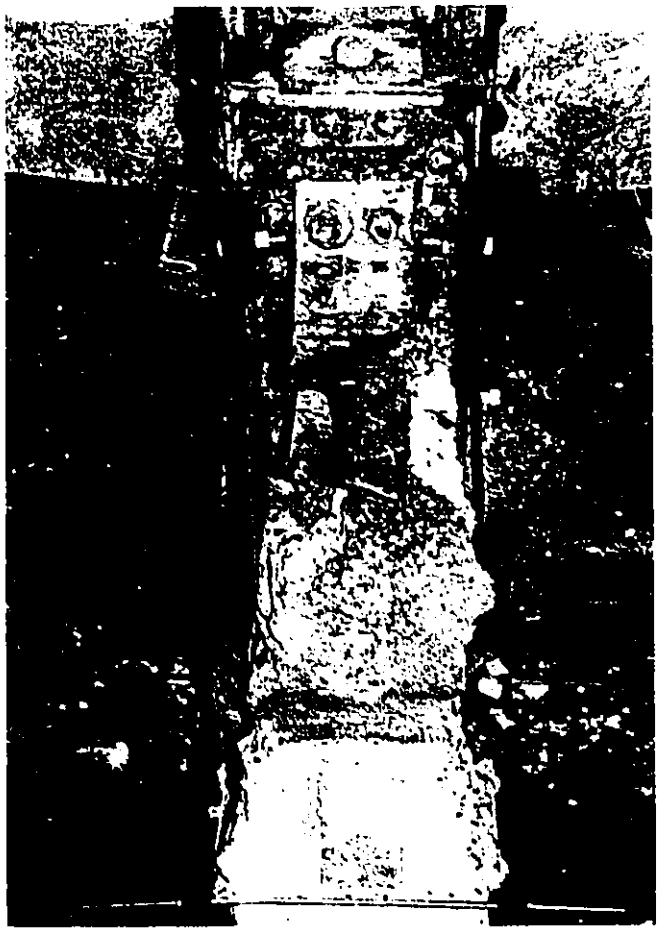

Figure 4.40 Failure of the connection detail 2, specimen 4

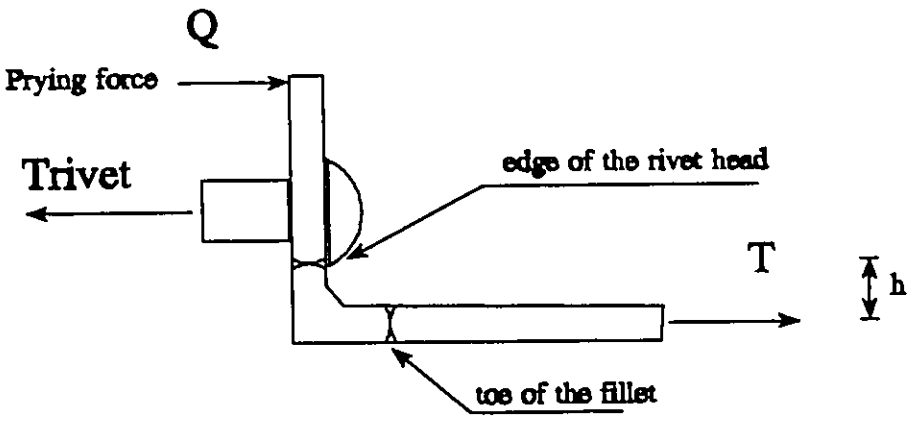

Location of plastic hinges

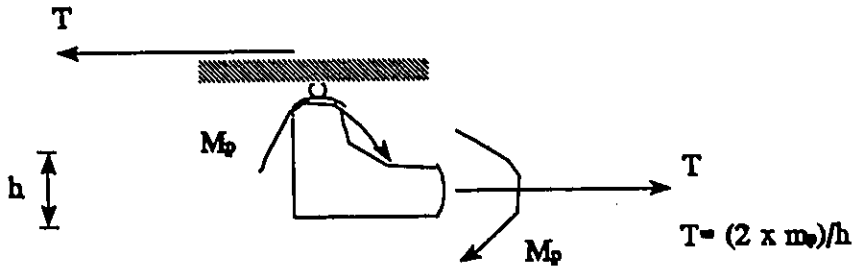

Free body diagram of the angle fillet

Figure 5.1 Assumed model used for calculation of load corresponding to formation of hinge mechanism in the top angle

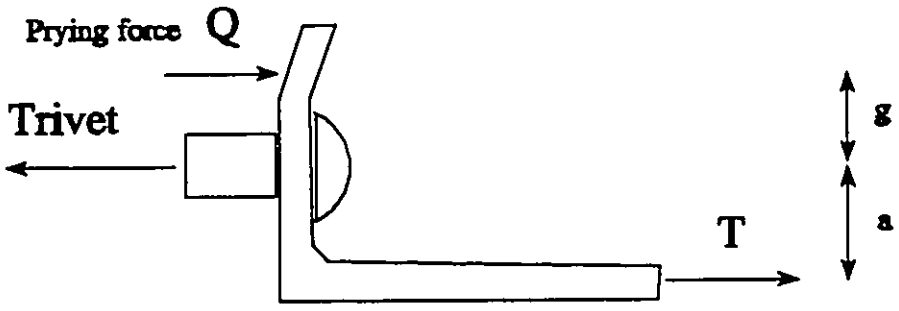

$$Q = (T \times a) / g$$

Figure 5.2 Change in position of the prying force

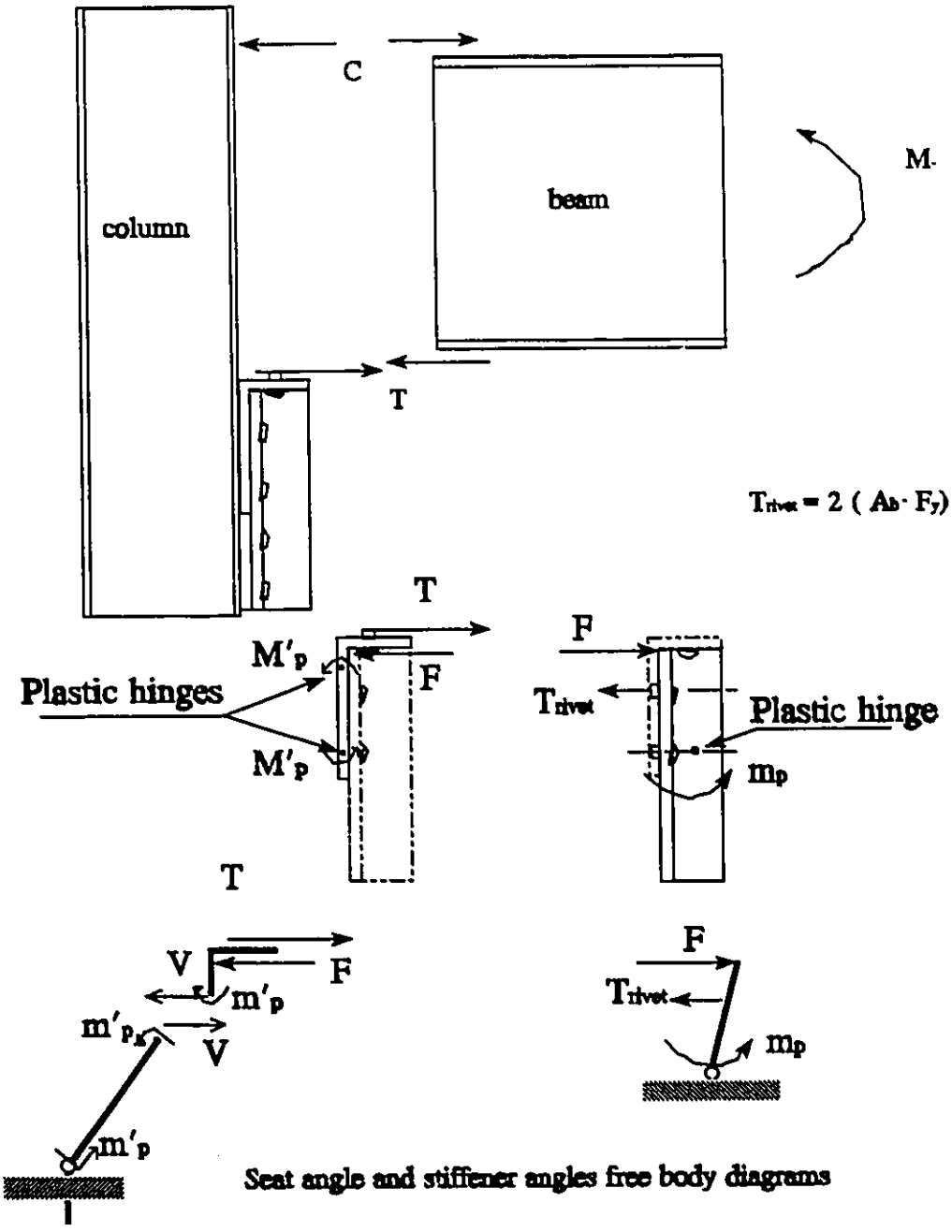

Figure 5.3 Hinge mechanism in the stiffened seat connection (connection detail 2)

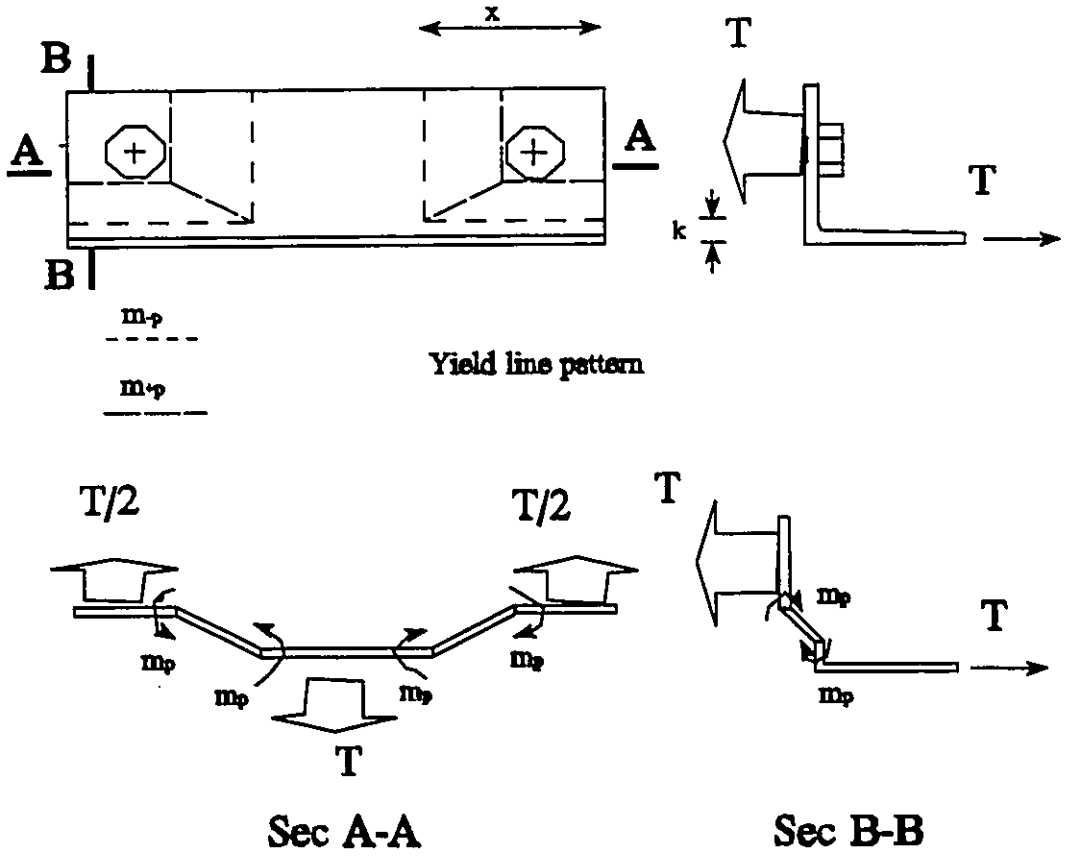

Figure 5.4 Yield line pattern of the angle in connection detail 2

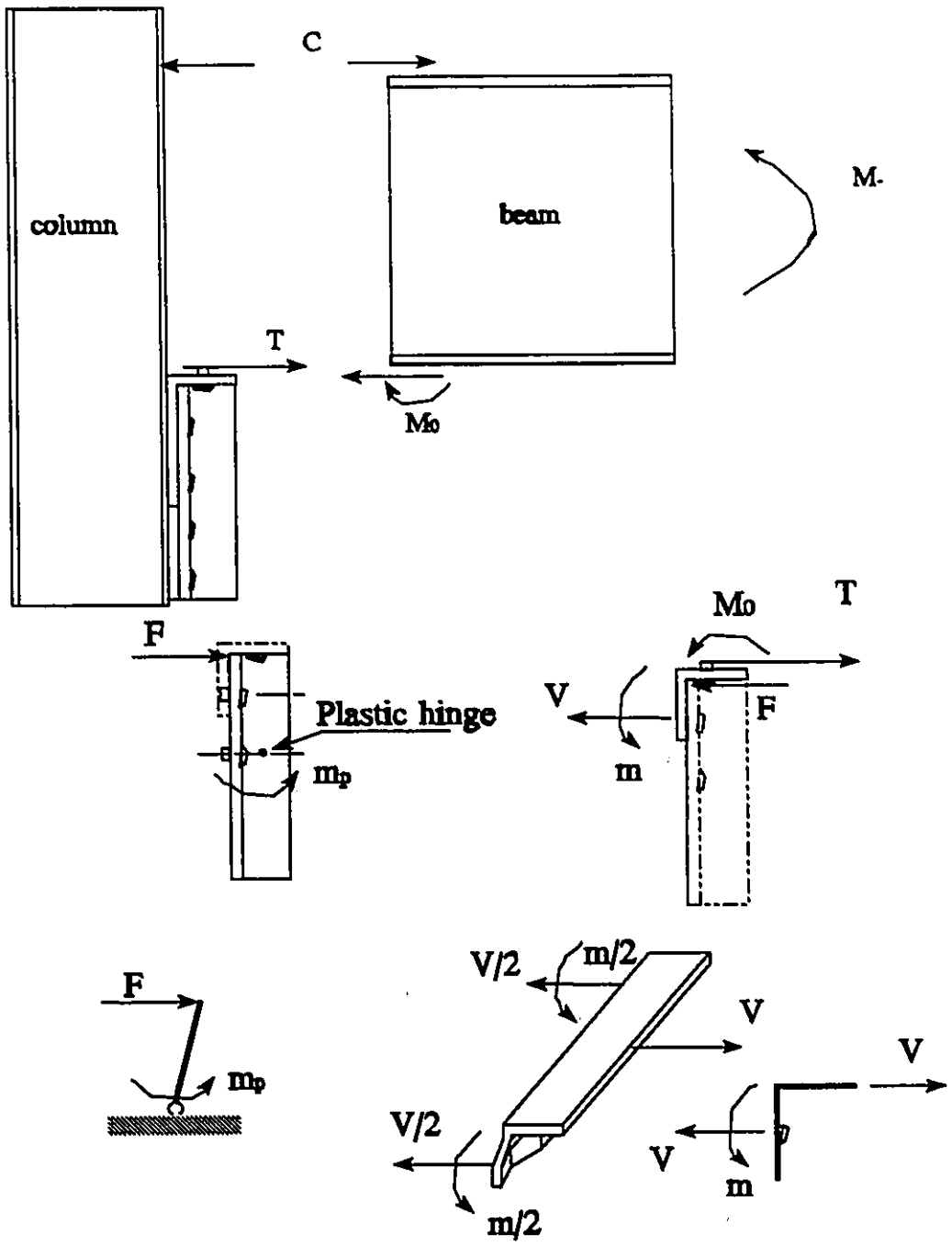

V, force corresponding to formation of yield lines

Figure 5.5 Yielding mechanism in the seat angle and stiffener angles of connection detail 2

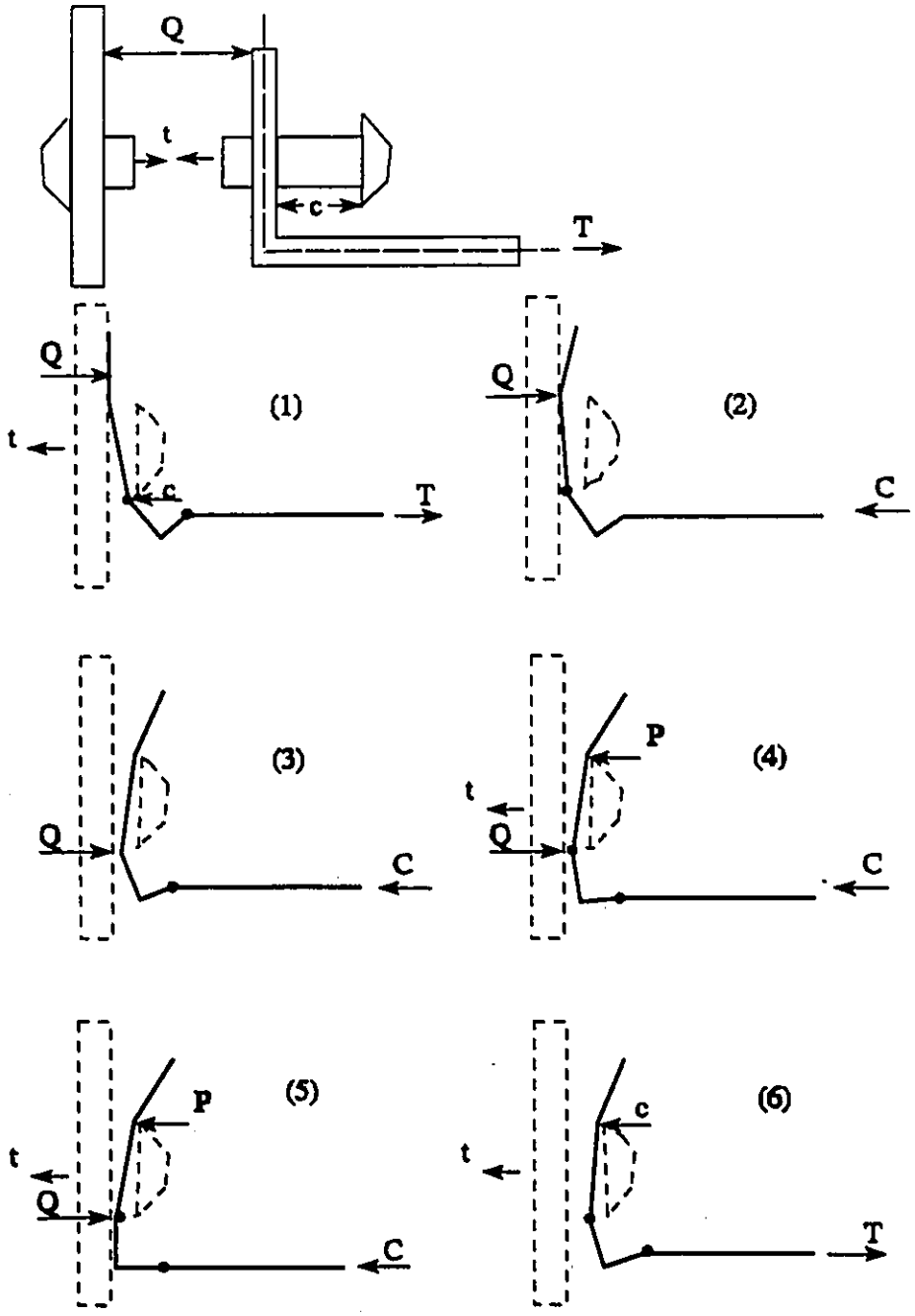

Figure 5.6 Different stages of response of top angle of the connection detail 1 to the horizontal force produced by moment.

Appendix A

Prediction of Moment Capacity of the Connection Detail 1 and 2

A.1 Prediction of the positive moment capacity for connection detail 1

A.1.1 Failure Mode 1:

Formation of hinge mechanism in top angle

$$m_p = \frac{b \times t^2}{4} \quad (1)$$

b=161 mm, t=9.5 mm,

F_y=225 MPa

Therefore, m_p=0.817 kN.m

$$T = \frac{2 \times m_p}{h'} \quad (2)$$

h'=17.37 mm,

m_p=0.817 kN.m

Therefore, T=94 kN

As shown in Fig. a.2

m_p=0.817 kN.M

U_1=31.8 mm, U_2=35 mm

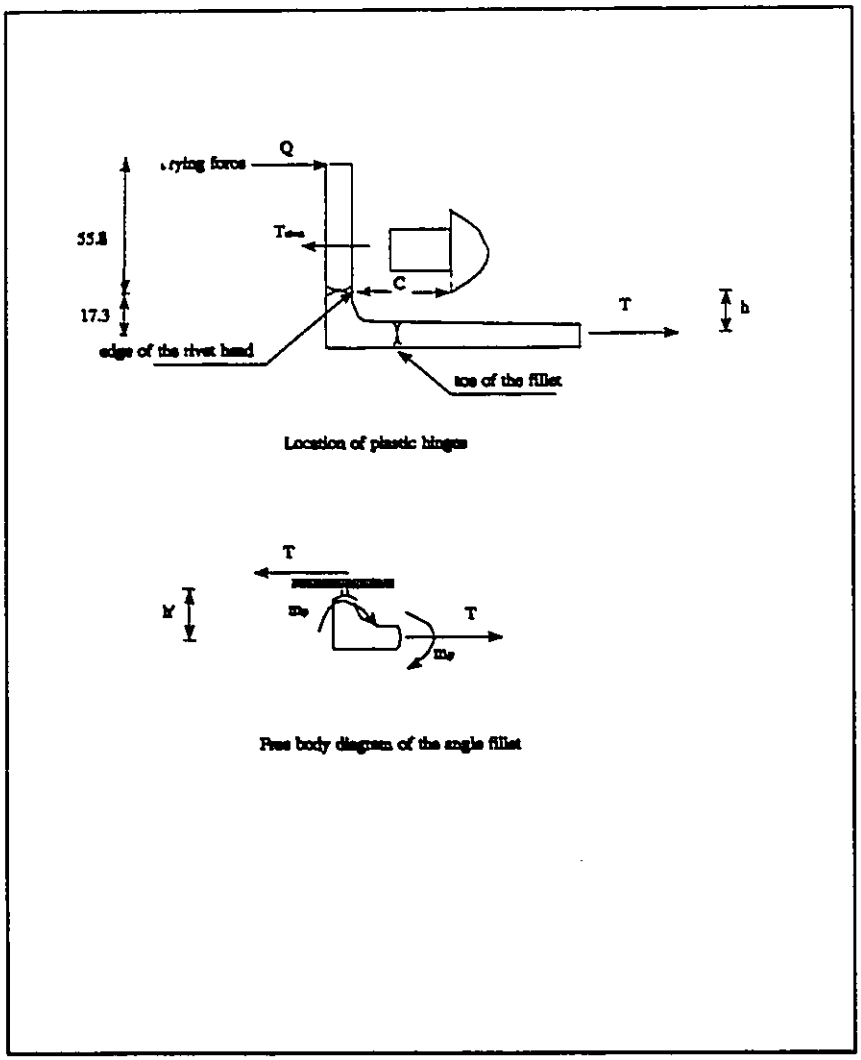

Figure a.1

Figure a.2

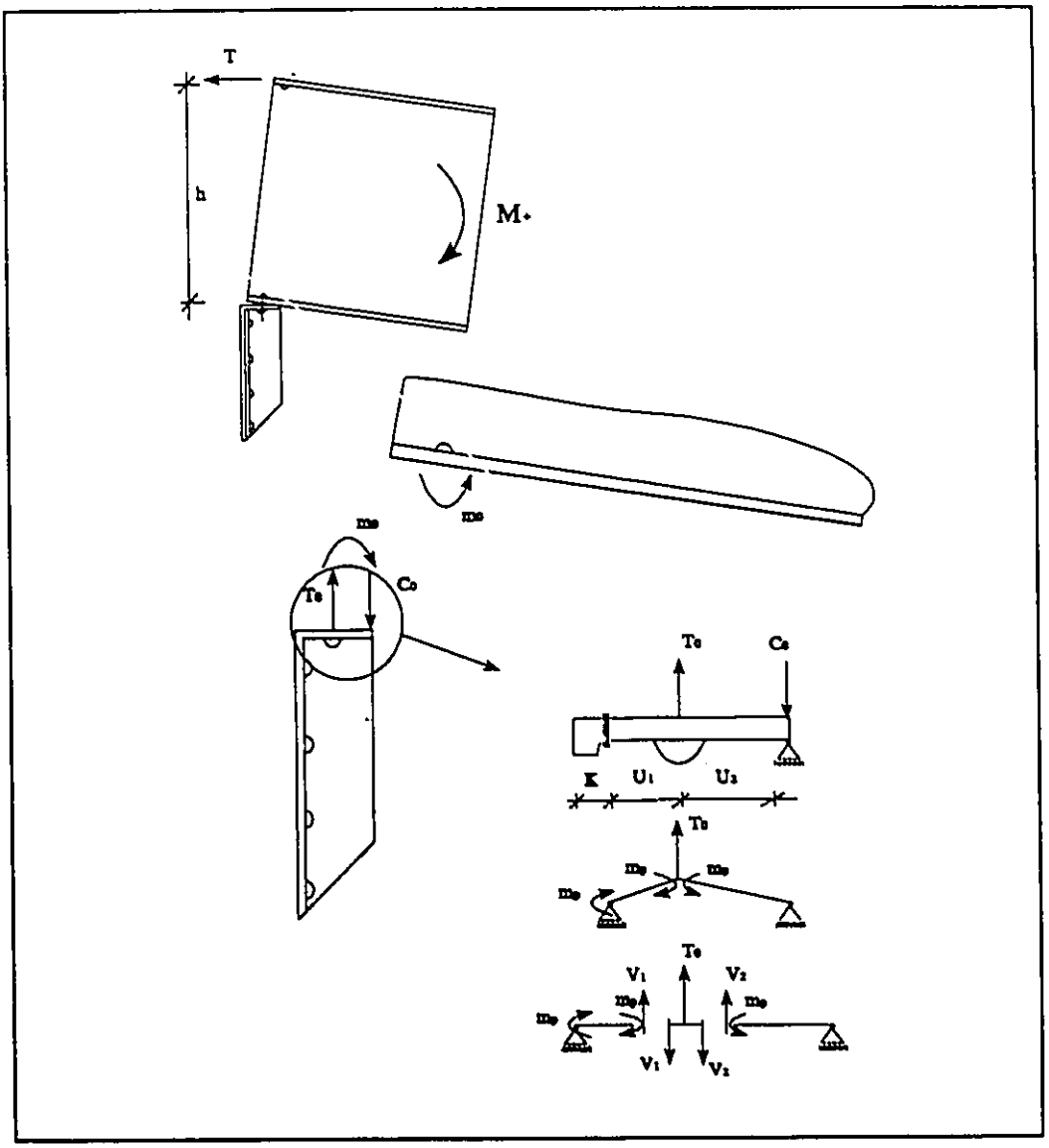

$T_0 < A_b \cdot F_y = 172.4$ kN (Load correspond to tensile yielding of the rivet)

$$V_1 = \frac{m_p \times 2}{U_1} \tag{3}$$

$$V_2 = \frac{m_p}{U_2} \tag{4}$$

$T_0 = V_1 + V_2$

V_1=51.3 kN , V_2=23.34 kN

Therefore, T_0= 74.kN

$m_0 = T_0 . U_2$

m_0=74.6 x 35 = 2.6 kN.M

To find total moment corresponding to this failure mode we have:

$M = T . h + m_p + m_j$ (5)

M = 94 x 0.507 + 0.817 + 2.6 = 51 kN.m (Failure Mode 1)

As observed, m_0 and m_0 both have very small contribution to the total resistance.

A.1.2 Failure Mode 2:

Yielding in column flange due to concentrated load from rivets

To find the load which causes this failure, yield line patterns are assumed, as shown in Fig. a.3.

If virtual displacement at the point of applied load p is equal to **u**, from the geometry we get:

$s = L . \tan \phi$

$t = (L . u) / a$

$\alpha = t / s$

external work done = $W_e = P . u$

Internal work done = W_i

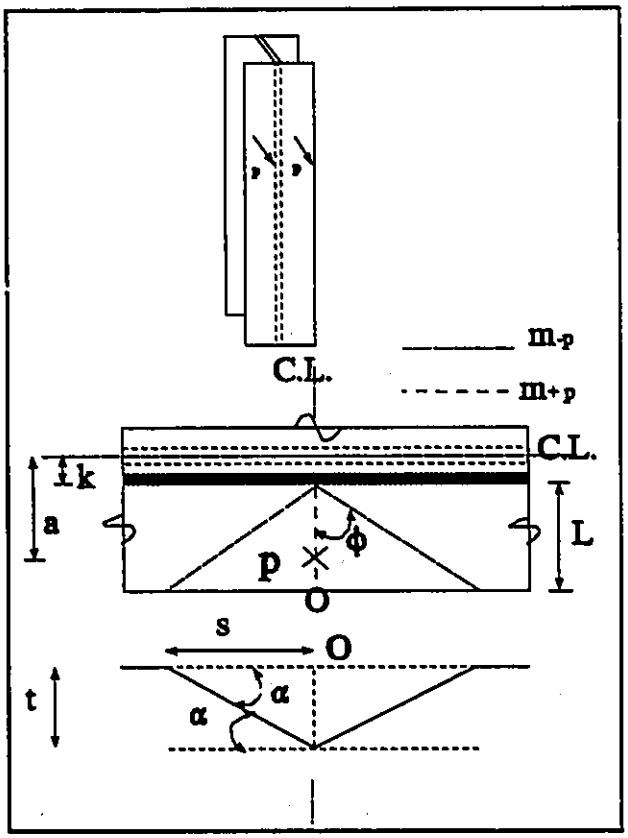

Figure a.3

$$W_i=2(m_p^- \times L)\times\alpha+2(m_p^- \times L\times tang\alpha)\times(\frac{u}{a})+2(m_p^+ \times L)\times\alpha$$

$W_i=W_e$,

by omitting u and assuming that $m^+_p = m^-_p = m_p$ we have:

$$P=2\frac{L}{a}\times(\frac{2}{tang\phi}+tang\phi)$$

By minimizing P with respect to ϕ, it is resulted that $\phi \approx 55°$ therefore;

$$P=\frac{5.66m_p\times L}{a} \qquad (6)$$

Where, L and a are distances as shown in Fig.3.1 and m_p is plastic moment per unit length of the column flange.

Now, for the existing column having flanges of thickness of 10 mm , $m_p = (t^2/4).F_y$

m_p=5625 N.mm/mm

k = 9/16" (fillet length) , b = 182 mm (width of the column flange)

L = b/2 - k = 76.76 mm

a = 36.71 mm (based on the measurements)

Using Equation 6, we obtain P = 66.55 kN

Total horizontal force acting at the top of the beam (T) will be 2xP and therefore, corresponding moment is:

M = 2 . p . h

M = 2 x 66.55 x 0.506 = 67 kN.m

A.1.3 Failure mode 3:

Yielding of the top angle rivets in tension

Q, as illustrated in Fig. a.3, can be at maximum equal to m_p/55.8 mm = 14.6 kN

also, T_{rivet} is assumed to be the tensile capacity of rivet in tension therefore;

$T_{rivet} = 2 . A_b . F_y$ (F_y, here, is tensile strength of the rivet obtained from the test)

F_y= 258 MPa and A_b=334.2 mm^2

T_{rivet}= 172 kN

From equilibrium of the top angle we have;

$T = T_{rivet} - Q$

To obtain the corresponding moment, therefore;

$M = T . h$

$T = 172 - 14.6 = 157.8$ kN

$M = 157.8 \times 0.506 = 80$ kN.m

A.1.4 Failure mode 4:

Bearing failure at the rivet holes in the top angle

(Note that # refers to CAN/CSA S16.1-M89 clause number)

Using #13.10.1(C) and assuming ϕ=1.0;

$Br = t . e . n . F_u$ (1)

$Br = 3 . d . t . n . F_u$ (2)

For the top angle we already have, F_u=400 MPa, e=30.5 mm, n=2, d=20.63, t=9.5 mm using (1) Br=231.8 kN and using (2) Br=470.4 Therefore the minimum value of 231.8 is governing.

The corresponding moment to cause this failure is :

$M = T . h = Br . h$

$M = 231.8 \times 0.506 = 117$ kN.m

A.1.5 Failure mode 5:

Crippling of the column web under compressive load from beam flange

Using # 21.3.(a) and assuming ϕ=1.0 for the given dimension of the column and its

connections we have; $B_r = 8 (t_b + 5 k_c) F_{yc}$

$t_b = k_{angle} = 20.6$ mm (since the beam flange is not in direct contact with column flange)

$k_c = 22.7$ mm

$t_w = 8$ mm

$F_{yc} = F_y = 225$ MPa

Therefore, $T = B_r = 241.4$ kN and corresponding failure load will be:

$M = T . h$

$M = 241.4 \times 0.506 = 122$ kN.m

A.1.6 Failure mode 6:

Shear failure of the rivets connecting top and seat angles the beam

To find shear capacity of the two rivets in the top we have;

$V_r = 2 A_b . F_v$

Knowing that shear to tensile capacity ratio of rivets has an average value of 0.75,

$F_v = 0.75 F_u$

experimentally obtained $F_u = 483$ MPa, then $F_v = 362$ MPa

knowing the section area of each rivet being 334 mm^2,

$V_r = 2 \times 334 \times 362 = 241.8$ kN

Therefore, corresponding failure load will be:

$M = T . h = V_r . h$

$M = 241.8 \times 0.506 = 122$ kN.M

A.1.7 Failure mode 7:

Gross section shear failure in the leg of the top angle

As shown in Fig. a.4, the moment corresponding to such a failure can be calculated as follows;

$V_{rivet} = A_g \cdot F_v$

Where A_g is gross section of the angle leg and F_v is shear capacity

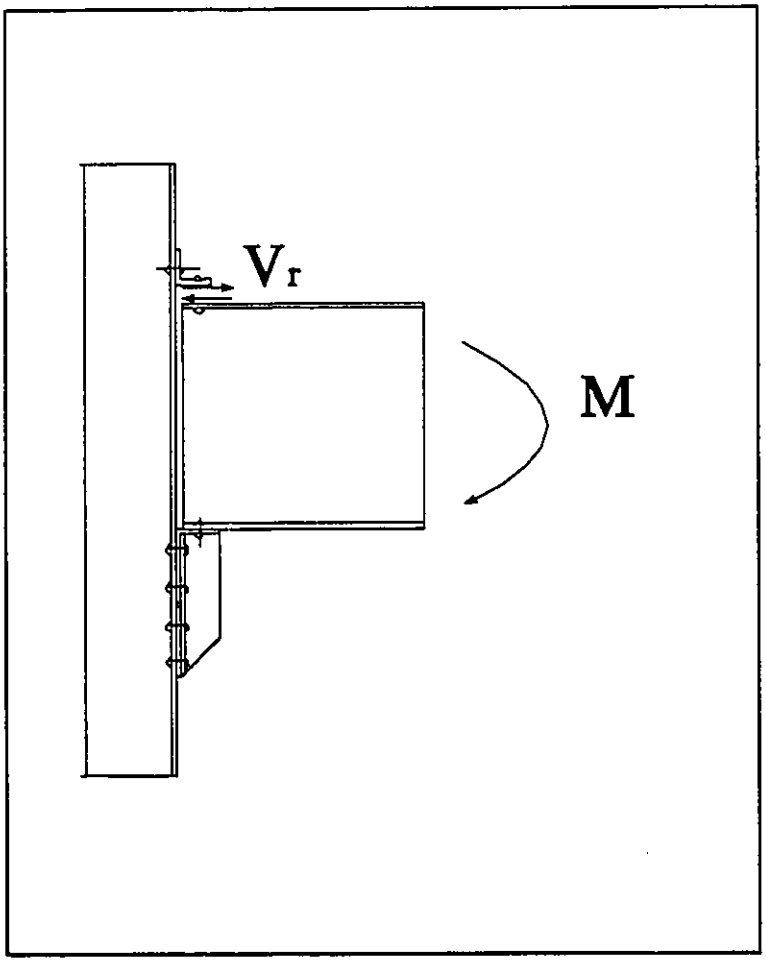

Figure a.4

having A_g = 9.5 mm x 161 mm = 1529 mm^2 and

$F_v = 0.6\ F_u = 0.6 \times 400$ MPa = 367 MPa

we get V_{angle} = 367 kN

Corresponding moment will be;

$M = V_{angle}\ (h + k)$

M = 367 (0.506 + 0.02) = 193 kN.M

A.1.8 Failure mode 8:

Net section tensile failure in the leg of the top angle

Using # 13.2 (a) by assuming $\phi = 1.0$ and ignoring reduction factor of 0.85.

$T_r = A_n \cdot F_u$

A_n = Net area of the leg, $A_n = A_g - 2\ d\ t$

$A_n = 161 \times 9.5 - 2 \times 20.61 \times 9.5$

$= 1137.5\ mm^2$

$T_r = 1137.5 \times 400 = 455$

Therefore, the corresponding moment is;

$M = T \cdot h$

$M = 455 \times 0.506 = 230\ kN.M$

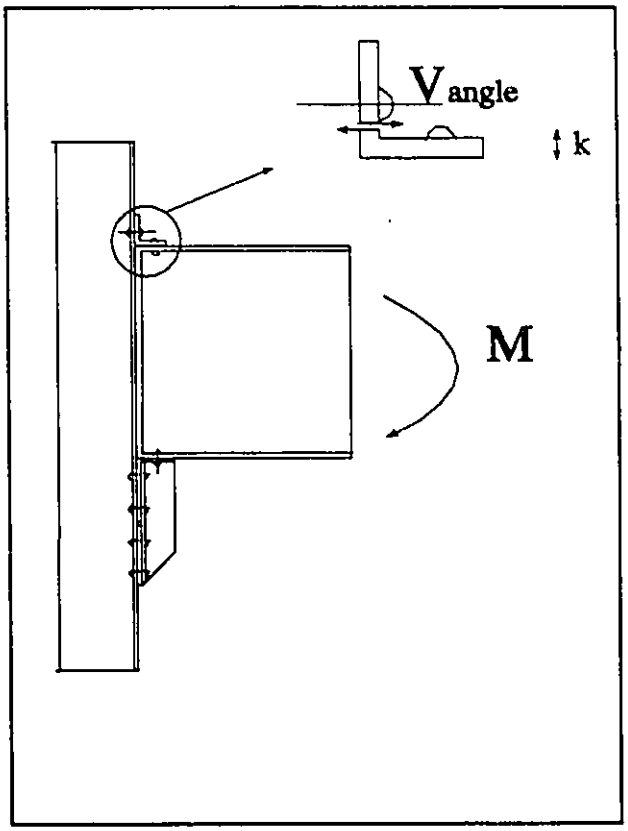

Figure a.5

A.1.9 Failure mode 9:

Gross section tensile yielding in the leg of the top angle

$T_r = A_g \cdot F_u$

$T_r = 161 \times 9.5 \times 400 = 611.8\ kN$

Therefore, corresponding moment is:

$M = T \cdot h = 309\ kN.M$

A.2 Prediction of the negative moment capacity for connection detail 1

A.2.1 Failure mode 1:

Formation of plastic hinge mechanism in the stiffener angles

In order to find the failure mechanism of the stiffener first it is assumed that stiffener angles behave as a beam with concentrated loads acting at one end and at the location of rivets then

the values of these loads are determined in terms of portion of applied load at the end of the beam. Here a method similar to that used for distribution of stresses in a concrete section subjected to moment is used to determine relative amount of tensile force in the rivets. Then the moment diagram of this beam can be drawn in order to find location of maximum moment and therefore the point where first

plastic hinge forms. Figure a.6, shows the free body diagram for the seat angle.

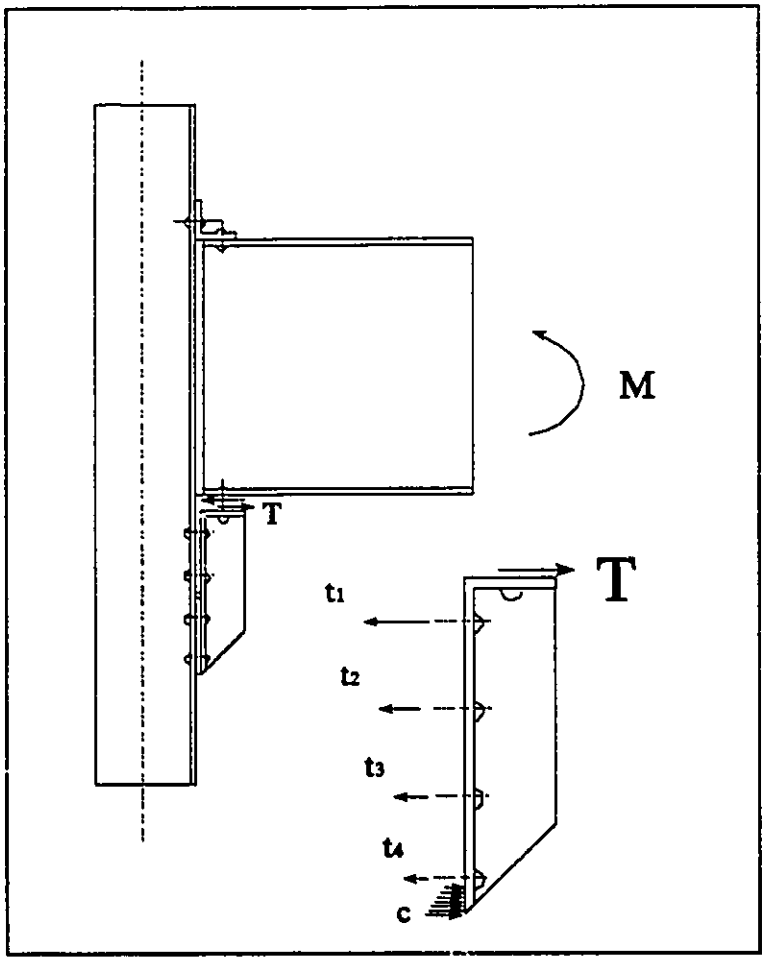

Figure a.6

Elastic analysis of the stiffeners treated as a beam under such loading when stress in the rivets remain within elastic range and for the given dimensions and property of stiffener and rivets results;

$t_1 = 0.733\ T$

$t_2 = 0.491\ T$

$t_3 = 0.249\ T$

$t_4 = 0.005\ T$

and $C = -0.48\ T$

Moment diagram of the stiffener angles shows that maximum moment will occur at the level of the second row of the rivets, meaning where plastic hinge forms. Now, to find force F, corresponding to development of plastic hinge at that point, we have;

$m_p = 9.43$ (kN.m)

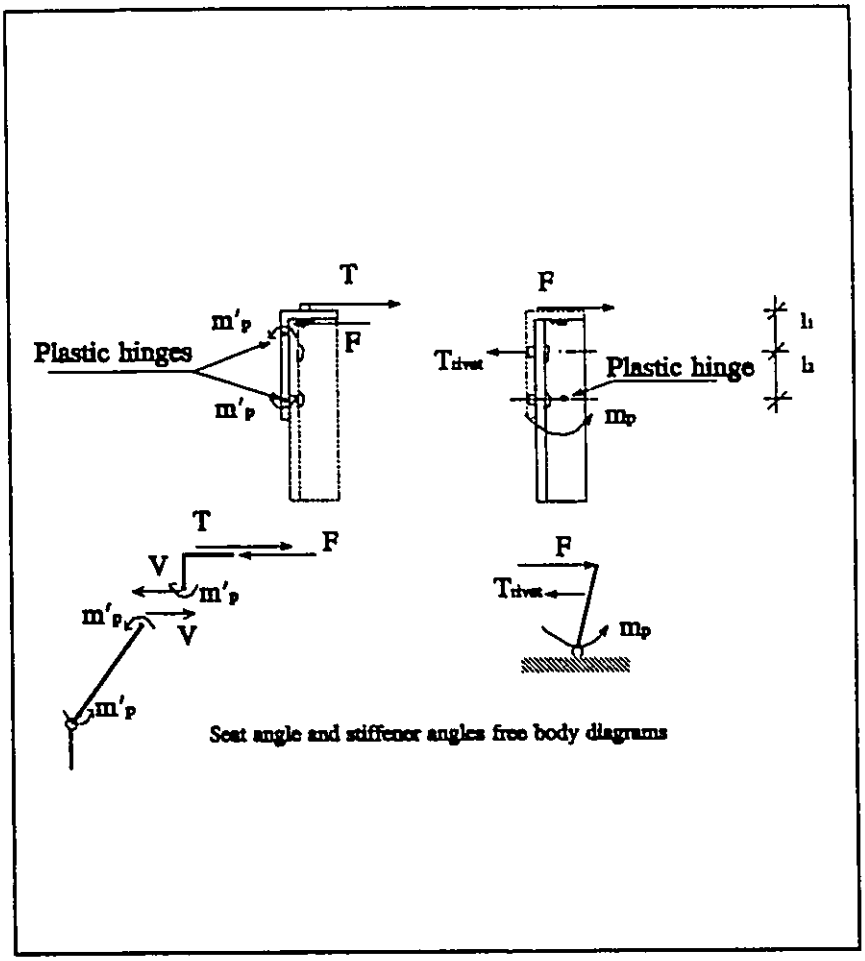

Figure a.7

As shown in Fig. a.7 By equating this value to the maximum moment in the beam as a function of F, T_{rivet}, and their distance (l_1 = 45 mm, l_2 = 75 mm).

$$M = F \cdot (l_1 + l_2) - T_{rivet} \cdot l_2 = m_p \qquad (7)$$

and knowing that $T_{rivet} = t_1 = 0.733\ F$, we get F = 145 kN

To find V, first we have to calculate m'_p (plastic moment capacity of the seat angle leg). from the geometry of the seat angle leg of the connection detail 1, we know the total length of 161 mm and thickness of 9.5 mm. Deducting the void part of the section due to the holes of two rivets, we get

$m'_p = 0.607$ kN.m

From here, value of shear force V (shown in Fig. a.7), knowing the distance l_2, will be;

$V = (2 \cdot m'_p)/l_2$

or, V = 14.33 kN

By equilibrium of the horizontal forces on the seat angle we have;

$T = F + V$

for the obtained values of F and V we get T = 159.33 kN

Therefore, moment corresponding to this failure mechanism will be simply given by;

$M = T \cdot h$

which, for known values of T and h yields;
M = 80 kN.m

A.2.2 Failure mode 2:
Tensile yielding of first row of stiffener rivets under seat angle

Although in the previous failure mode plastic hinge mechanism developed, but tensile force as portion of force F, produced in the first row of the rivets of the stiffener angles do not seem to cause yielding. This means force F, can still increase until tensile yielding in these rivets occur. Therefore, similar to the calculation of the previous failure mode but assuming;

$T_{rivet} = 2\ A_b \cdot F_y$ or $T_{rivet} = 172$ kN

and consequently by equilibrium, it is resulted that;
M = 101 kN.m

A.2.3 Failure mode 3:
Crippling of the column web under compressive load from beam flange

the same as the value obtained in **A.1.5**, M = 122 kN.m.

A.2.4 Failure mode 4:

Shear failure of the rivets connecting top and seat angles the beam

The same as the value obtained in section **A.1.6**, M = 122 kN.m

A.2.5 Failure mode 5:

Bearing failure at the rivet holes in the top angle

Similar to that obtained in section **A.1.4**, but using value of end distance e equal to 30.5 mm, yields ;

M = 117 kN.m

A.2.6 Failure mode 6:

Tensile Failure of first row of stiffener rivets under seat angle

Similar to the value obtained in **A.2.2**, but assuming that

$T_{rivet} = 2 \cdot A_b \cdot F_u$

results; M = -149 kN.m

A.2.7 Failure mode 7:

Gross section shear yielding in stiffener angles

Since force F, as described in Fig.a.7 can produce direct shear on the section of the stiffener angles, one possible scenario is to have gross section shear failure on the pair of angles. Force F, then, can be equal to the shear capacity of the stiffeners, calculated as follows;

$F = F_{v,\ stiffeners} = 0.6\ F_y \cdot A_{double\ angle}$

F = 0.6 x 225 MPa x 2(78mm x 8mm + 70mm x 8mm) = 350 kN

Since V (14.3 kN) is small compare to F, therefore; T = F

corresponding moment M = T . h ,

which for the known values of T and h, yields M = 178 kN.m

A.2.8 Failure mode 8:

Net section tensile failure in the leg of the seat angle

The same as that calculated in section **A.1.8**, M = 230 kN.m

A.2.9 Failure mode 9:

Gross section tensile failure in the leg of the seat angle

The same as that calculated in section **A.1.9**, M = 309 kN.m

A.3 Prediction of the positive moment capacity for connection detail 2

A.3.1 Failure mode 1:

Yielding of the column flange due to concentrated load from high strength bolts

Using the equation (6) developed in section **A.1.2**, with new values for thickness of the column flange (8 mm), **a** (14.2 mm), **l** (40.7 mm) and **k** (23.8 mm) as described in Fig.a.3, to find critical load **P** we have;

m_p = 3600 N.mm/mm

P = 5.66 m_p . l / a = 58.4 kN (per bolt)

M = 2 P. h = 59 kN.m

A.3.2 Failure mode 2:

Formation of hinge mechanism in top angle

Since the distance between the edge of the bolt head and the toe of fillet in the vertical leg of the top angle is large enough to allow formation of two hinges as shown in Fig.2.4, using Kishi and Chen's model we have;

g_2 = 14 mm, m_p = 0.993 kN.m (angle leg plastic moment capacity)

$V_p = 2\ m_p / g_2$

V_p = 141.8 kN

and finally by ignoring contribution from m_0 (as shown in Fig. a.2),

$M = V_p \cdot h$

M = 72 kN.m

A.3.3 Failure mode 3:

Cross section shear failure in leg of top angle

Similar to the method used in Section **A.1.7** but by using new value for A_g (276x8 mm2), we get;

M = 151 kN.m

A.3.4 Failure mode 4:

Shear failure of weld in top angle

based on #13.13.2 Table 3(A) for shear resistance of the weld with following known values, we have;

ϕ_w = 0.67, X_u = 480 MPa

A_w = (161 mm + 2 x 40 mm) x 8 mm x 0.707 (provided area of weld in the top and seat connection as retrofit)

$V_r = 0.67\ \phi_w \cdot A_w \cdot X_u$

V_r = 293.8 kN,

un-reduced moment capacity will be;

$M = (V_r / \phi_w) \cdot h$

$M = 222$ kN.m

A.3.5 Failure mode 5:

Gross section tensile yielding in leg of top angle

similar to that obtained in section **A.1.9**, using the dimensions of top angle of connection detail 2 (thickness 8.6 mm and length 276 mm), we get;

$M = 270$ kN.m

A.3.6 Failure mode 6:

Net section tensile failure in leg of top angle

similar to that obtained in section **A.1.8**, using the dimensions of the top angle of connection detail 2 , we get;

$M = 409$ kN.m

A.4 Prediction of the positive moment capacity for connection detail 2

A.4.1 Failure mode 1:

Formation of hinge mechanism in the stiffener angles and the seat angles

By using the same method as used in section **A.2.2**, but accounting for difference in size and configuration of the seat angle and stiffener angles in connection 2, we have;

$m_p = F \cdot (l_1 + l_2) - T_{rivet} \cdot l_2$ (7)

$m_p = 7.6$ kN.m (for a double angles of the size 2 x 2 x 3/8")

$l_1 = 45$ mm , $l_2 = 75$ mm

$T_{rivet} = 2 \cdot A_b \cdot F_y$

T_{rivet} = 172 kN

Solving (7) for Unknown force F we get,

F = 170.4 kN

Since in this connection hinge mechanism in the vertical leg of the seat angle, as assumed for connection detail 1, can not be developed (since the vertical leg of the seat angle in this case does not extend to the level of the second row of the rivet, where the plastic hinge in the stiffener angles are expected to form), therefore; force $_V$ as described in Section **A.2.1** is not taken into account, and we simply have;

T = F

and finally the corresponding moment will be;

M = T. h

M = 186 kN.m

A.4.2 Failure mode 2:

Gross section sear yielding of stiffener angles

By applying the same method as used in Section **A.2.7**, but using new section are of the stiffener angles of connection detail 2, we get

M = 169 kN.m

A.4.3 Failure mode 3:

Crippling of column web under compressive load from beam flange

Following the same procedure as that of Section **A.1.5**, but using different values for column flange and web thickness (since the column in this case is a built-up section, made of two channels) we get;

M = 201 kN.m

A.4.4 Failure mode 4:

Shear failure of weld in leg of seat angle

The same as value (M = 222 kN.m) as calculated in Section A.3.4.

A.4.5 Failure mode 5:

Gross section tensile yielding in leg of seat angle

The same as value (M = 270 kN.m) as calculated in Section A.3.5.

A.4.6 Failure mode 6:

Gross section tensile yielding in leg of seat angle

The same as value (M = 409 kN.m) as calculated in Section A.3.6.

Appendix B

Design of Knee Braces

B.1 Mechanism of Knee braces and design procedure

In order to design knee braces as retrofit, it is assumed that the existing connection do not develop any tensile resistance when subjected to horizontal forces acting at their contact point with the beam but they can develop end shear at the beam support. This assumptions are made due to the actual conditions of the failed connection in which the top and seat angles are highly deformed or the rivets, transforming shear from the couple of forces at the beam end, can no longer develop any considerable resistance. This assumption can also be true to a large extent and used to simplify the design, even for the case that the connections have not failed. The reason is that contribution of connections moment resistance compared to the resistance of the knee braces are very small, since these connections have relatively low flexural stiffness compared to stiffness of bracing members owing to their truss action. However, by modelling the connections as a spring with known stiffness, less conservative solution can be obtained.

Assumed model for design of the knee braces and internal forces in the members are shown in Fig. b.1. The moment capacity of this system can then be determined by assuming both members have reached their plastic capacity. knowing the geometry and taking moment about point **O**, we get;

(Note that # refers to CAN/CSA S16.1-M89 clause number)

Σ M/o = 0

$$M=C_r\times x\times\sin(45^\circ)+T_r\times(x+h)\times\sin(45^\circ) \qquad (1)$$

where, using #13.3.1,

$$C_r=A_g\times F_y\times(1.035-0.202\lambda-0.222\lambda^2) \qquad (2)$$

and

$$\lambda = \frac{kl}{r} \times \sqrt{\frac{F_y}{\Pi^2 \times E}} \qquad (3)$$

When,

$$0.15 < \lambda \leq 1.0$$

Now, in order to find a section for the knee braces which can develop moment **M**, we have to express C_r as a function of A_g, **r** and length **X**. Therefore, we first from **(3)** we have;

K = 0.5 (assuming weld and gusset plate connection provides 100% fixity at the member supports in for in plane buckling)

$l = \sqrt{2}\ X$

$\lambda = (0.5\ \sqrt{2}\ X)/r\ .\ (F_y / 9.87\ E)^{0.5}$

by substituting λ in **(2)**,

We get, C_r as a function of A_g, **r, X** and other parameters are known.

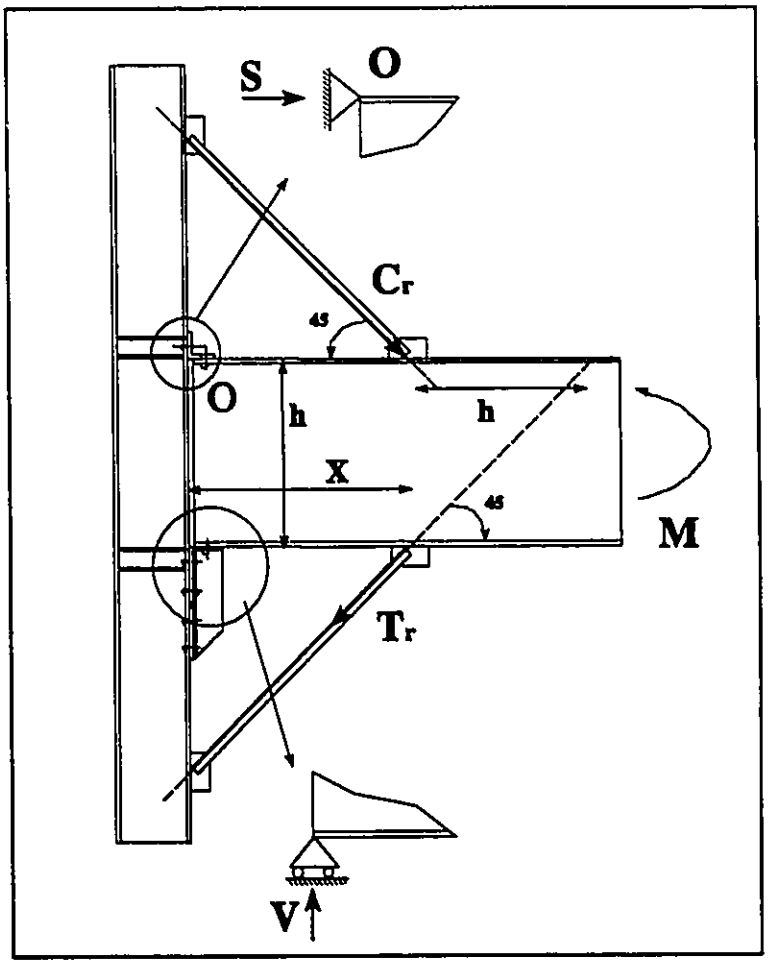

Figure b.1

Substituting C_r and T_r in eq. **(1)** gives an expression in which only A_g, **r, X** are unknown (E, F_y, h and E are all know values). This means from this expression for a given section (A_g,

r are known), length **X** can be found by try and error. Therefore, the problem is to find the best section which meets the followings;

a) C_r/T_r ratio as close as possible (in order to minimise effect of buckling in the compressive member for more energy dissipation)

b) The calculated length **X** is large enough so that gusset plates and welding can be practically performed.

c) Since the in-plane buckling of the knee braces is the most governing failure mode for a particular section, we have to ensure that other failure modes (out-of-plane buckling of the member, single buckling and torsional buckling) occur at higher loads than C_r.

B.2 Design of the knee braces

Following the design guidelines as described in Section **B.2**, by try and error and using a double angle 1"x1"x " (F_y = 320 MPa), beam hight **h** = 0.506 m for **M** = 190 kN.m, yields;

X = 542.8 mm

now, to check C_r/T_r ratio we have;

r_{xx} = 7.37 mm, A_g = 565 mm^2

$\lambda = (0.5 \times 542.8 \text{ mm} \times \sqrt{2})/ 7.37 \text{ mm} \times (320/ 9.87 \times 2E5)^{0.5}$

$\lambda = 0.633 < 1.0$ and > 0.15

$C_r = (1.035 - 0.202 \times 0.633 - 0.222 \times (0.633)^2) A_g F_y = 0.803 A_g F_y$

Therefore, $C_r/T_r = 0.803$ good

also,

$C_r = 0.803 \times 565 \text{ mm}^2 \times 320 = 145$ kN

T_r = 180 kN

Check for Out-of-plane buckling

Assuming that back-to-back distance between the double angles is 10 mm, we get;

r_{yy} = 15.5 mm

since providing a gusset plate of 10 mm thickness, can reduce **K** from conservative value of 1.0 (pin-pin model), we assume **K** = 0.8, therefore;

$\lambda_{yy} = 0.76\ \lambda_{xx} = 0.481$

$C_{r,yy} = (1.035 - 0.202 \times 0.481 - 0.222 \times (0.481)^2)\ A_g\ F_y = 160$ kN $> C_r = 145$ kN O.K.

Check for buckling of a single angle

To ensure that a single buckling of a single angle does not occur before overall buckling of the member a number of batten plates are provided at a required distance calculated as follows;

r_{min} = 4.98 mm (for a single angle)

$(kl/r)_{member}$ = 49.5 (for double angle)

therefore, l_{max}' = 246 mm

we chose l'= l/4 = 191.9 mm < 246 O.K.

Check for torsional buckling of a single angle

Since torsional buckling of a single angle is more governing than that of the hole member in this case, for a single angle with following parameters we have using the related expressions (Steel Structures, Charles G. Salmon, 2nd edition, P431-437), we have;

A = 279 mm^2 , t = 6.4 mm , b = 25 mm

$I_{xx} = I_{yy} = 0.015 \times 10\ e^6\ mm^4$

$r_x = r_y$ = 7.24 mm

$r_z = 4.98$

$J = 1/3 \Sigma b_i (t_i)^3 = 2/3 \times 21.8 \times (6.4)^3 = 3809.8 \text{ mm}^4$

$C_w = 1/36 (b^3 . t_1^3 + h^3 . t_2^3) = 0.1508 e^6 \text{ mm}^6$

$I_p = I_z + I_y + A y_0^2 = 46392 \text{ mm}^4$, $y_0 = 7.66$

$r_p = \sqrt{(I_p/A)} = 12.89 \text{ mm}$

$r_{z,max} = \sqrt{(I_{max}/A)} = 10.6 \text{ mm}$

substituting all the parameters in the following expression we get;

$r_E = (C_w/I_p + 0.04 J l'^2/I_p)^{0.5}$

$r_E = 11.14 \text{ mm}$

again by substituting the values for r_E , r_y (for axis of symmetry in this case $r_y = r_{z,max}$) and r_p in the following equation,

$$\frac{1}{r_e^2} = \frac{1}{2r_E^2} + \frac{1}{2r_y^2} + \sqrt{\left(\frac{1}{2r_E^2} - \frac{1}{2r_y^2}\right)^2 + \left(\frac{y_0}{r_E r_y r_p}\right)^2} \qquad (4)$$

we finally get, $r_e = 8.6 \text{ mm} > r_z = 4.98 \text{ mm}$ O.K.

therefore, torsional buckling will not occur.

Appendix C

Additional Experimental Data

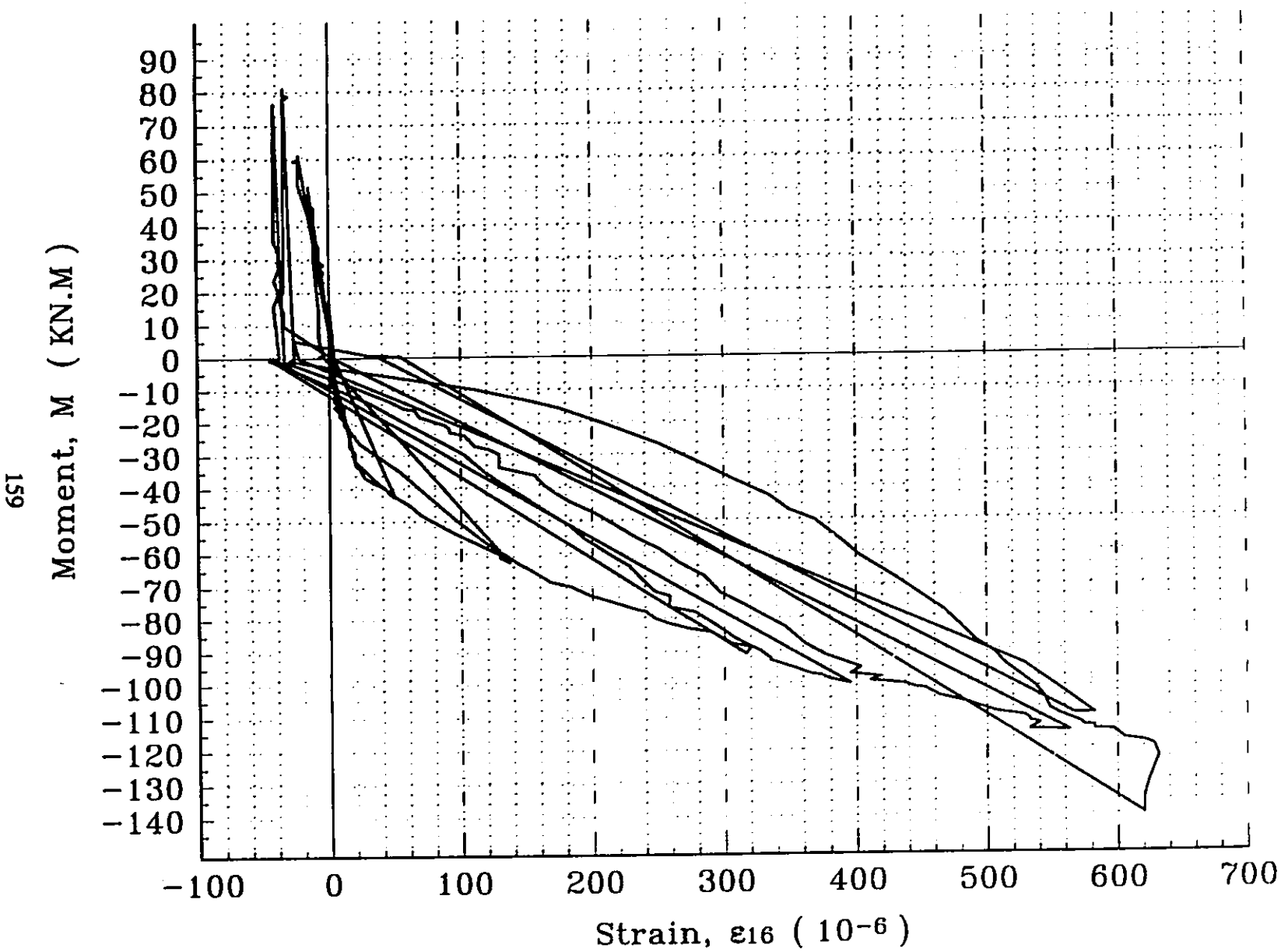
Moment, M (KN.M)
90
80
70
60
50
40
30
20
10
0
-10
-20
-30
-40
-50
-60
-70
-80
-90
-100
-110
-120
-130
-140
-100
0
100
200
300
400
500
600
700
Strain, ε16 (10-6)

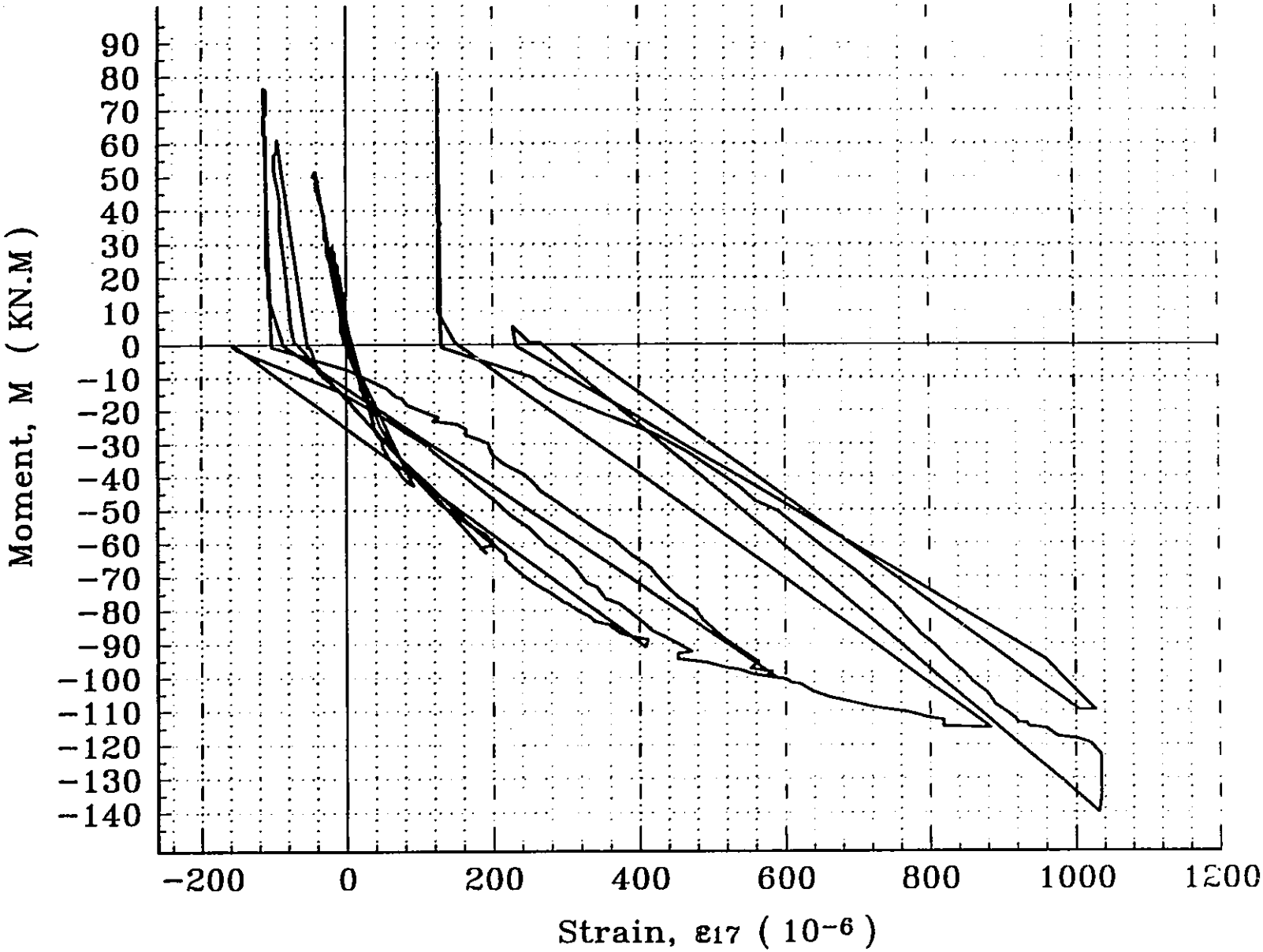
Moment, M (KN.M)
90
80
70
60
50
40
30
20
10
0
−10
−20
−30
−40
−50
−60
−70
−80
−90
−100
−110
−120
−130
−140
−200
0
200
400
600
800
1000
1200
Strain, ε17 (10−6)

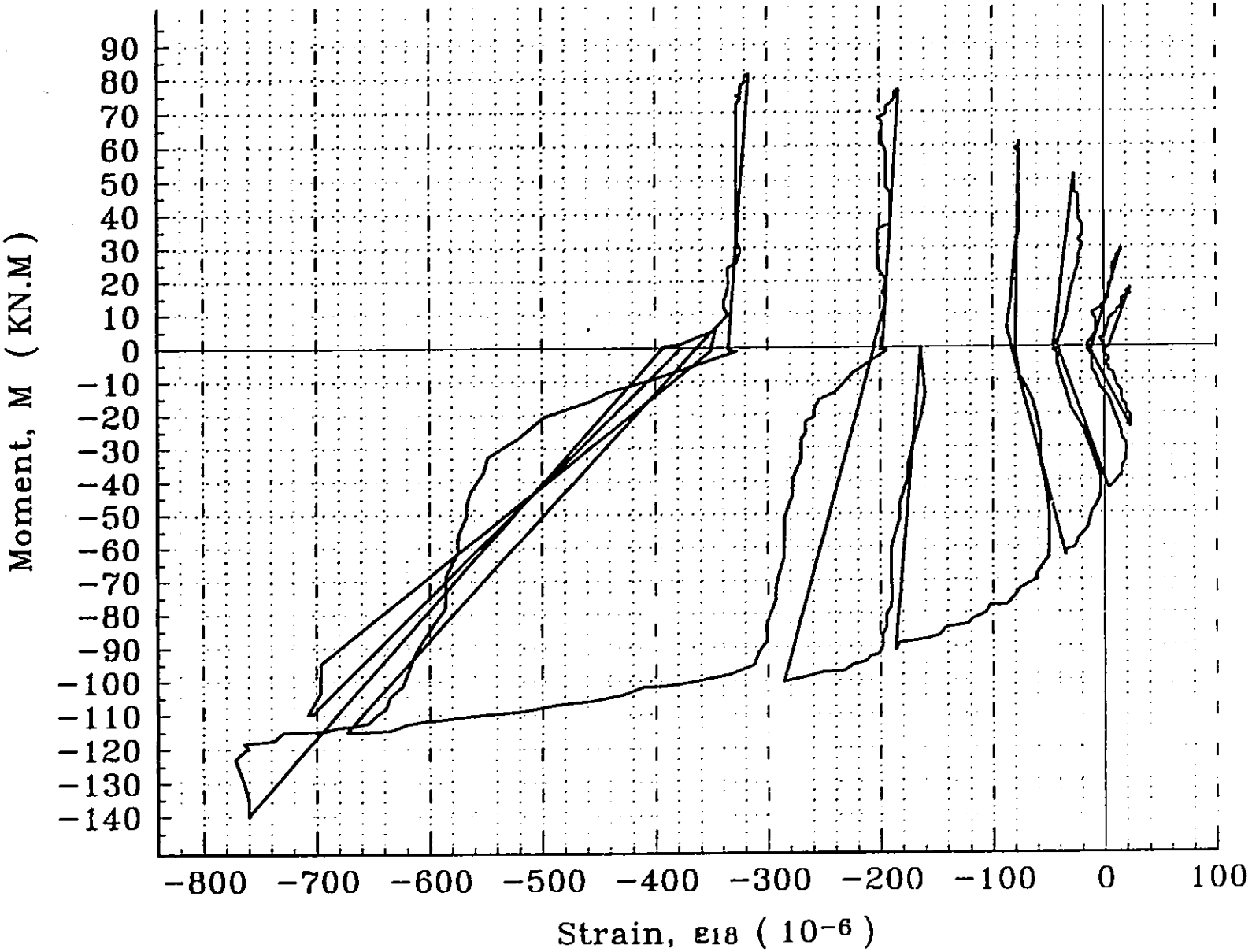
Moment, M (KN.M)
90
80
70
60
50
40
30
20
10
0
−10
−20
−30
−40
−50
−60
−70
−80
−90
−100
−110
−120
−130
−140
−800
−700
−600
−500
−400
−300
−200
−100
0
100
Strain, ε18 (10−6)

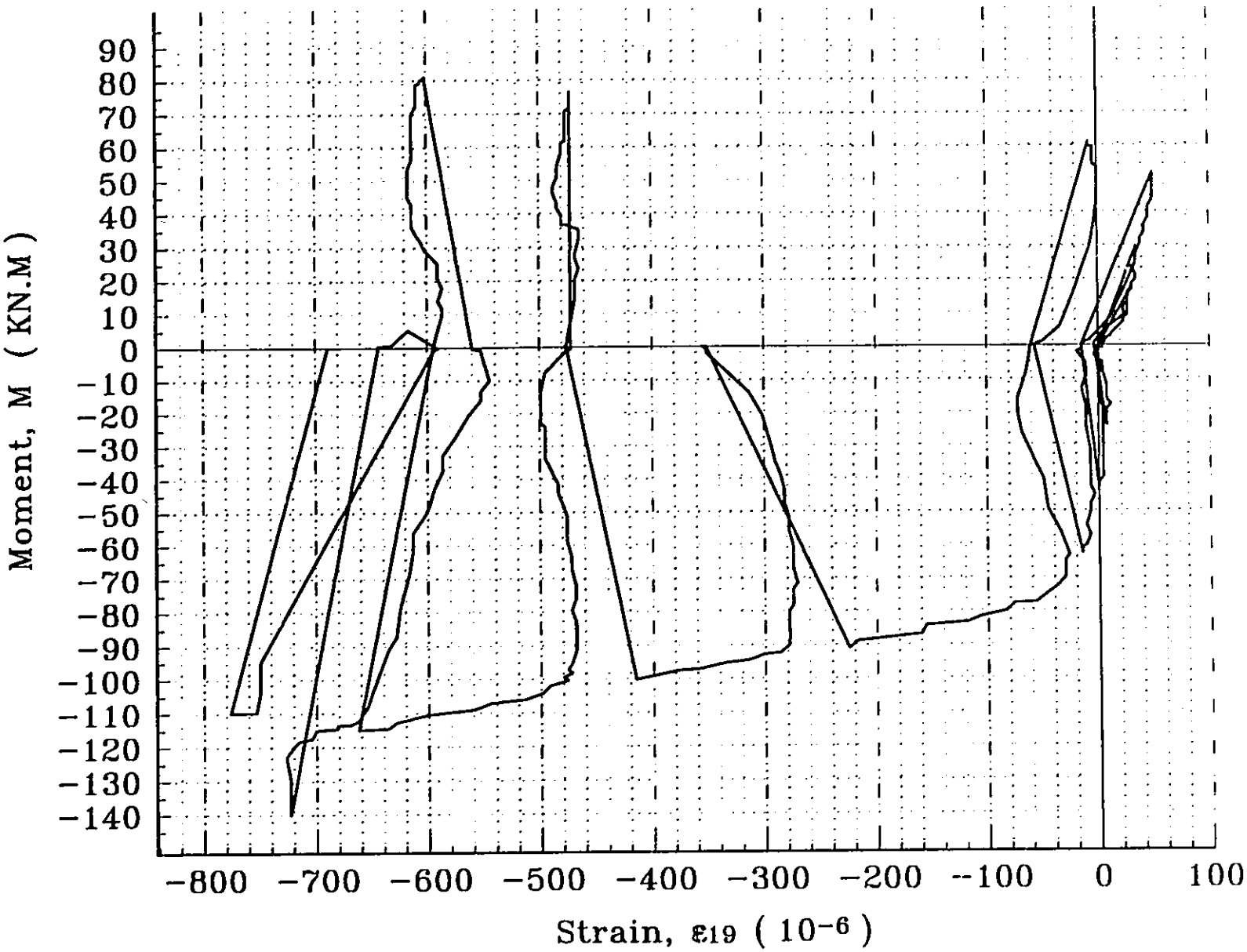
Moment, M (KN.M)
90
80
70
60
50
40
30
20
10
0
-10
-20
-30
-40
-50
-60
-70
-80
-90
-100
-110
-120
-130
-140
-800
-700
-600
-500
-400
-300
-200
-100
0
100
Strain, ε19 (10-6)

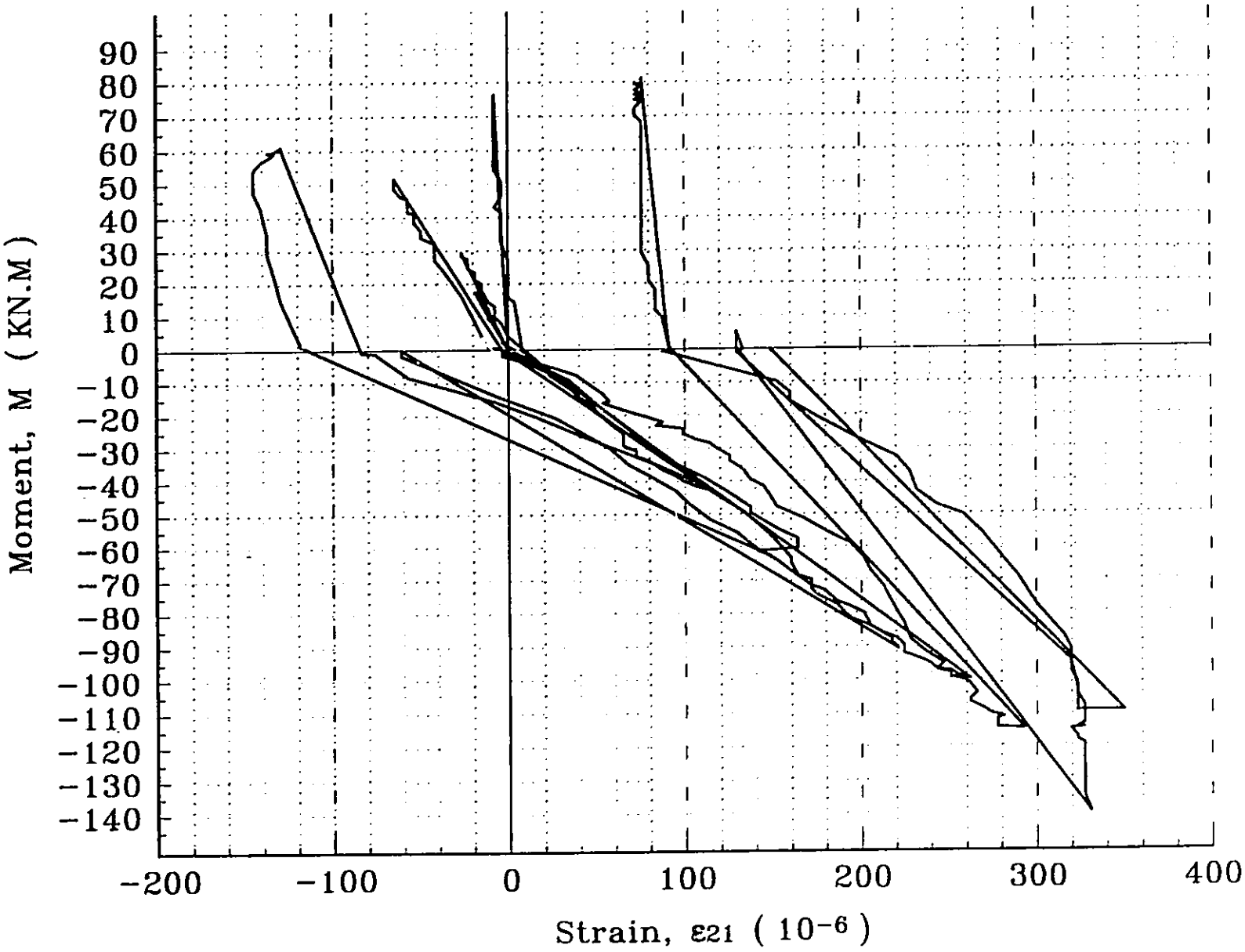
90
80
70
60
50
40
30
20
10
0
−10
−20
−30
−40
−50
−60
−70
−80
−90
−100
−110
−120
−130
−140
Moment, M (KN.M)
−200
−100
0
100
200
300
400
Strain, ε21 (10−6)

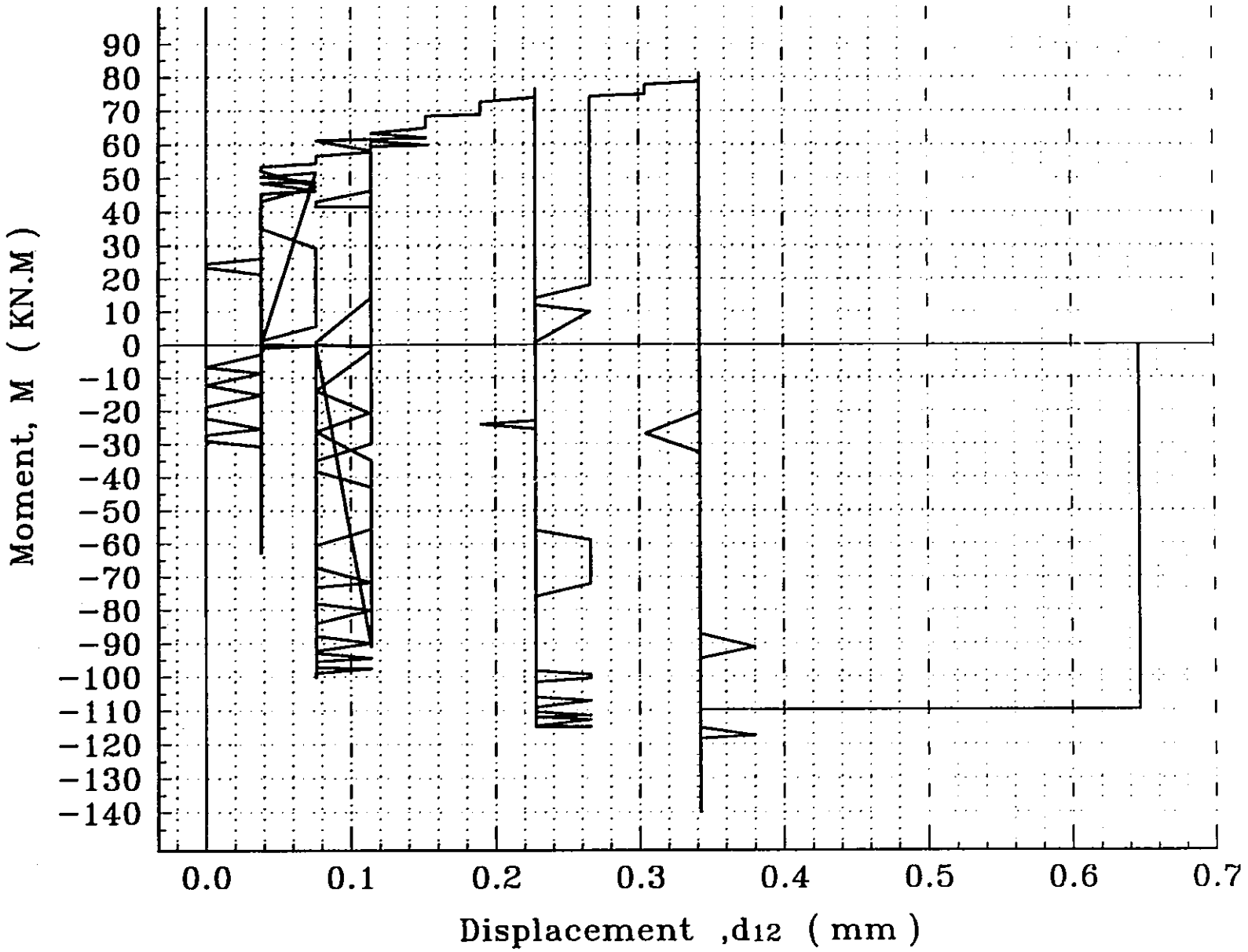
Moment, M (KN.M)
90
80
70
60
50
40
30
20
10
0
-10
-20
-30
-40
-50
-60
-70
-80
-90
-100
-110
-120
-130
-140
0.0
0.1
0.2
0.3
0.4
0.5
0.6
0.7
Displacement ,d12 (mm)

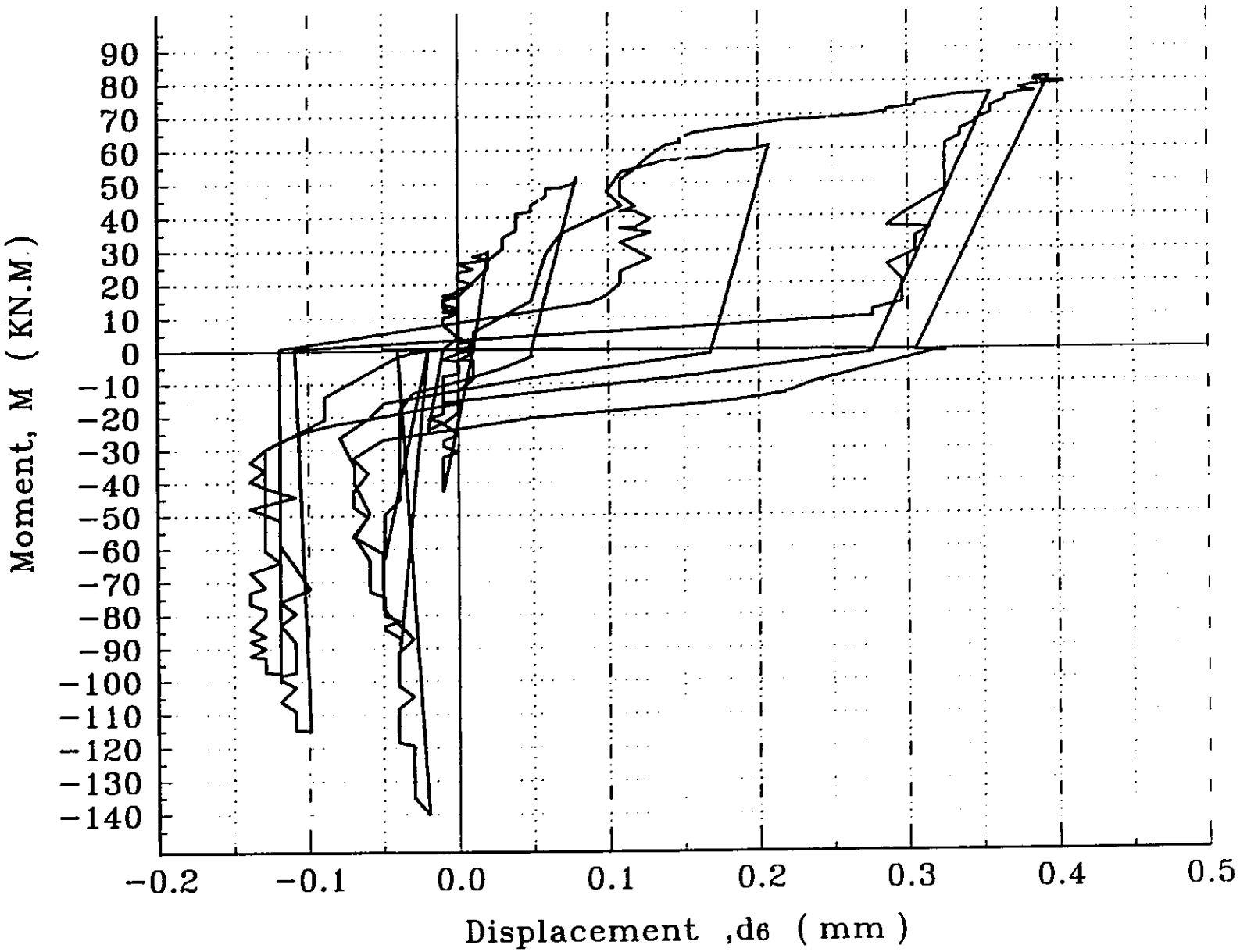
Moment, M (KN.M)
90
80
70
60
50
40
30
20
10
0
-10
-20
-30
-40
-50
-60
-70
-80
-90
-100
-110
-120
-130
-140
-0.2
-0.1
0.0
0.1
0.2
0.3
0.4
0.5
Displacement ,d6 (mm)

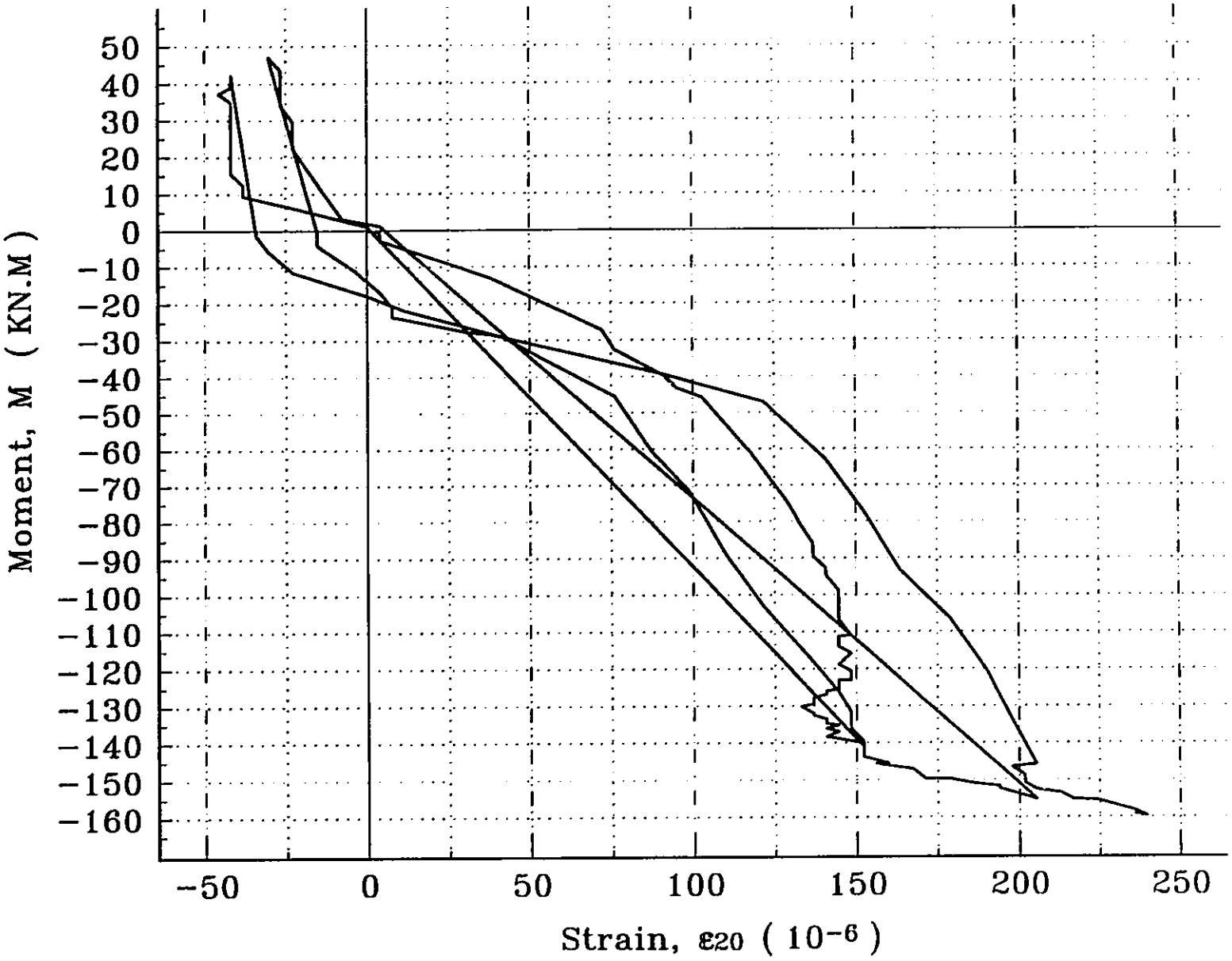
Moment, M (KN.M)
50
40
30
20
10
0
−10
−20
−30
−40
−50
−60
−70
−80
−90
−100
−110
−120
−130
−140
−150
−160
−50
0
50
100
150
200
250
Strain, ε20 (10−6)

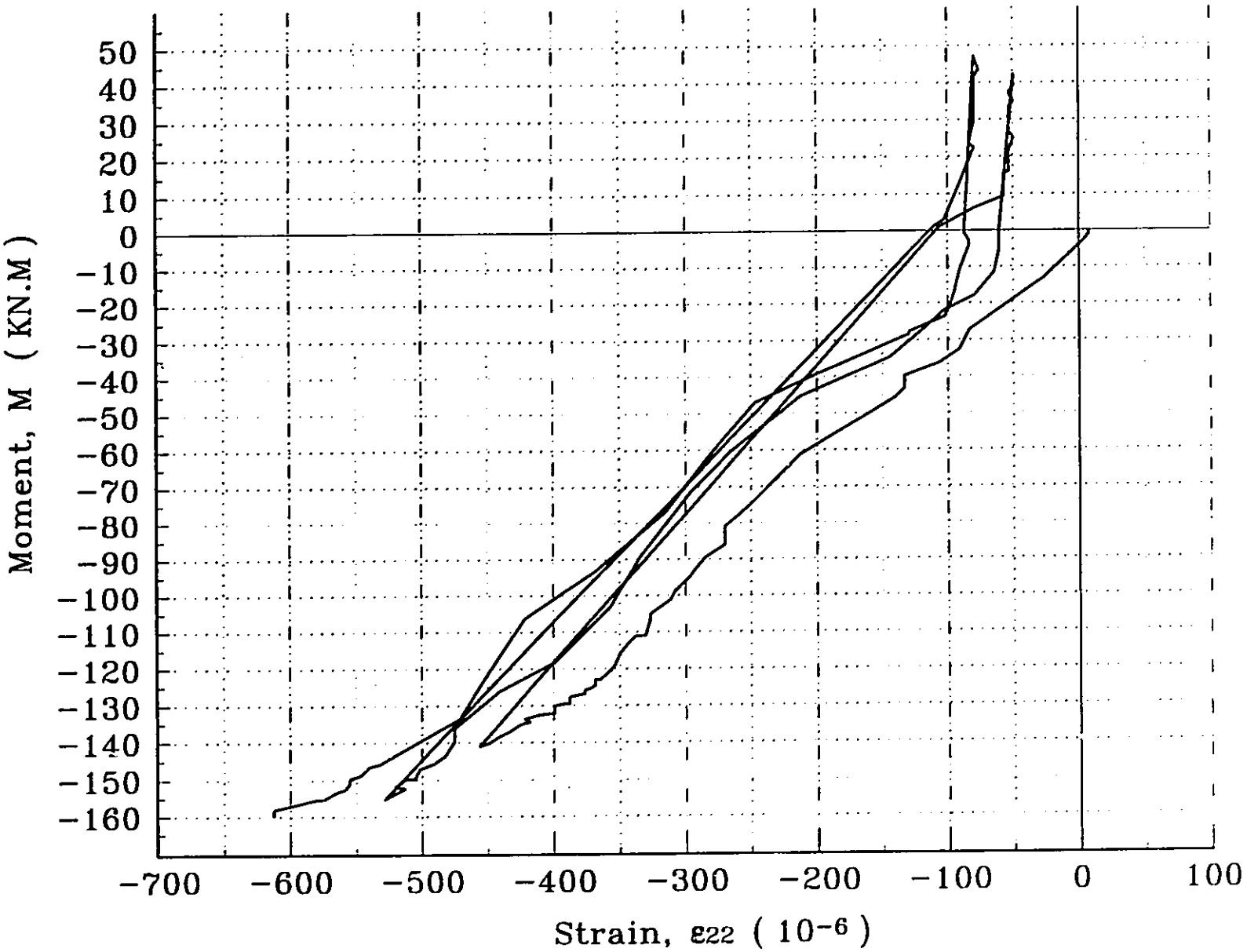
50
40
30
20
10
0
−10
−20
−30
−40
−50
−60
−70
−80
−90
−100
−110
−120
−130
−140
−150
−160
Moment, M (KN.M)
−700
−600
−500
−400
−300
−200
−100
0
100
Strain, ε22 (10−6)

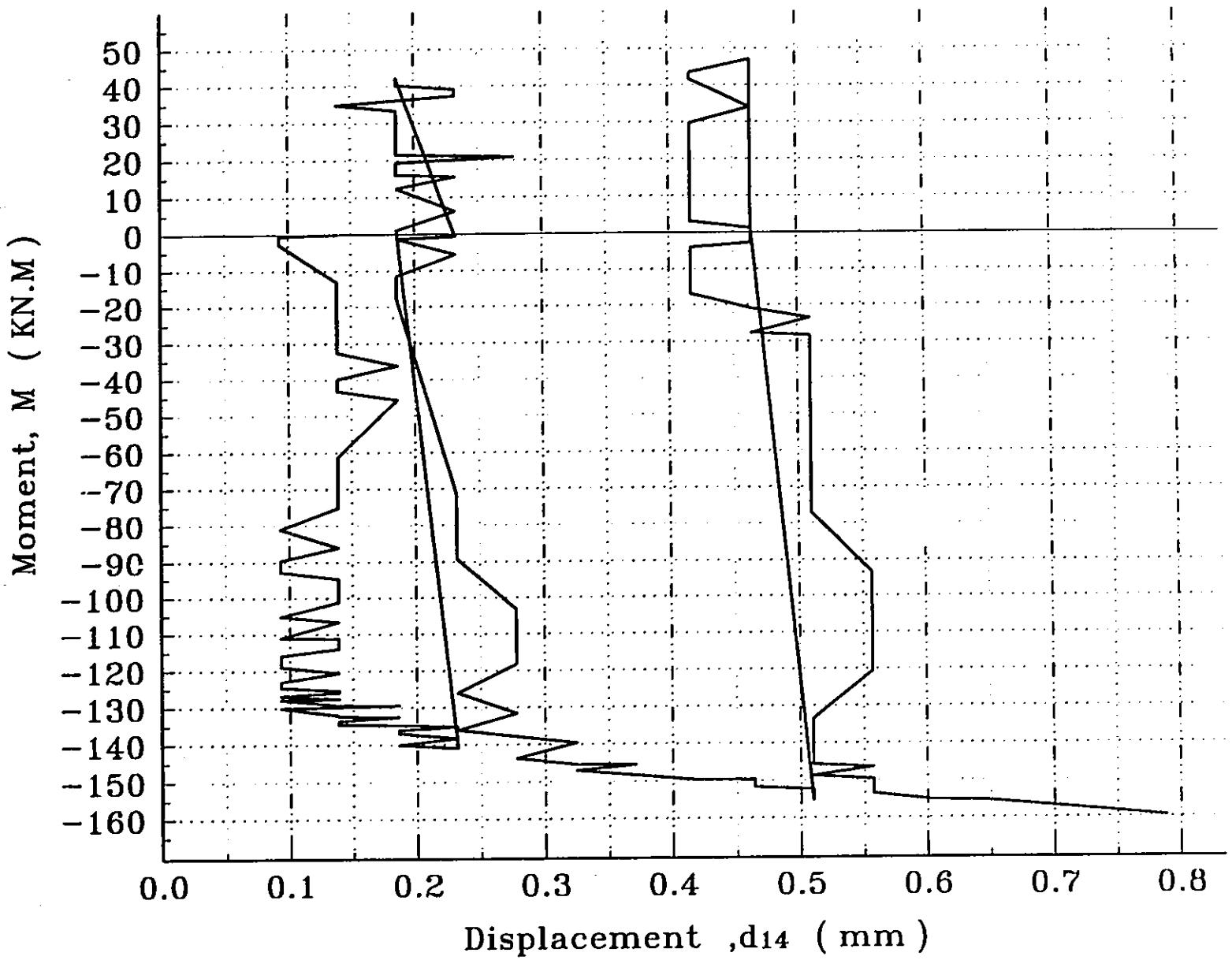
Moment, M (KN.M)
50
40
30
20
10
0
-10
-20
-30
-40
-50
-60
-70
-80
-90
-100
-110
-120
-130
-140
-150
-160
0.0
0.1
0.2
0.3
0.4
0.5
0.6
0.7
0.8
Displacement ,d14 (mm)

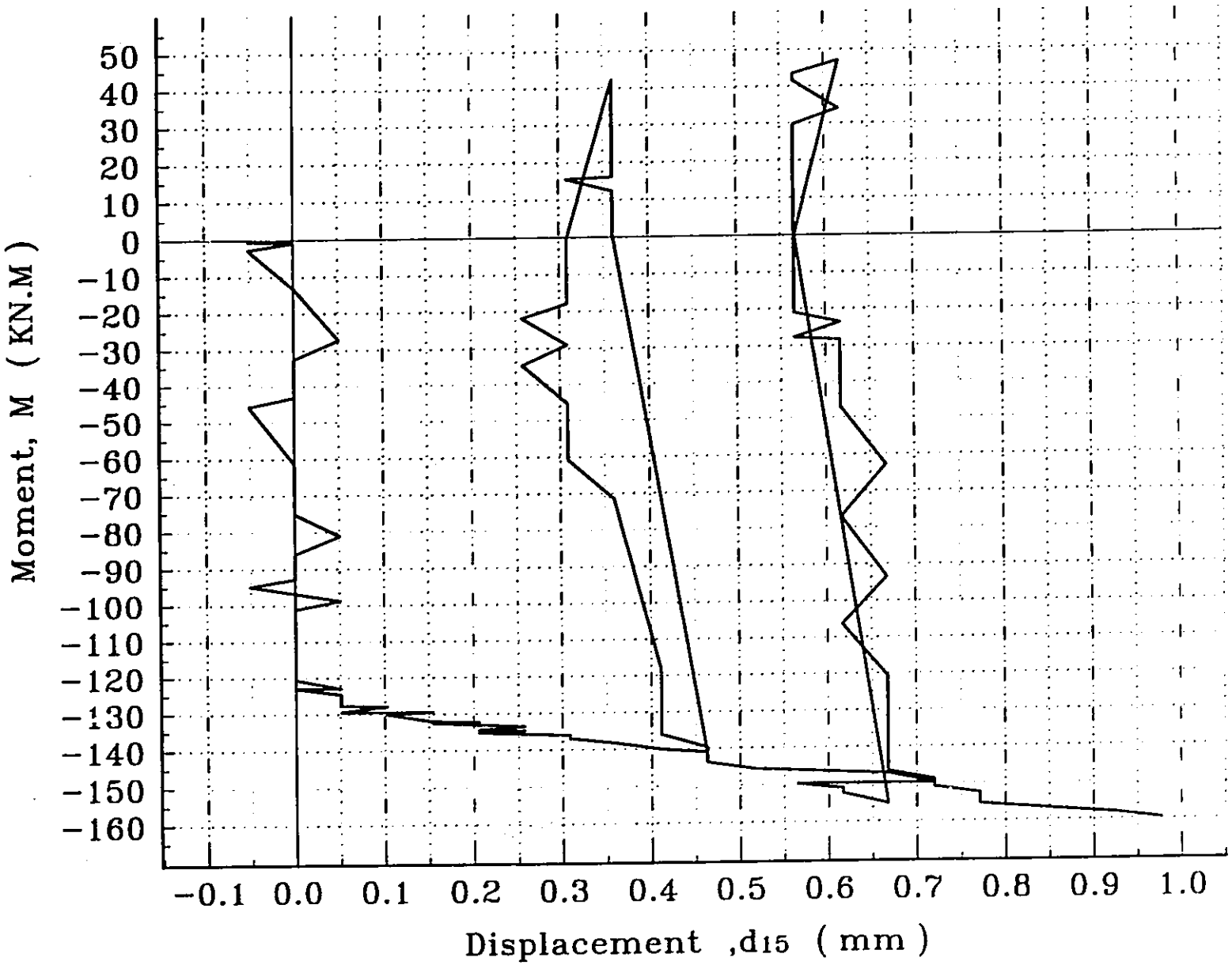
Moment, M (KN.M)
50
40
30
20
10
0
-10
-20
-30
-40
-50
-60
-70
-80
-90
-100
-110
-120
-130
-140
-150
-160
-0.1
0.0
0.1
0.2
0.3
0.4
0.5
0.6
0.7
0.8
0.9
1.0
Displacement ,d15 (mm)

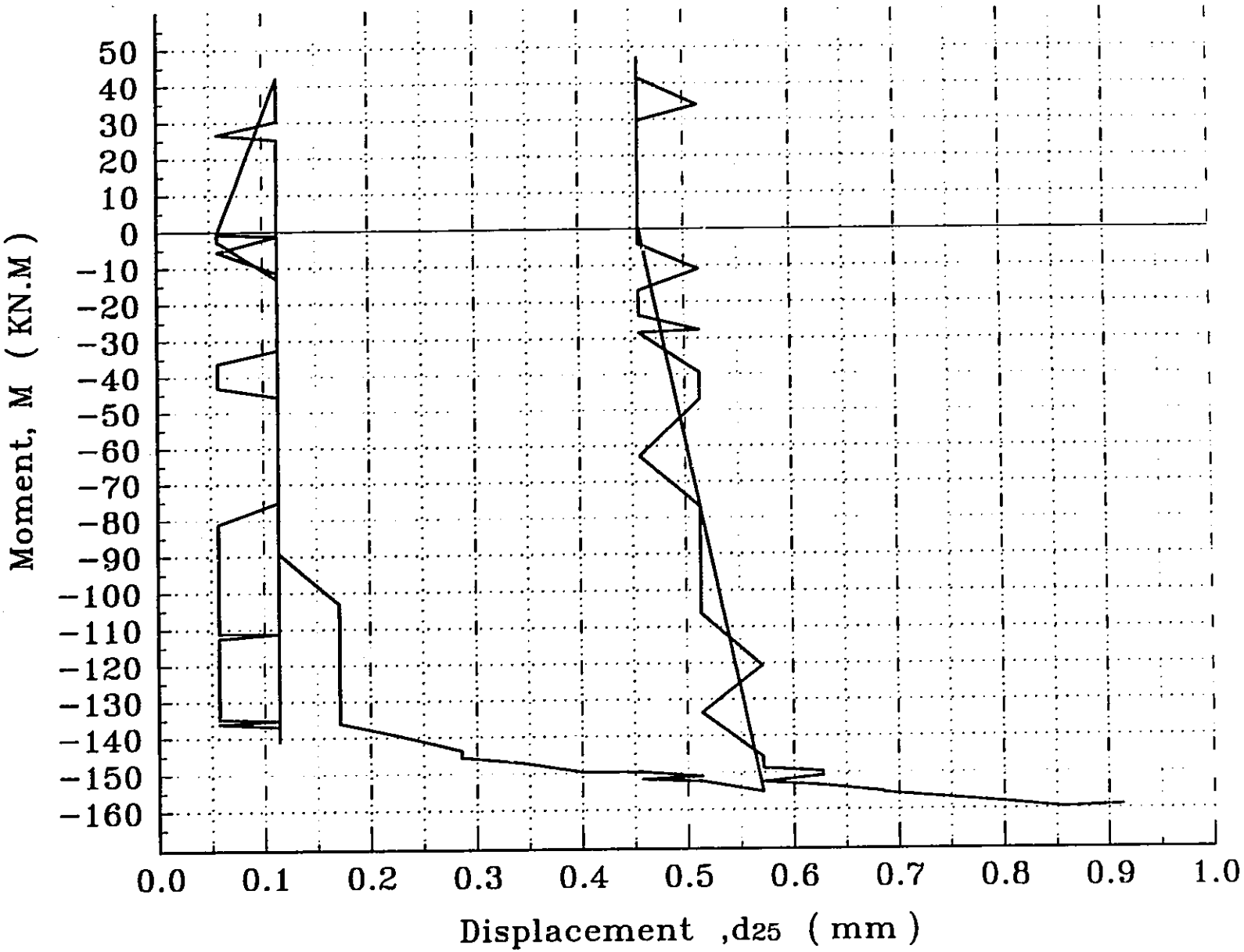
Moment, M (KN.M)
50
40
30
20
10
0
-10
-20
-30
-40
-50
-60
-70
-80
-90
-100
-110
-120
-130
-140
-150
-160
0.0
0.1
0.2
0.3
0.4
0.5
0.6
0.7
0.8
0.9
1.0
Displacement ,d25 (mm)

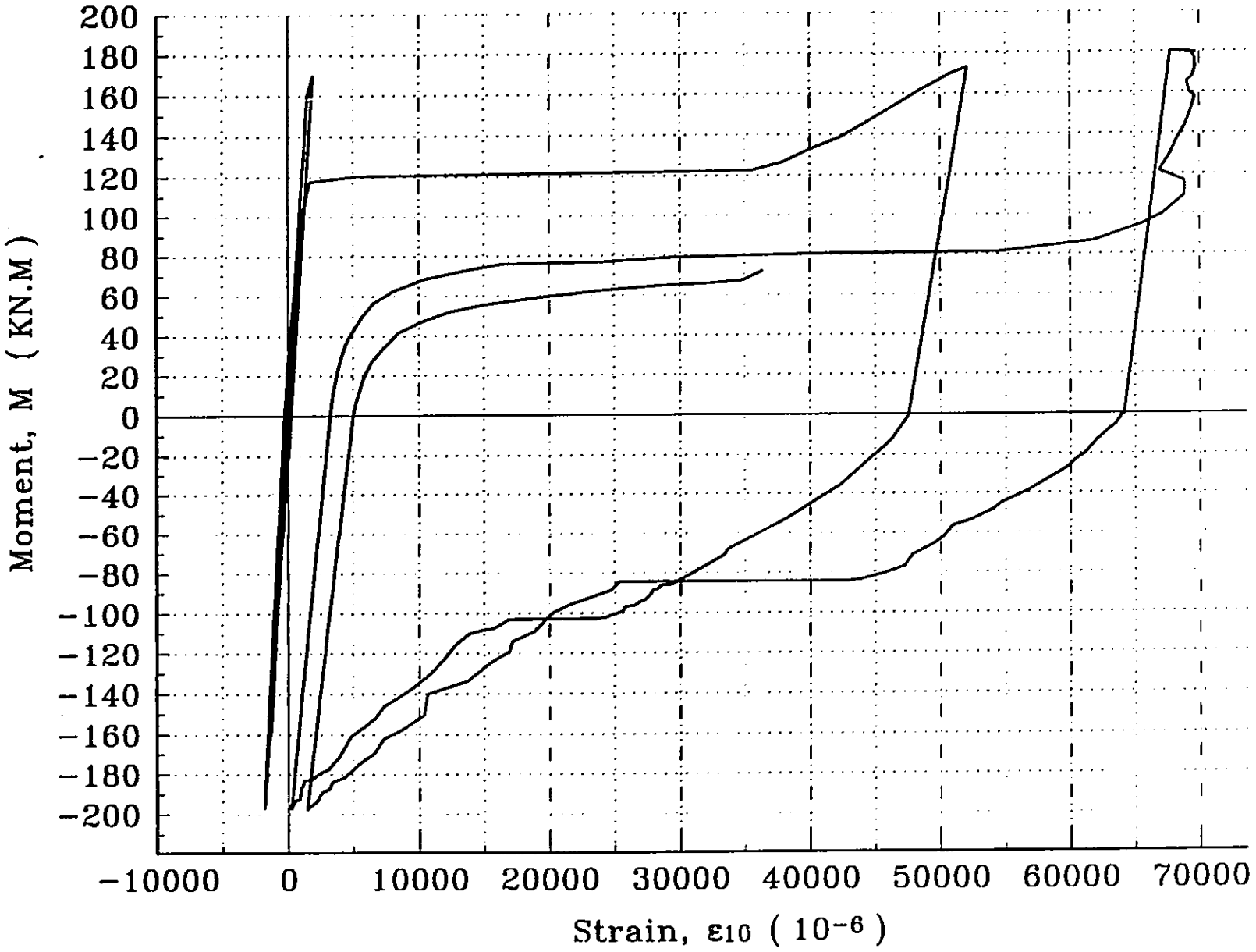
200
180
160
140
120
100
80
60
40
20
0
−20
−40
−60
−80
−100
−120
−140
−160
−180
−200
−10000
0
10000
20000
30000
40000
50000
60000
70000
Moment, M (KN.M)
Strain, ε10 (10−6)

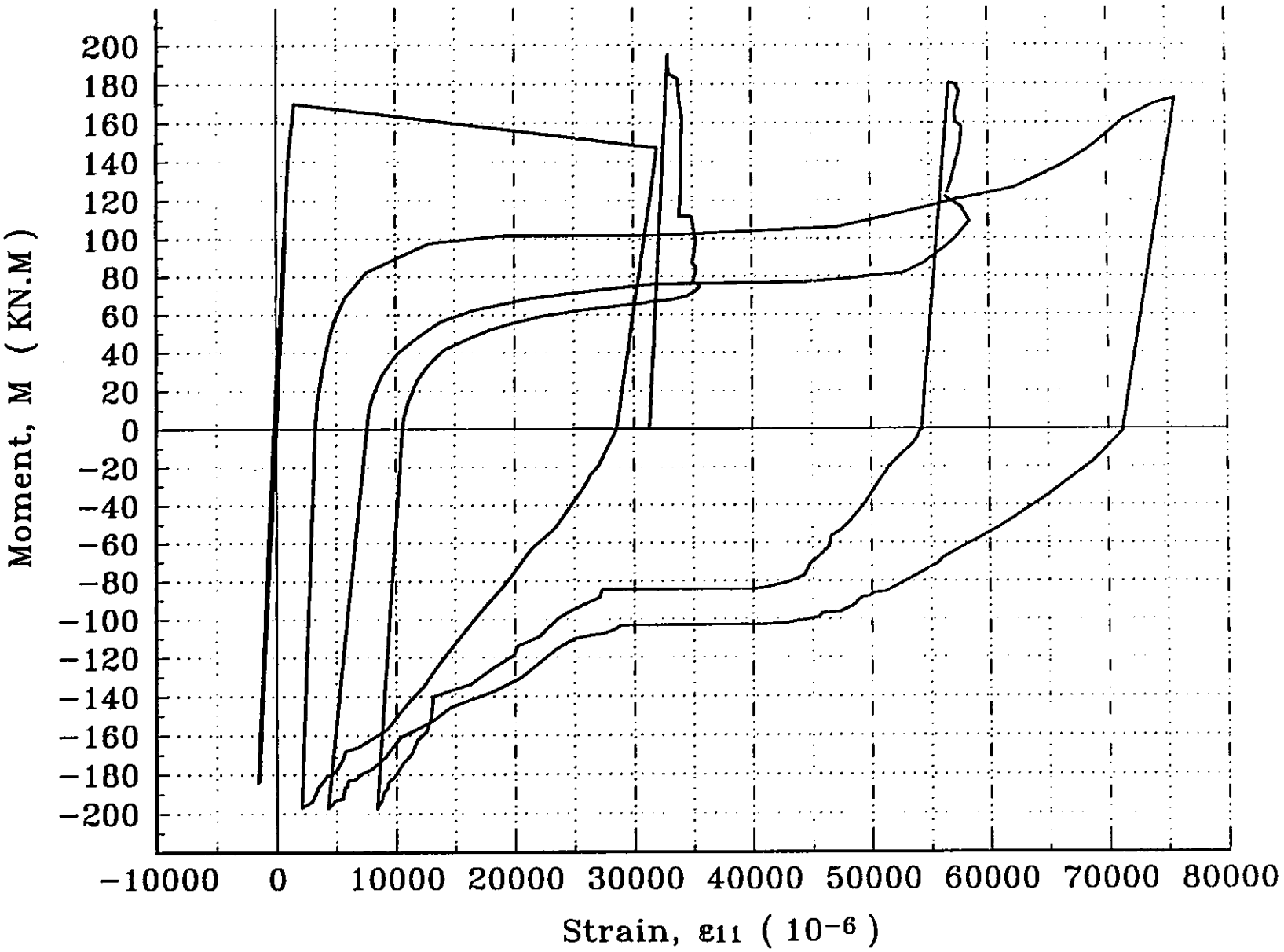
Moment, M (KN.M)
200
180
160
140
120
100
80
60
40
20
0
-20
-40
-60
-80
-100
-120
-140
-160
-180
-200
-10000
0
10000
20000
30000
40000
50000
60000
70000
80000
Strain, ε11 (10-6)

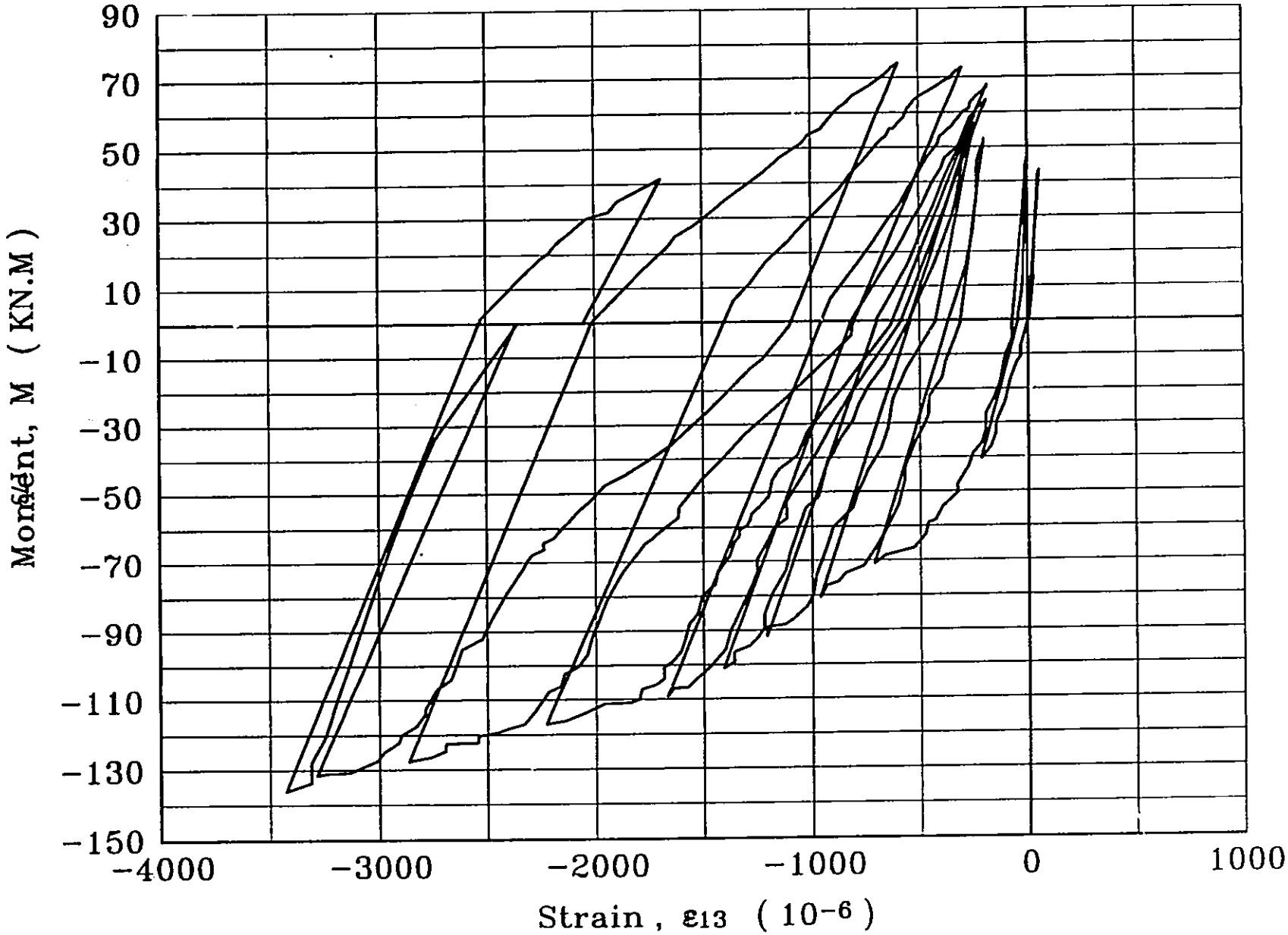
90
70
50
30
10
-10
-30
-50
-70
-90
-110
-130
-150
Moment, M (KN.M)
-4000
-3000
-2000
-1000
0
1000
Strain , ε13 (10-6)

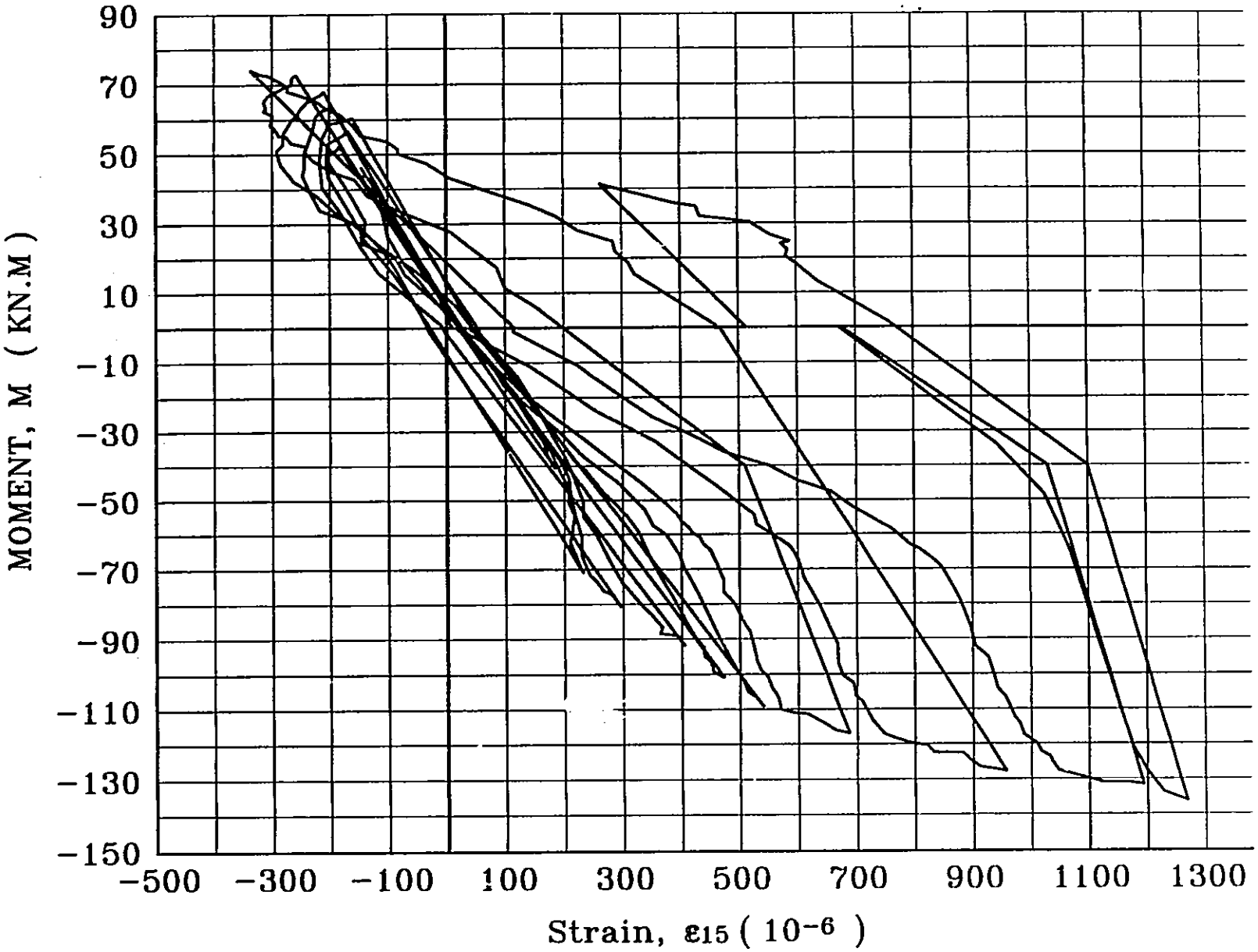
90
70
50
30
10
−10
−30
−50
−70
−90
−110
−130
−150
MOMENT, M (KN.M)
−500
−300
−100
100
300
500
700
900
1100
1300
Strain, ε15 (10−6)

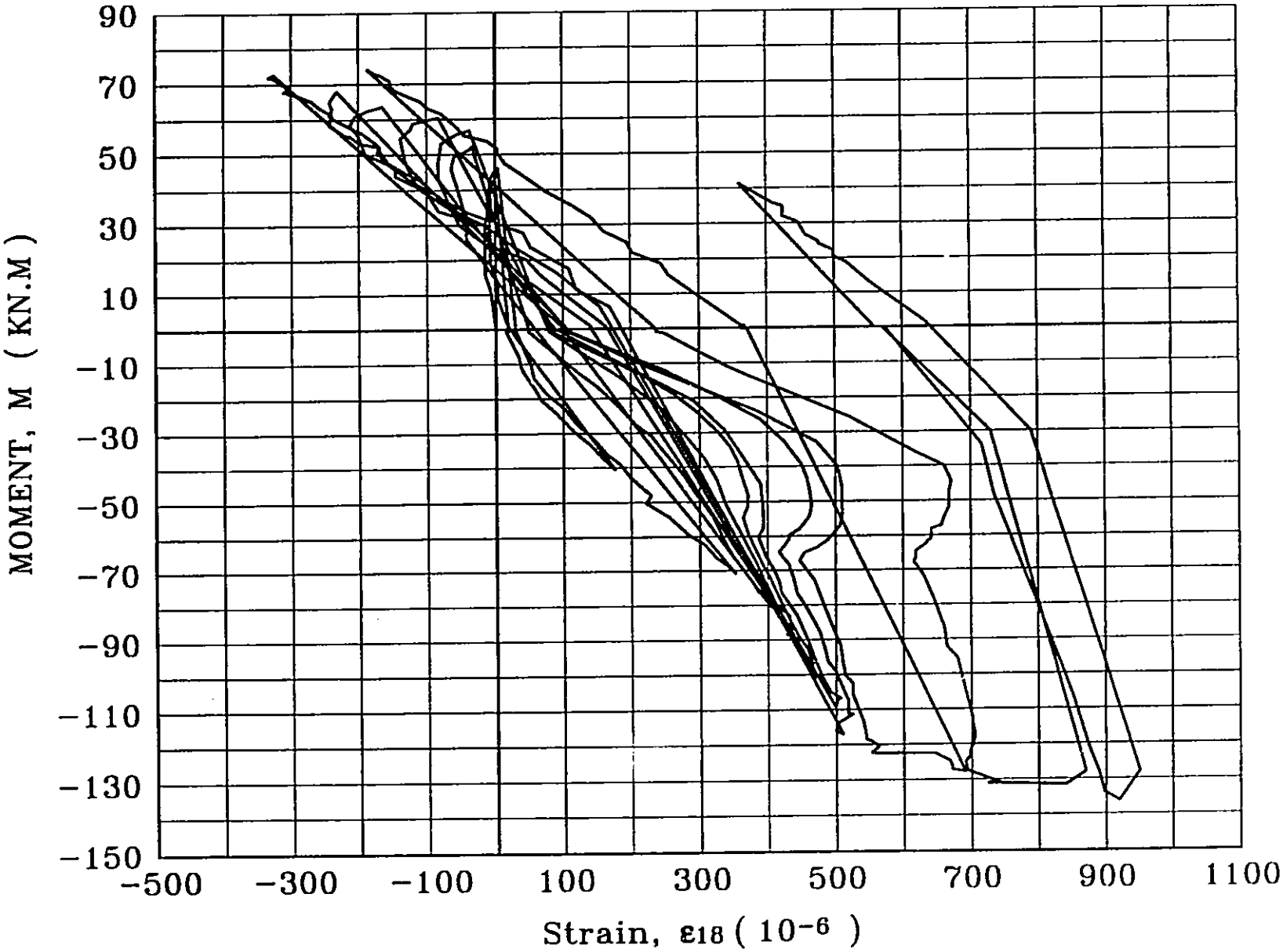
MOMENT, M (KN.M)
90
70
50
30
10
−10
−30
−50
−70
−90
−110
−130
−150
−500
−300
−100
100
300
500
700
900
1100
Strain, ε18 (10−6)

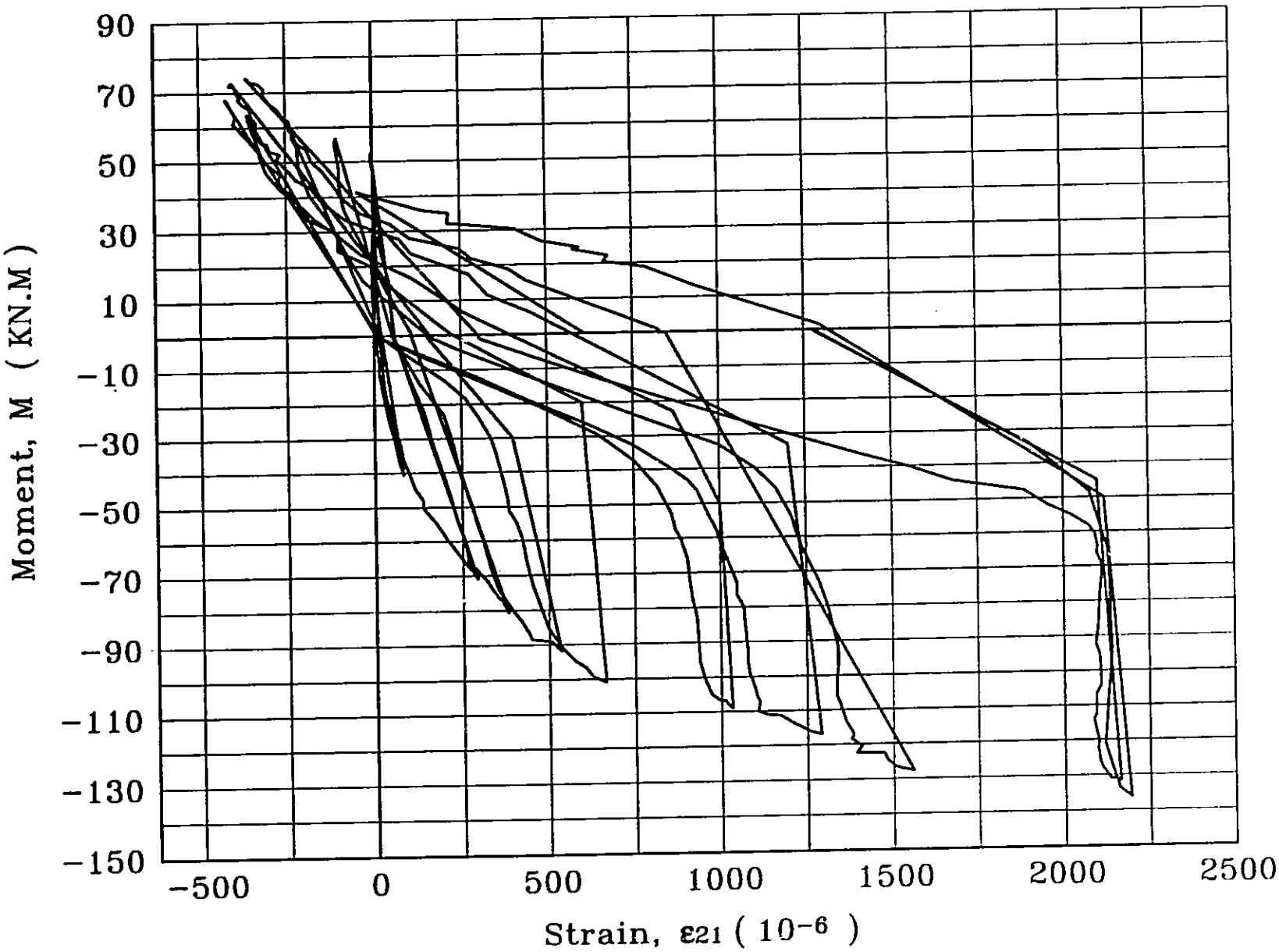
90
70
50
30
10
-10
-30
-50
-70
-90
-110
-130
-150
-500
0
500
1000
1500
2000
2500
Moment, M (KN.M)
Strain, ε21 (10-6)

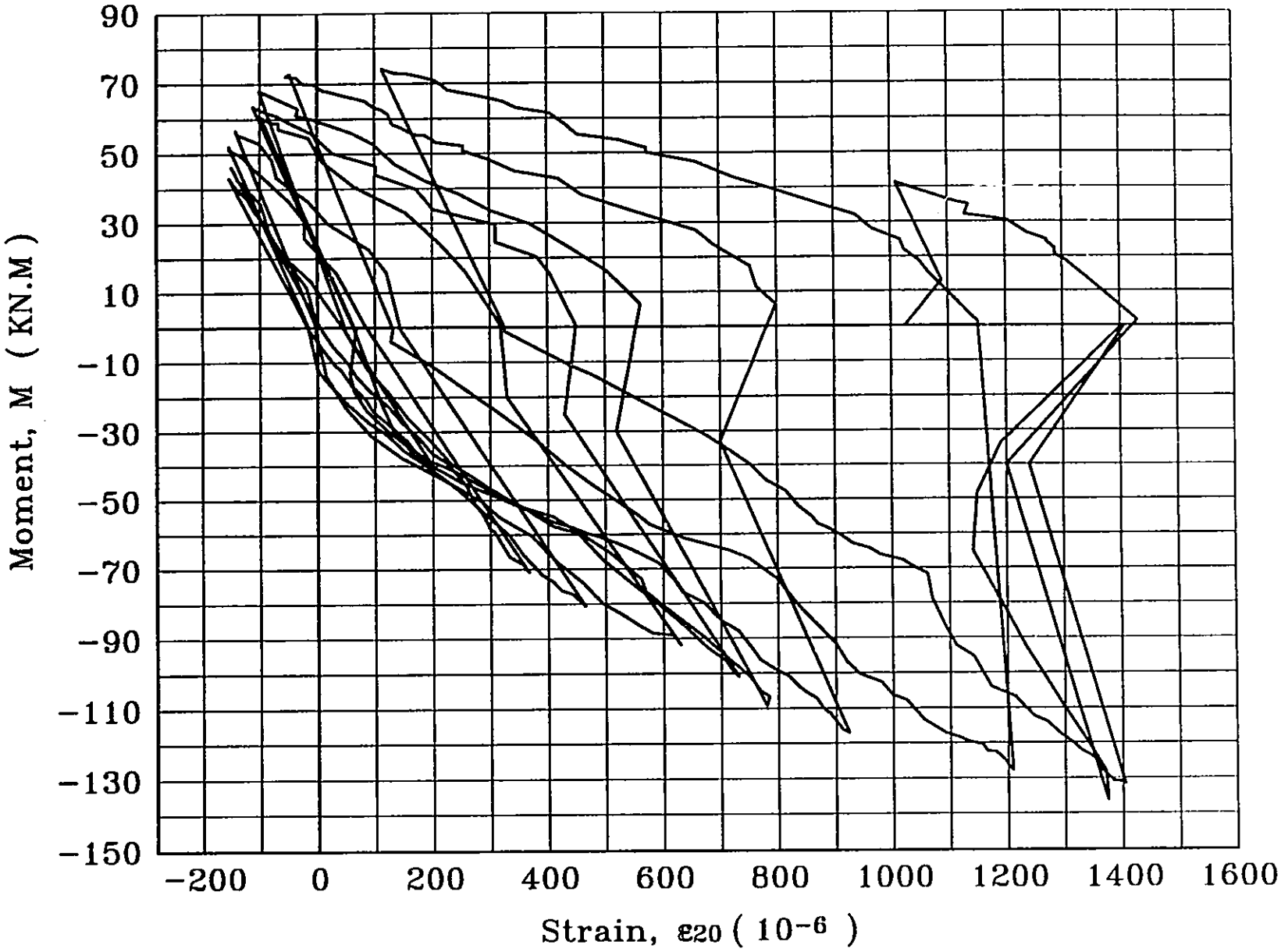
90
70
50
30
10
-10
-30
-50
-70
-90
-110
-130
-150
-200
0
200
400
600
800
1000
1200
1400
1600
Moment, M (KN.M)
Strain, ε20 (10-6)

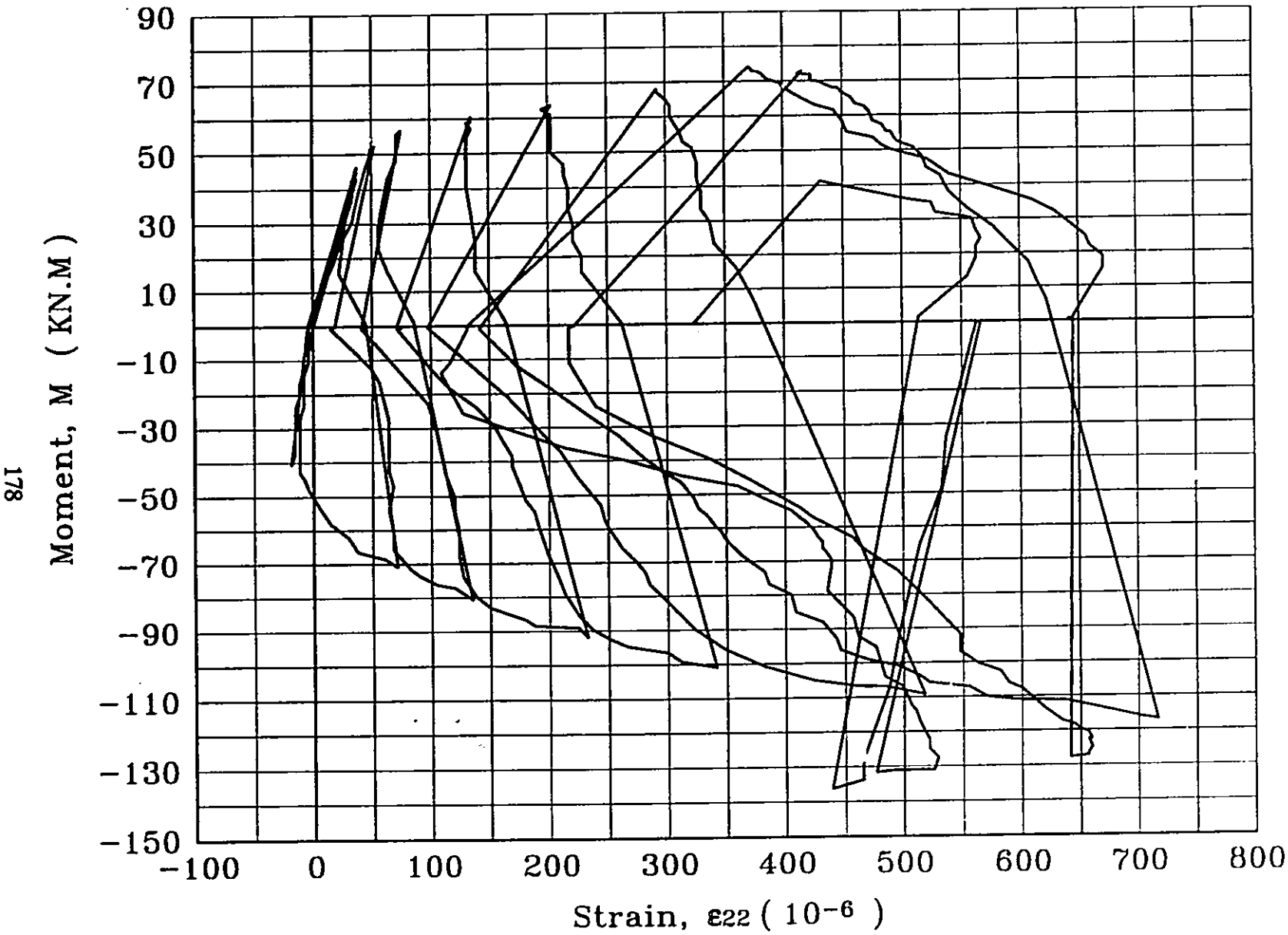
90
70
50
30
10
-10
-30
-50
-70
-90
-110
-130
-150
-100
0
100
200
300
400
500
600
700
800
Moment, M (KN.M)
Strain, ε22 (10-6)

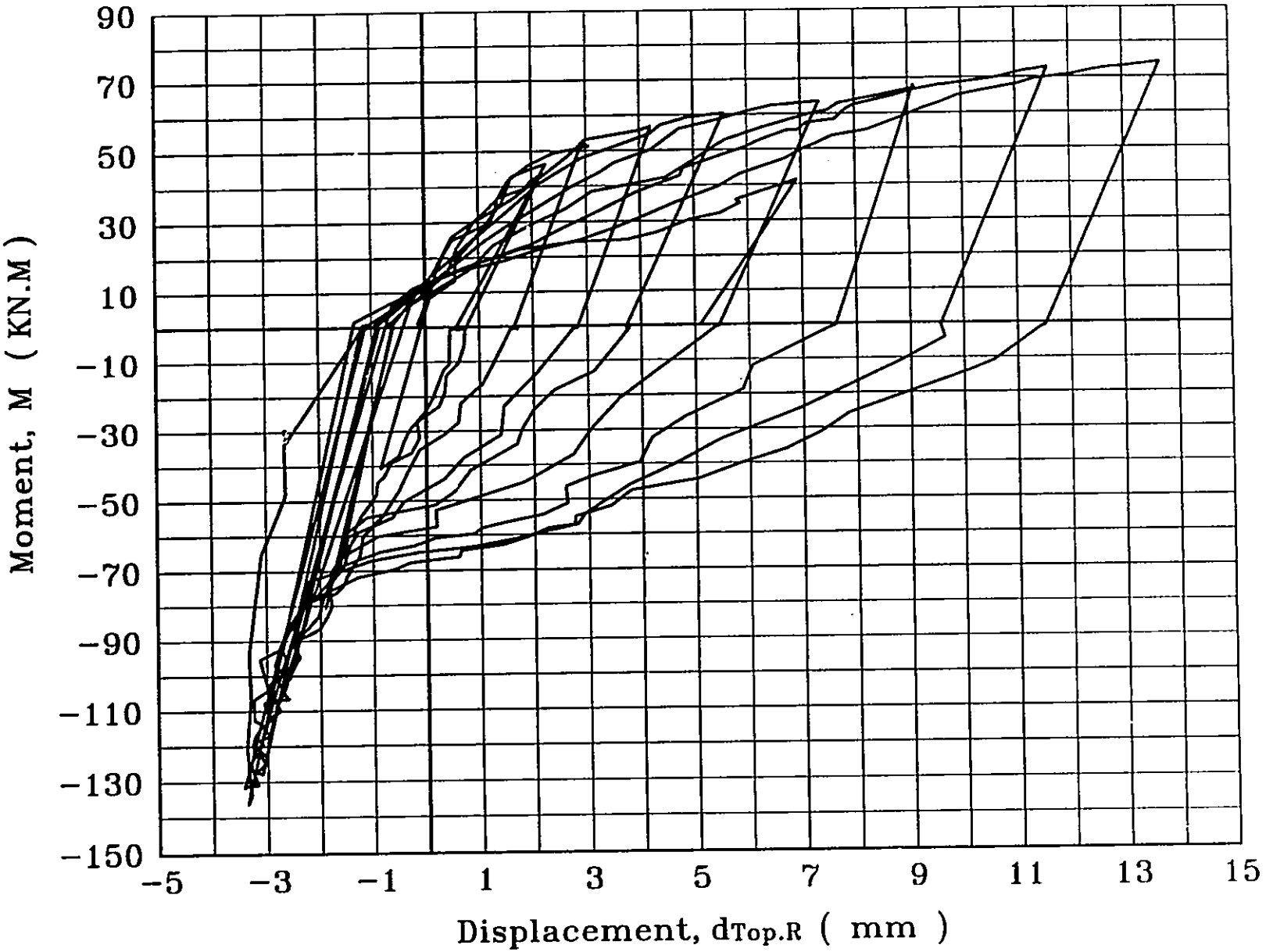
90
70
50
30
10
-10
-30
-50
-70
-90
-110
-130
-150
-5
-3
-1
1
3
5
7
9
11
13
15
Moment, M (KN.M)
Displacement, dTop.R (mm)

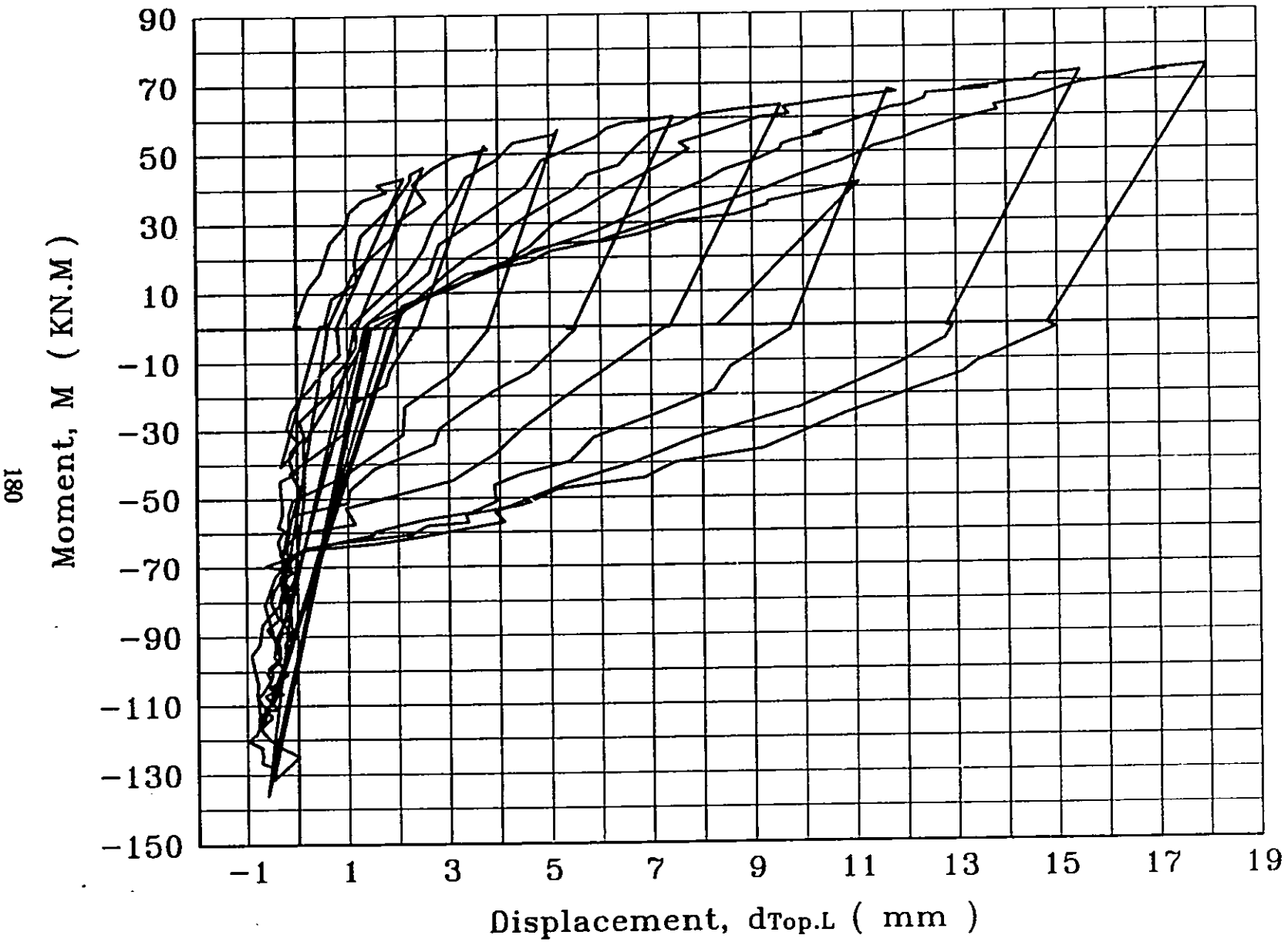
90
70
50
30
10
-10
-30
-50
-70
-90
-110
-130
-150
-1
1
3
5
7
9
11
13
15
17
19
Moment, M (KN.M)
Displacement, dTop.L (mm)

Appendix D

Data Reduction Program

```
10 INPUT A$
15 INPUT B$
20 OPEN A$ FOR INPUT AS #1
30 OPEN B$ FOR OUTPUT AS #2
40 INPUT #1, Y1, X1, t
49 PRINT Y1; X1
50 IF Y1 < 0 THEN GOTO 1000
60 YTR = Y1
61 XTR = X1
62 YMAX = YTR
63 XMAX = XTR
70 INPUT #1, Y2, X2, t
79 PRINT Y2; X2
80 IF Y2 < .01 THEN GOTO 1000
90 IF YTR > YMAX THEN GOTO 120
100 YTR = Y2
101 XTR = X2
110 GOTO 70
120 IF Y2 > YTR THEN GOTO 100
130 YMAX = YTR
131 XMAX = XTR
140 WRITE #2, YMAX, XMAX
150 GOTO 100
1000 X1 = X2
1001 Y1 = Y1
1010 YTR = Y1
1011 XTR = X1
1012 YMAX = YTR
1013 XMAX = XTR
1020 INPUT #1, Y2, X2, t
1029 PRINT Y2; X2
1030 IF Y2 > -.01 THEN GOTO 2000
1040 IF YTR < YMAX THEN GOTO 1070
1050 YTR = Y2
1051 XTR = X2
1060 GOTO 1020
1070 IF Y2 < YTR THEN GOTO 1050
1080 YMAX = YTR
1081 XMAX = XTR
1090 WRITE #2, YMAX, XMAX
1100 GOTO 1050
2000 X1 = X2
2001 Y1 = Y2
2010 GOTO 50
3000 STOP
```

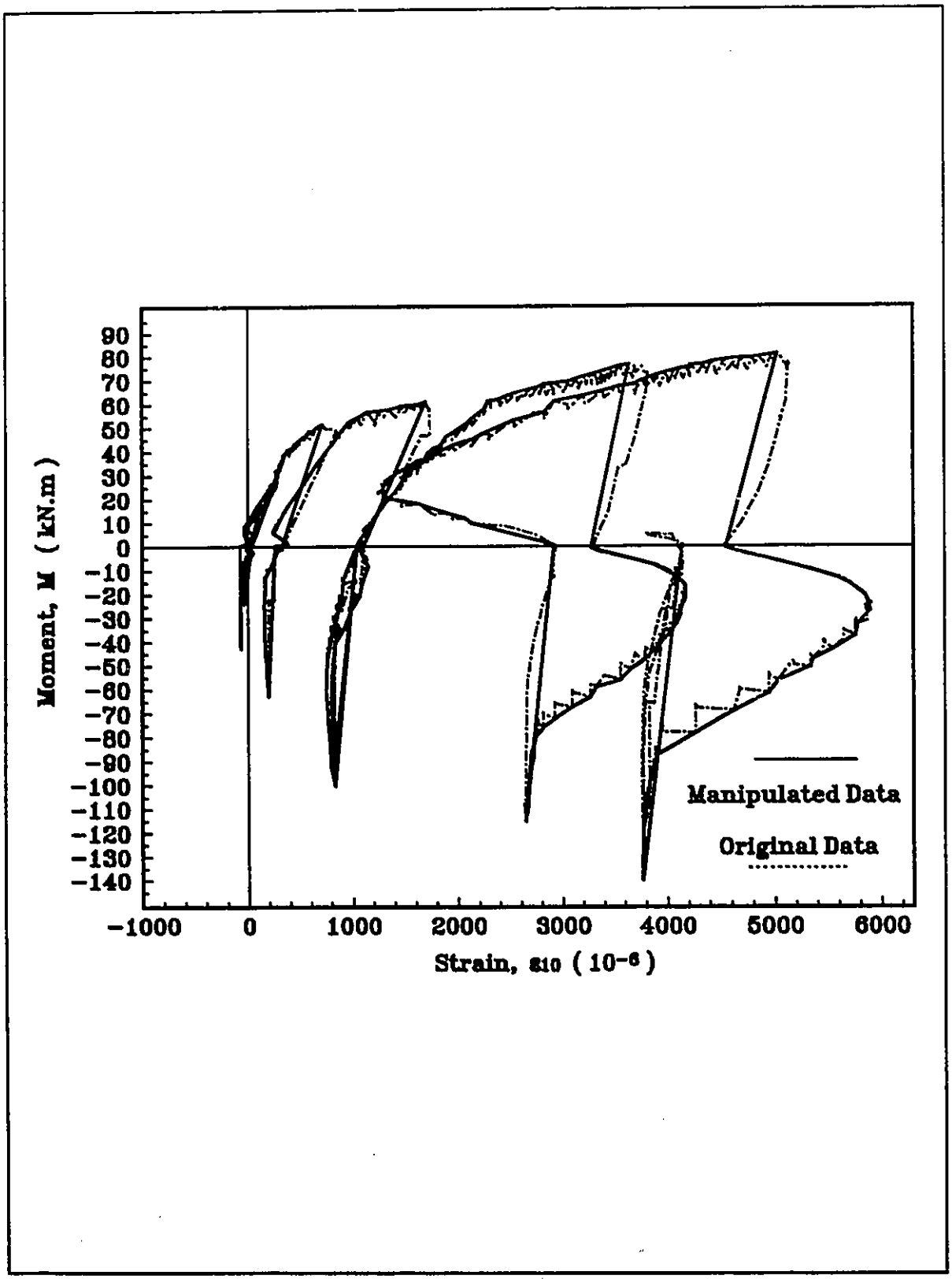
Moment, M (kN.m)
90
80
70
60
50
40
30
20
10
0
-10
-20
-30
-40
-50
-60
-70
-80
-90
-100
-110
-120
-130
-140
-1000
0
1000
2000
3000
4000
5000
6000
Strain, ε10 (10-6)
Manipulated Data
Original Data

Appendix E

Application of Yield line Theory in Determination of Angle Connections Capacity

E.1 Capacity of a Long Angle Subjected to Tensile Load

Since prediction of capacity based on simple assumption of formation of yield lines parallel to longitudinal axis of an angle does not give realistic result, as it was also observed during experiment 4, instead a more complex yield line pattern is considered. The new yield line pattern, as shown in Fig. e.1, should be then used to determine corresponding load **P** which relates to capacity of the connections with top and/or seat angles. **Figure e.1**

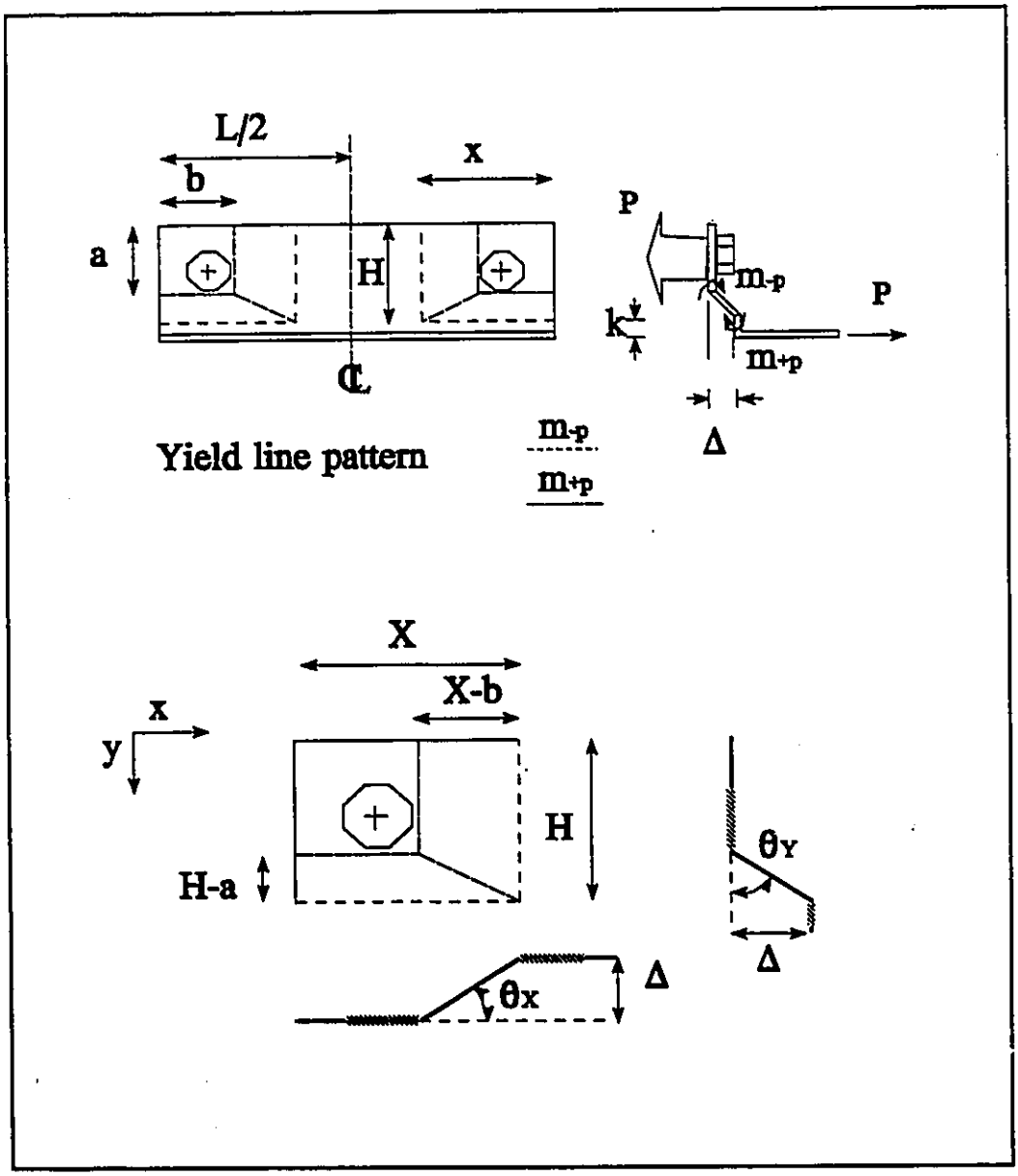

Assuming virtual displacement Δ and using virtual work method, for half an angle, we have;

Internal work $= W_i = (m^+ . H)\,\theta_x + (m^- . H)\,\theta_x + (m^+ . X)\,\theta_y + (m^- . X)\,\theta_y$ (1)

where, by geometry of the figure we have $\theta_x = \Delta/(X-b)$ and $\theta_y = \Delta/(H-a)$.

substituting these parameters in the equation for W_i we get;

$w_i = (m^+ + m^-)\,\{H/(X-b) + X/(H-a)\}\Delta$

assuming that $m^- = m^- = m_p$ (for a uniform steel section)

$w_i = 2\,m_p\,\{H/(X-b) + X/(H-a)\}\Delta$

Also, external work $= W_e = (P.\Delta)/2$

where, P is the total load acting on the hole angle.

Equating external work and internal work, to solve for **P**, we get;

$$P = 4m_p\left[\frac{H}{(X-b)} + \frac{X}{(H-a)}\right] \quad (1)$$

To minimize **P**, we take its derivative with respect to **X** and by setting that equal to zero, we get;

$$X = b + \sqrt{H^2 + Ha} \qquad (2)$$

Note that X must always be smaller than half length of the angle. $X <= L/2$

E.2 Practical Application in Determination of Moment Capacity of Connection Detail 2

E.2.1 Positive Moment

Knowing the size and configuration of the angle and stiffeners in the top angle of connection detail 2, we have;

H = 59 mm, b = 58 mm, a = 45 mm, L = 276 mm, thickness t = 8 mm, F_y = 225 MPa

substituting these values in eq.(2) we get; X = 86.7mm < L/2 =138mm

Also, $m_p = t^2 F_y/4 =$ 3600 N.mm/mm

substituting the obtained values in eq.(1) we get,

P = 118 kN

Corresponding moment will be simply,

M = p . h (h is the beam hight)

M = 118 x 0.506 m = 60.2 kN.m

E.2.1 Negative Moment

Using the same method as above, for the seat angle of connection detail 2 with known values of parameters used in eq.(2), we have;

H = 67.5 mm, b = 55.8 mm, a = 56 mm, L = 276 mm, thickness t = 8.6 mm, F_y = 225 MPa

$X = 83.6$ mm $< L/2 = 138$ mm

also, we have $m_p = t^2 F_y/4 = 4160$ N.mm/mm

substituting these values in eq.(1) we get,

$P = 161.4$ kN

Now, as shown in Fig. 5.5, total negative moment capacity can be obtained if force **T** and moment $\mathbf{M_0}$ are known. To find force **T**, fist we need to determine horizontal force **F** which can cause formation of plastic hinge in the stiffener angles. Therefore;

$m_p = 7.5 \times 10^6$ N.mm (for double angle of size 63.5mm x 63.5mm x 9.5mm)

In contrary to what considered in similar case for connection detail 1, to find force **F** the first row of rivets connecting the stiffener angles to the seat angle are not considered. This is due to the fact that these rivets are located where the seat angle and stiffener angles move together. therefore, knowing that distance between plastic hinge (second row of rivet) and the tip of the angles is equal to 114 mm, we simple have,

$F = 7.5 \times 10^6 / 114 = 65.8$ kN

By writing the equation of equilibrium for horizontal forces acting on the seat angle, to find total force **T** we get,

$T = F + V$

where, $V = P = 161.4$ kN , therefore; $T = 227.2$ kN

knowing that moment $\mathbf{M_0}$, acting on the horizontal leg of the seat angle, at the maximum, can reach plastic moment of the leg which is equal to:

$M_0 = L \times t^2 F_y/4 = 276$mm x 4160 N.mm/mm $= 1.14$ kN.m

Therefore, total negative moment for the connection will be

$M = T.h + M_0$ (h, is the hight of the beam)

$M = 227.2 \times 0.507 + 1.14$ kN.m

$M = 116.2$ kN

Note that $\mathbf{M_0}$ is small compare to total moment **M.**